Journal of Research

of the

National Bureau of Standards

UNIVERSITY
OF MICHIGAN

OCT 29 1956

PHYSICS
LIBRARY

OCTOBER 1956

VOLUME 57 NUMBER 4

U. S. DEPARTMENT OF COMMERCE
Sinclair Weeks, Secretary
NATIONAL BUREAU OF STANDARDS
A. V. Astin, Director

OCTOBER · 195
VOLUME · 5
NUMBER ·

JOURNAL OF RESEARCH

of the

NATIONAL BUREAU OF STANDARDS

PERIODICALS OF THE NATIONAL BUREAU OF STANDARDS

(Published monthly)

The National Bureau of Standards is engaged in fundamental and applied research in physics, chemistry, mathematics, and engineering. Projects are conducted in fifteen fields: electricity and electronics, optics and metrology, heat and power, atomic and radiation physics, chemistry, mechanics, organic and fibrous materials, metallurgy, mineral products, building technology, applied mathematics, data processing systems, cryogenic engineering, radio propagation, and radio standards. The Bureau has custody of the national standards of measurement and conducts research leading to the improvement of scientific and engineering standards and of techniques and methods of measurement. Testing methods and instruments are developed, physical constants and properties of materials are determined, and technical processes are investigated.

JOURNAL OF RESEARCH

The Journal presents research papers by authorities in the specialized fields of physics, mathematics, chemistry, and engineering. Complete details of the work are presented, including laboratory data, experimental procedures, and theoretical and mathematical analyses. Annual subscription: domestic, $4.00; $1.25 additional for foreign mailing.

TECHNICAL NEWS BULLETIN

Summaries of current research at the National Bureau of Standards are published each month in the Technical News Bulletin. The articles are brief, with emphasis on the results of research, chosen on the basis of their scientific or technologic importance. Lists of all Bureau publications during the preceding month are given, including Research Papers, Handbooks, Applied Mathematics Series, Building Materials and Structures Reports, Miscellaneous Publications, and Circulars. Each issue contains 12 or more two-column pages; illustrated. Annual subscription: domestic, $1.00; 35 cents additional for foreign mailing.

BASIC RADIO PROPAGATION PREDICTIONS

The Predictions provide the information necessary for calculating the best frequencies for communication between any two points in the world at any time during the given month. The data are important to all users of long-range radio communications and navigation, including broadcasting, airline, steamship, and wireless services, as well as to investigators of radio propagation and ionosphere. Each issue, covering a period of one month, is released three months in advance and contains 16 large pages, including pertinent charts, drawings, and tables. Annual subscription: domestic, $1.00; 25 cents additional for foreign mailing.

Order all publications from the Superintendent of Documents
U. S. Government Printing Office, Washington 25, D. C.

Use of funds for printing this publication approved by the Director of the Bureau of the Budget (May 14, 1956).

Journal of Research of the National Bureau of Standards Vol. 57, No. 4, October 1956 Research Paper 2708

Infrared Spectra of D-Talose Monobenzoate and Related Substances[1]

H. S. Isbell, J. E. Stewart, H. L. Frush, J. D. Moyer, and F. A. Smith

Infrared absorption spectra for D-talose monobenzoate, α-D-talose, β-D-talose, penta-acetyl-α-D-talose, tetraacetyl-α-D-talose, and β-L-rhamnose 1,2-(methyl orthoacetate) show that the previously held, orthoacid structure for D-talose monobenzoate is not correct. The spectrum and the method of synthesis of D-talose monobenzoate indicate that the compound is a 1-benzoyl-D-talopyranose. The infrared absorption of the alpha and beta pyranose modifications of D-talose was found to be anomalous in that each form shows absorption heretofore considered characteristic of the alpha modification as well as that considered characteristic of the beta.

1. Discussion

By the action of perbenzoic acid on D-galactal (D-talal), Pigman and Isbell [1] [2] obtained a D-talose monobenzoate for which they suggested an orthoester structure because of its unusual properties. The substance showed a rapid, complex mutarotation in methanol, a similar but somewhat slower mutarotation in pyridine, and almost no mutarotation in dilute hydrochloric acid. In light of the properties of certain orthobenzoates of ribose recently described by Fletcher and Ness [2], it seemed desirable to reinvestigate the structure of the talose derivative.

A sample of the product prepared by Pigman and Isbell in 1937 was available, but had turned slightly brown. After two recrystallizations from dimethoxyethane, the melting point was sharper and higher than that reported earlier, and the mutarotation in methanol followed the same course, but at a slightly lower rate. The recrystallized compound, like the original, did not yield a phenylhydrazone; hence the reducing group must be blocked by the benzoyl group, which could be present either as the normal ester (I) or as the orthoester (II). However, only the normal ester would show infrared absorption characteristic of a carbonyl group.

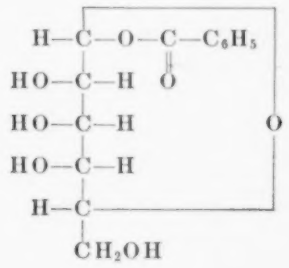

I

D-Talopyranose 1-benzoate.

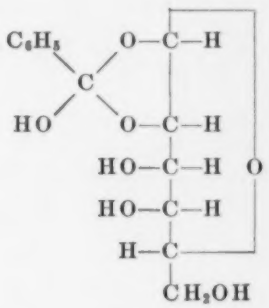

II

β-D-Talose 1,2-(orthobenzoic acid).

It has now been found that the infrared absorption spectrum of the original D-talose monobenzoate (fig. 1), which is identical with the spectrum of the recently repurified product, shows a strong absorption at 5.77 μ, characteristic of the ester carbonyl group. In contrast, β-L-rhamnose 1,2-(methyl orthoacetate), which has been characterized as an orthoester by means of its ultraviolet absorption spectrum [3,4], shows no absorption near this wavelength. Thus, it can be concluded that the D-talose monobenzoate is not an orthoester but a normal benzoic ester possessing a carbonyl group. This conclusion is also supported by the observed absorption at 7.93 μ, because normal benzoates show characteristic absorption in this region [5,6]. The lack of formation of a hydrazone, in conjunction with the infrared absorption, requires that the product be a D-talose 1-benzoate.

It seemed possible that a study of infrared absorption might aid in assigning alpha or beta configuration to the D-talose 1-benzoate. A study of the spectra of over 75 hexoses and substituted hexoses had previously shown that the alpha anomers of the more common configurations have bands in the 11.6- to 12.4-μ region, whereas the beta anomers have bands in the 11.2- to 11.7-μ region.[3] These regions

[1] This work was sponsored by the Chemistry Branch of the Office of Naval Research, Department of the Navy, Washington, D. C.

[2] Figures in brackets indicate the literature references at the end of this paper.

[3] The spectra will be presented in papers now in preparation.

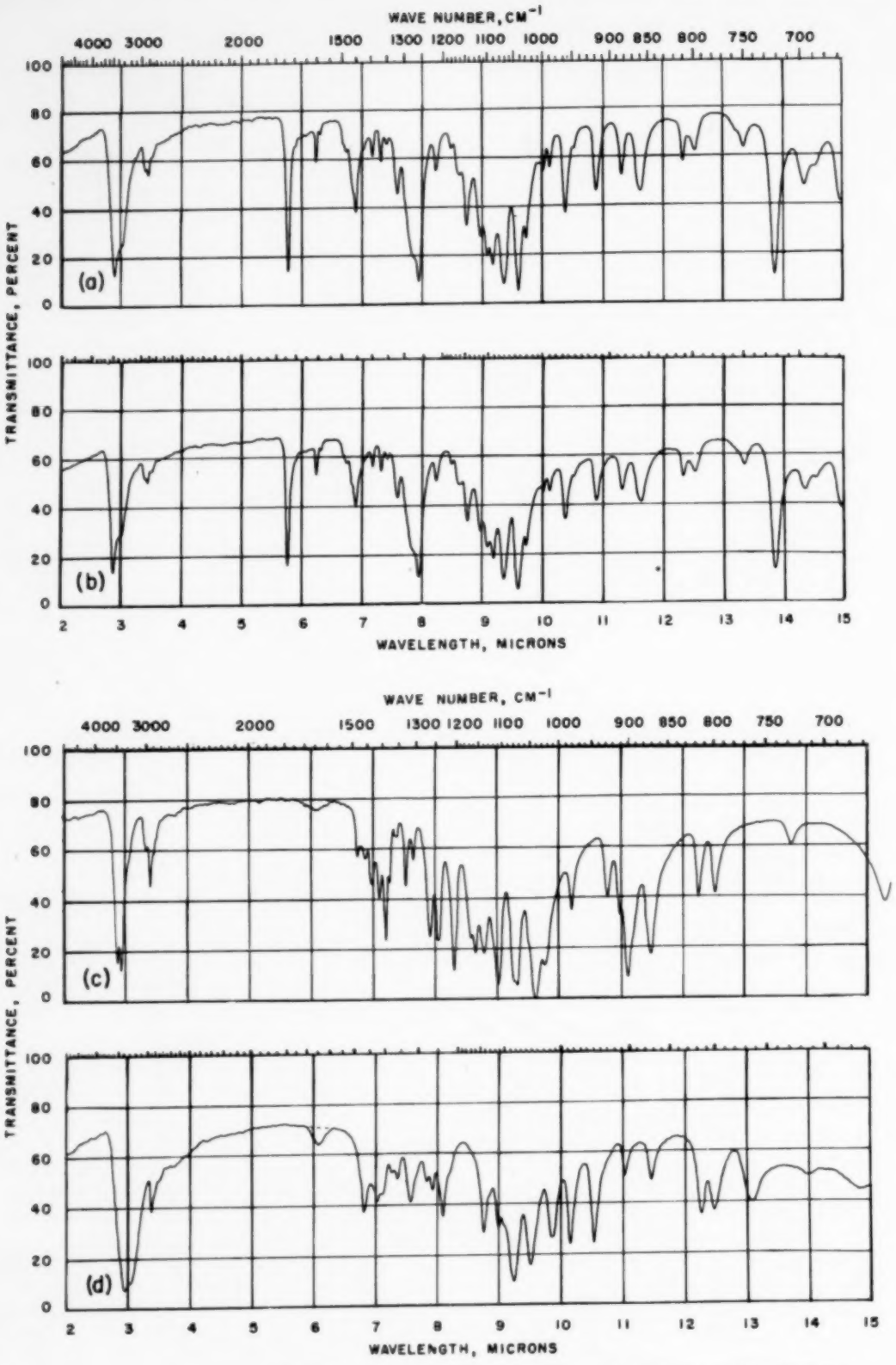

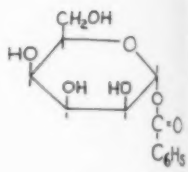

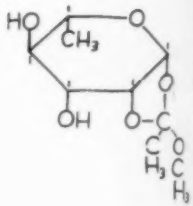

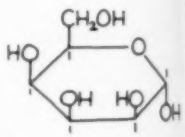

FIGURE 1. *Spectrograms of materials in potassium chloride pellets*

a, D-Talose monobenzoate (original sample); b, D-talose monobenzoate (recrystallized); c, β-L-rhamnose 1,2-(methyl orthoacetate); d, α-D-talopyranose.

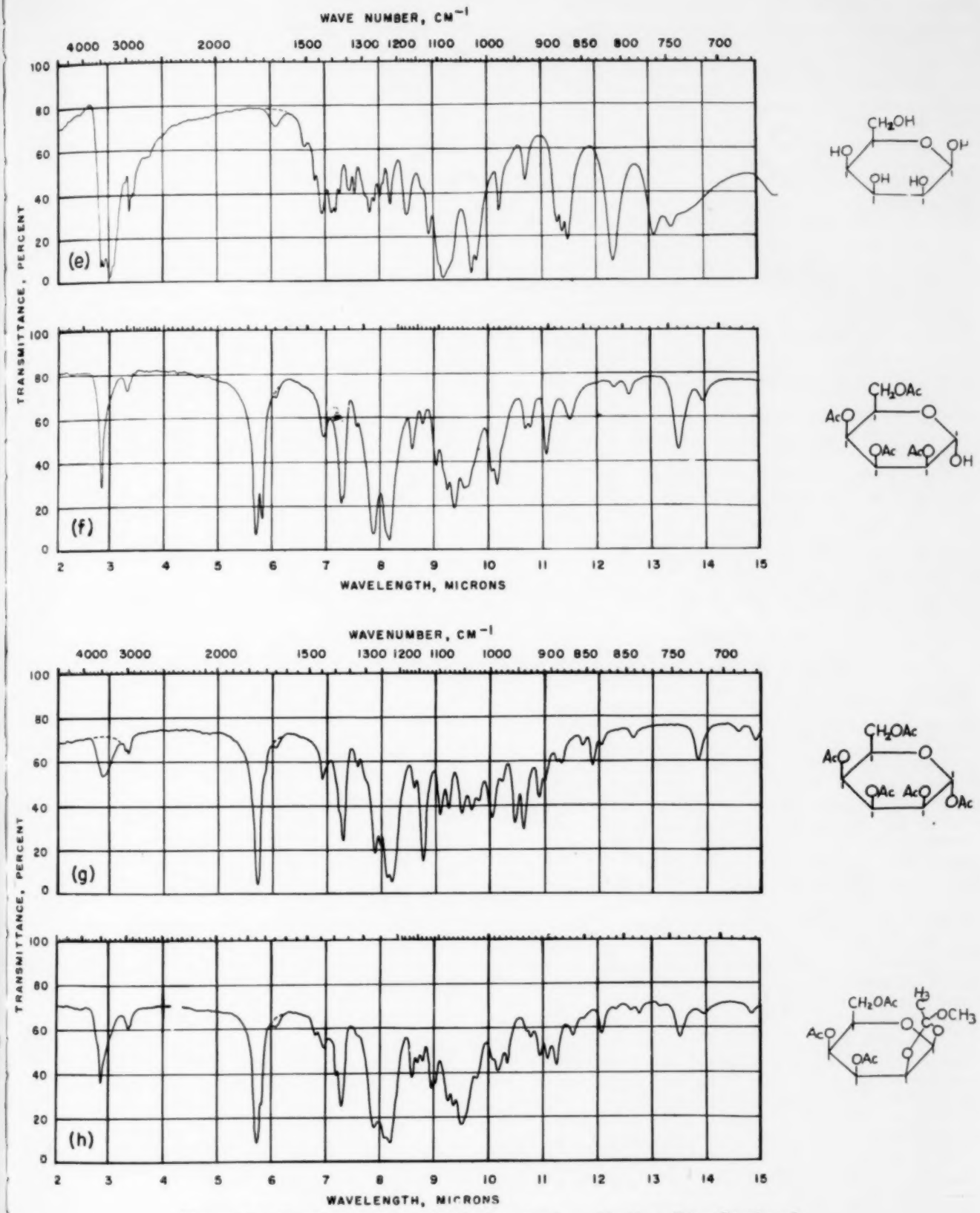

FIGURE 1. *Spectrograms of materials in potassium chloride pellets*—Continued

e, β-D-talopyranose; f, tetraacetyl-α-D-talopyranose; g, pentaacetyl-α-D-talopyranose; h, triacetyl-β-D-talose 1,2-(methyl orthoacetate) (old sample).

are much narrower for specific hexose types. The existence of characteristic infrared absorption for the common hexose types is in agreement with the observations of Barker et al. [7]. It now appears, however, that the infrared absorption of the D-talopyranoses and a number of related derivatives is anomalous in that bands occur in both of the regions mentioned (see table 1 and fig. 1).

In light of this fact, one cannot assign an alpha or beta configuration to D-talose 1-benzoate on the basis of absorption in the so-called "alpha and beta regions." It follows also that absorption in these regions cannot be used indiscriminately for the assignment of alpha or beta configuration to all types of pyranose derivatives. Whatever the difference between the absorption found for talose and that found for other hexoses, it is apparent that infrared measurements must be extended to all possible pyranose types before generalizations as to characteristic absorption can be held valid.

TABLE 1. *Absorption bands of* D-*talose derivatives in the 11.2- to 12.7-μ region*

Compound	Wavelength of bands	Curve in fig. 1
	μ	
D-Talose monobenzoate	11.31, 11.63, 12.32, 12.52	b
α-D-Talopyranose	11.44, 12.25, 12.45	d
β-D-Talopyranose	11.28, 11.38, 11.48, 12.31	e
Tetraacetyl-α-D-talopyranose	11.49, 12.32, 12.59	f
Pentaacetyl-α-D-talopyranose	11.40, 11.68, 11.87, 12.02, 12.61	g
Triacetyl-β-D-talose 1,2-(methyl orthoacetate).	11.23, 11.54, 12.06, 12.31, 12.58	h

Although infrared studies do not distinguish satisfactorily between the alpha and beta anomers of talose derivatives, the mode of synthesis of D-talose 1-benzoate provides a basis for assigning the configuration at carbon 1. The compound was prepared by the oxidation of D-galactal (III) with perbenzoic acid. Reaction of ethylenic compounds with perbenzoic acid gives anhydrides by the process clearly described by Waters [8]. Thus D-galactal, on oxidation with perbenzoic acid, forms, as intermediates, 1,2-anhydro-D-talopyranose, IV, and 1,2-anhydro-D-galactopyranose, V. The products isolated are obtained by cleavage of these 1,2-anhydrides. In accordance with the concept presented by one of us in 1940, cleavage of the anhydrides takes place by a mechanism in which the entering group approaches the face of one of the carbons from the side opposite the ring oxygen and combines with inversion [9]. Reaction of carbon 2 of IV with benzoate ion by an opposite-face mechanism would give β-D-galactopyranose 2-benzoate, and reaction of carbon 2 of V would give α-D-talopyranose 2-benzoate. These compounds have not been found. However, reaction of carbon 1 of IV would give α-D-talopyranose 1-benzoate I, and reaction of carbon 1 of V would give β-D-galactopyranose 1-benzoate.[4] Hence the talose 1-benzoate found experimentally should have the alpha pyranose structure. This structure does not account for the mutarotation of the substance observed in methanol and in pyridine. Explanation of these unusual properties must await further experimental study.

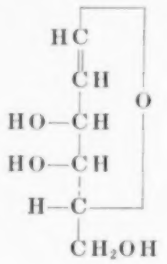

III

D-Galactal.

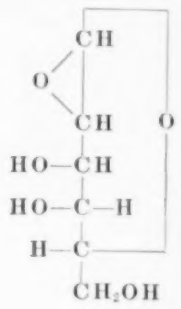

IV

1,2-Anhydro-D-talopyranose.

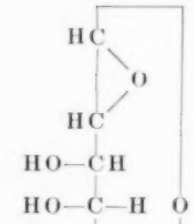

V

1,2-Anhydro-D-galactopyranose.

2. Experimental Details

2.1. D-Talose Monobenzoate

The product prepared by Pigman and Isbell in 1937 melted at 160° to 175° C in 1955, and showed the infrared absorption given in curve *a* of figure 1. Two recrystallizations from dimethoxyethane changed the melting point to 180° to 182° C without an appreciable change in absorption (curve *b*). Hence recrystallization from dimethoxyethane occurred without change in structure. When dissolved in anhydrous methanol, the recrystallized product gave the mutarotation reported in table 2. The rate of

TABLE 2. *Rotation of* D-*talose monobenzoate in methanol at 20°C*

(0.0512 g made up to 10 ml with anhydrous methanol, and read in a 2-dm tube.)

Time	$[\alpha]_D^{20}$	Time	$[\alpha]_D^{20}$
min		*min*	
5.3	+14.0	120	−33.7
7.1	+13.1	150	−30.2
9.8	+10.2	225	−23.5
15.0	+6.4	1,100	+3.5
27.5	−3.0	1,350	+6.6
50	−15.8	1,590	+7.5
60	−19.8	2,655	+8.6
90	−26.8	7,200	+9.8

[4] By perbenzoic acid oxidation of triacetyl-D-galactal, Levene and Tipson [10] obtained tri-*O*-acetyl-β-D-galactopyranose 1-benzoate, the product to be expected by the mechanism indicated here.

mutarotation is somewhat lower than that observed in 1937, but the over-all change is essentially the same.

2.2. β-L-Rhamnose 1,2-(Methyl Orthoacetate)

This compound was prepared by the method of Fischer, Bergmann, and Rabe [11]. The product, after two recrystallizations from hot ethyl acetate, melted at 143° to 144° C, in agreement with the reported value.

2.3. α-D-Talopyranose

The material used for the spectrogram was obtained by crystallization of the sugar from water with the addition of methanol. The product had a melting point of 131° to 134° C, and gave a complex mutarotation like that reported previously [12]. The specific rotation, $[\alpha]_D^{20}$, extrapolated to zero time, was +67°, in substantial agreement with the recorded value of +68°.

2.4. β-D-Talopyranose

The optical rotation of the β-D-talopyranose prepared in 1937 showed that the material had changed in large measure to the more stable alpha modification. Hence a new sample was prepared. α-D-Talose (15 g) was dissolved in about 50 ml of water. After 18 hr, the solution was diluted with 150 ml of absolute ethanol and cooled by immersing in a bath at about −10° C. The solution was seeded with 0.5 g of finely powdered α-D-talose, and shaken for 45 min. The crystals that formed were then separated by filtration. On standing at a low temperature, the filtrate yielded a small crop of β-D-talose. The process was repeated, to obtain a total of about 1 g of β-D-talose. The combined crops were then dissolved in 3 ml of ice-cold water, and 5 ml of cold, absolute ethanol was added; crystallization began immediately. After 1 hr, the crop was removed by filtration, washed first with ethanol and then with 2-propanol, and finally thoroughly dried.

The specific rotation, $[\alpha]_D^{20}$, of this material, extrapolated to zero time, was +13.3°, and the melting point was 121° to 123° C. The values agree with those previously recorded [1] ($[\alpha]_D^{20}$ +13.2° and mp 120° to 121° C).

2.5. Pentaacetyl-α-D-talopyranose

A sample of the compound previously reported [1] was recrystallized from hot ethanol. The specific rotation, $[\alpha]_D^{20}$, of the recrystallized substance was +70° and the melting point 106° to 107° C, in agreement with the published values.

2.6. Tetraacetyl-α-D-talopyranose

A sample of tetraacetyl-α-D-talose, prepared in 1937, was recrystallized from hot water. The melting point was 114° to 116° C and the initial specific rotation, $[\alpha]_D^{20}$, was +41.5° in U. S. P. chloroform. The constants differ slightly from those reported [1] ($[\alpha]_D^{20}$, +42.8° and mp 112° to 113° C), but the amount of material available was not sufficient for further study.

2.7. Triacetyl-β-D-talose 1,2-(Methyl Orthoacetate)

The few milligrams of this material remaining from the original preparation of Pigman and Isbell was found to have a melting point of 77° to 83° C (reported, 91.5° to 92.5° C). Because of lack of material, the infrared absorption spectrum was determined without prior recrystallization.

2.8. Measurement of Infrared Absorption

The spectrograms recorded in figure 1 were made with a Perkin-Elmer model 21 spectrophotometer, using the alkali halide pellet technique. The pellets were prepared from a mixture of 100 mg of potassium chloride and 0.4 mg of the sample. The material was pressed in a 3-piece die, 9.5 mm in diameter, patterned after one described by Anderson and Woodall [13]. Pressure was applied with a shop vise. The spectra were run without compensation for reflection or scatter by the pellet.

3. References

[1] W. W. Pigman and H. S. Isbell, J. Research NBS **19,** 189 (1937) RP1021.
[2] H. G. Fletcher, Jr., and R. K. Ness, J. Am. Chem. Soc. **77,** 5337 (1955).
[3] E. Braun, Ber. deut. chem. Ges. **63,** 1972 (1930).
[4] E. Pacsu, Advances in Carbohydrate Chem. **1,** 107 (1945).
[5] L. J. Bellamy, The infrared spectra of complex molecules, p. 163 (Methuen & Co., Ltd., London, or J. Wiley & Sons, Inc., New York, N. Y., 1954)
[6] R. N. Jones, P. Humphries, F. Herling, and K. Dobriner, J. Am. Chem. Soc. **73,** 3215 (1951).
[7] S. A. Barker, E. J. Bourne, R. Stephens, and D. H. Whiffen, J. Chem. Soc. **1954,** 3468.
[8] W. A. Waters, Gilman's organic chemistry, vol. 4, p. 1165 (J. Wiley & Sons, Inc., New York, N. Y., 1953).
[9] H. S. Isbell, Ann. Rev. Biochem. **9,** 65 (1940).
[10] P. A. Levene and R. S. Tipson, J. Biol. Chem. **93,** 631 (1931).
[11] E. Fischer, M. Bergmann, and A. Rabe, Ber. deut. chem. Ges. **53,** 2362 (1920).
[12] H. S. Isbell and W. W. Pigman, J. Research NBS **18,** 141 (1937) RP969.
[13] D. H. Anderson and N. B. Woodall, Anal. Chem. **25,** 1906 (1953).

WASHINGTON, April 9, 1956.

Journal of Research of the National Bureau of Standards Vol. 57, No. 4, October 1956 Research Paper 2709

Small Oil-Free Bearings

Hobart S. White

An investigation was made of materials that may be suitable for use as oil-free bearings in aircraft clocks and similar instruments between −55° and +70° C, to replace lubricated jewels that do not give satisfactory operation at subzero temperatures because of congealing of the oil. Another advantage of an oil-free instrument is the freedom from cleaning and oiling periodically during shelf storage. Materials included in the investigation were plastics, plastics with fillers, impregnated metals, and impregnated carbon. Friction tests were made with an inclined-plane type of static-friction apparatus, and with shafts rotating in loaded journal bearings, at temperatures from −55° to +70° C. With bearings of typical materials stored on steel shafts, the effect of shelf storage on static friction was investigated. Wear tests were made with loaded bearings on ¼-inch-diameter rotating shafts made of different types of steel. With oscillating ⅛-inch-diameter shafts and 1,000-gram loads, wear data were obtained on bearings of the more promising materials. Using an endstone wear testing machine, wear data were obtained for end-thrust bearings made of typical bearing materials. The performance of oil-free bearings in 18 timepieces was investigated.

1. Introduction

It is essential that aircraft instruments and devices operate satisfactorily over a wide temperature range. At subzero temperatures, increased viscosity and congealing of lubricating oils result in high friction with lubricated bearings. In aircraft clocks, similar jeweled instruments, and some mechanical fuzing devices, the power supplied for normal operation is not sufficient to overcome the excessively high friction at low temperatures. Some devices may be made to operate at low temperatures by having a surplus of power supplied, but this is not feasible in timepiece mechanisms. The nonspreading watch and clock oils conventionally used for lubricating jewel (sapphire) bearings are not satisfactory at −50° C, and at ordinary temperatures the necessity of periodic cleaning and oiling during shelf storage and during service is not desirable.

Because of the unsatisfactory performance of lubricated aircraft clocks at low temperatures, a project [1] was initiated to investigate materials that may be suitable for use as oil-free bearings in timepieces, between −55° and +70° C. to replace jewels that require lubrication. In addition to the primary objective of satisfactory operation at low temperature, another important advantage of an oil-free timepiece is freedom from cleaning and oiling periodically during shelf storage.

Bearing materials included in the investigation were plastics, plastics with fillers, impregnated metals, and impregnated carbon. Corrosion-resistant shaft materials were investigated. The work consisted of investigations of the friction and the wear characteristics of the materials, and trial of the more promising materials in timepieces.

[1] This project was initiated in October 1951, and was sponsored by the Bureau of Aeronautics, Department of the Navy.

2. Bearing Materials

The bearing materials tested are identified by sample number and composition in table 1. The percentages given are approximate; they are computed either from the densities of the samples and the densities of the ingredients, or from the composition of the suspension or dispersion as given by the manufacturer in conjunction with the known amount of fillers added. In some cases the samples from commercial firms are specially prepared materials; in other cases they are products that the manufacturers considered promising for the application.

For convenience, the abbreviations PTFE and PTFCE are used in this paper to symbolize polytetrafluoroethylene and polytrifluorochloroethylene, respectively.

2.1. Plastics

The low-friction characteristics of PTFE (polytetrafluoroethylene) were largely responsible for the inception of this project. This resin [1][2] is waxy in appearance, and white or gray in color, except that thin sheets are transparent. It is a crystalline solid with good stability from −320° to +500° F, and is chemically inert to known reagents and solvents except molten alkaline metals and gaseous fluorine under pressure. Its relative softness and poor heat conductivity limit its suitability as a bearing material to applications involving low speeds and low unit pressures.

The PTFCE (polytrifluorochloroethylene) used in this investigation is a relatively hard thermoplastic, with good stability from −320° to +375° F. It is chemically inert to most organic solvents and reagents. It may vary from the amorphous to the crystalline state, depending largely on the rate of cooling in its preparation [2]. The amorphous material is transparent; and crystalline material is

Figures in brackets indicate the literature references at the end of this paper.

TABLE 1.—*Bearing material*

Sample	Material
101	Polytetrafluoroethylene (symbolized by PTFE).
102	Polytrifluorochloroethylene (symbolized by PTFCE).
103	Nylon, molded.
103a	Nylon, sintered and machined.
103b	Nylon, resintered after machining.
104	Polyethylene, high density, experimental.
201	No. 101+fiber glass+pigment.
202	No. 101+73% (40% vol) molybdenum powder.
202a	No. 101+85% (58% vol) molybdenum powder (0.5 to 5 μ).
202b	No. 101+83% (54% vol) molybdenum powder (0.5 to 5 μ).
202c	No. 101+65% (31% vol) molybdenum powder (0.5 to 5 μ).
203	No. 101+70% (33% vol) silver precipitated flowers.
204	No. 101+graphite.
204a	No. 101+graphite.
205	No. 101+copper powder.
206	No. 101+molybdenum disulfide.
206a	No. 101+61% (42% vol) molybdenum disulfide.
207	No. 102+graphite.
208	No. 101+90% (50% vol) tungsten powder (0.5 to 5 μ).
208a	No. 101+78% (29% vol) tungsten powder (0.5 to 5 μ).
209	No. 101+glass+molybdenum disulfide.
210	No. 101+glass.
211	No. 101+18% TiO_2+4% polymethylsiloxane.
212	No. 101+18% TiO_2+11% chlorinated biphenyl.
213	No. 102+molybdenum disulfide.
214	No. 102+14% (27% vol) No. 101+64%(28%vol) Mo (0.5 to 5 μ).
215	No. 102+56% No. 101, fused at 500° F.
215a	No. 102+56% No. 101, fused at 650° F.
216	First sample of No. 222, fused and molded again at NBS.
217	No. 101+28% (18% vol) titanium dioxide.
218	No. 102+51% No. 101+10% glass, fused 500°F, 13,000 psi.
218a	No. 102+51% No. 101+10% glass, fused 500° F, 3,000 psi.
219	No. 102+51% No. 101+13% chromium tetrahydrate.
220	No. 101+70% (34% vol) Mo+6% chromium tetrahydrate.
220a	No. 101+53% (20% vol) Mo+10% chromium tetrahydrate.
221	No. 101+glass+red pigment.
222	No. 101+glass+other fillers.
223	No. 101+glass+orange filler.
224	No. 101+glass+dark-gray filler.
225	No. 101+glass+light-gray filler.
226	No. 101+gray filler.
227	No. 101+80% (52% vol) tin, fused 650° F, 5,000 psi.
227a	No. 101+80% (52% vol) tin, fused 700° F, 10,000 psi.
228	No. 101+13% glass, 0.05 μ avg diam of fibers.
229	No. 101+13% glass, 2 μ avg diam of fibers.
230	No. 101+25% dental silicate.
231	No. 101+67% (33% vol) copper powder.
232	No. 101+36% silicon powder (2 to 10 μ).
233	No. 102+57% No. 101, fused at 500° F.
234	No. 102+67% No. 101, fused at 500° F.
234a	No. 102+40% No. 101, fused at 500° F.
235	No. 101+25% dental silicate.
236	No. 102+40% No. 101, fused at 500° F.
237	No. 102+20% No. 101, fused at 500° F.
237a	No. 102+30% No. 101, fused at 500° F.
237b	No. 102+40% No. 101, fused at 500° F.
237c	No. 102+10% No. 101, fused at 500° F.
238	No. 101+63% (29% vol) molybdenum powder (0.5 to 5 μ).
238a	No. 101+50% (20% vol) molybdenum powder (0.5 to 5 μ).
238b	No. 101+75% (42% vol) molybdenum powder (0.5 to 5 μ).
301	Sintered porous bronze+polytetrafluoroethylene.
302	Sintered porous bronze+graphite.
303	Sintered porous bronze+molybdenum disulfide.
304	Sintered porous bronze+molybdenum disulfide.
401	Carbon+graphite+silver.
402	Electrographitic carbon+silver.
403	Carbon+graphite+babbitt.
404	Electrographitic carbon+babbitt.
501	Silver amalgam.
601	Pyrex glass, lapped and polished.
602	Stainless steel (420), hardened, honed and polished.
603	Hard-coated 61S aluminum alloy.
604	Sapphire, lapped and polished.
605	Bearing bronze; copper, 83%; lead, 8%; tin, 8%.
606	Tungsten+molybdenum disulfide+plastic coating on brass.
607	Brass, ordinary.
608	Boron carbide, special superfine quality.
609	No. 102+20% small flake graphite, coating, fused on brass.
610	Diamond, polished.
611	No. 101+green pigment, 1-coat enamel, fused on brass.
612	Polytetrafluoroethylene, clear finish, fused on brass.

translucent, and is harder than the amorphous and more resistant to cold flow and heat distortion. Neither form has the low-friction characteristics of PTFE at ordinary temperatures.

The nylon material used in these tests was of the hardest type, and has been used to some extent for bearings and gears in certain applications. This material normally contains water; the amount of water varies with the ambient temperature, humidity, and time of exposure, but frequently is between 1 and 4 percent. The friction is not exceptionally low.

The high-density polyethylene tested was a relatively new type of polyethylene plastic produced by a commercial firm for experimental purposes. It is characterized by higher molding temperatures and greater strengths than those of ordinary polyethylene.

2.2. Plastics With Fillers

Because of the relative softness of PTFE, it is logical to expect that its load-carrying ability and its wear resistance might be improved by the addition of suitable fillers. Accordingly, several fillers were tried in combination with this plastic, including graphite, molybdenum disulfide, fiber glass, dental silicate, silicon, titanium dioxide, silver, copper, tungsten, and molybdenum.

Samples 202, 202a, 202b, 202c, 203, 204, 106a, 208, 208a, 214, 217, 227, 227a, 230, 231, and 232 were prepared (at the Bureau) by adding the filler in powder form to PTFE clear finish-type suspension (in water) and stirring to make a uniform paste. In general, after drying to the consistency of a very stiff paste, these samples were molded into cylinders, which were then more completely dried on a hotplate or by heating in the mold. To fuse the PTFE, the samples were dried and then heated to about 700° F at a pressure of about 10,000 psi in a heavy-walled steel tube with a loose-fitting steel rod at each end. Samples 211, 212, 228, 229, and 235 were prepared in a similar manner, except that they were thoroughly mixed in a blender after the addition of acetone in quantities sufficient to provide suitable fluidity for the blending action. After blending the samples, much of the acetone was removed by decanting, some was removed by pressing with absorbent paper and by compressing in the hands in the manner used for forming snowballs, and then the mixtures were dried by heating as above. Samples 238, 238a, and 238b were prepared as above, except that PTFE aqueous dispersion, designated by the manufacturer as TD–3, was used instead of the PTFE clear finish-type suspension; and samples 220 and 220a were prepared in a similar manner with PTFE one-coat enamel-type suspension instead of the clear finish-type suspension.

PTFCE was tried also as a resin binder with different fillers, such as graphite, molybdenum disulfide, and PTFE. Sample 215 was prepared by mixing PTFE clear finish-type suspension with PTFCE dispersion (in xylol) and then blending after dilution with acetone. After the drying operation, this sample was heated in the heavy-walled tube to about 500° F at a pressure of about 5,000 psi to fuse

the PTFCE. A trial at higher temperatures, to fuse the PTFE also, resulted in an inferior product because of decomposition of the PTFCE (sample 215a at 650° F). Samples 234 and 234a were prepared by adding PTFCE powder to PTFE clear finish and blending after the addition of acetone. In preparing sample 236, PTFCE powder was added to TD–3 dispersion (PTFE) and the mixture was diluted with acetone. In preparing samples 237, 237a, 237b, and 237c, the PTFCE powder was dispersed in acetone, and the dispersion was blended with TD–3 dispersion. Samples 214, 218, 218a, and 219 were prepared by methods similar to the above, except that they contained other fillers in addition to the PTFCE. Samples 214 and 233 were prepared by mixing in paste form, without the addition of acetone.

Samples 201, 204a, 205, 206, 207, 209, 210, 213, and 216 were commercial preparations of PTFE containing fillers. Examination of these with a 20-power stereomicroscope disclosed pockets of pure plastic much larger than some of the journals in timepieces. Sample 221 was similar to sample 201, except that it was mixed by the dispersion method instead of the micropulverizing method. This resulted in a more uniform mixture of the PTFE in sample 221 than in 201, but examination with a 20-power stereomicroscope revealed that the mixture was not as uniform as is desirable for bearings with a 0.005-in. bore. A few small pockets of glass without any binder were found in sample 221. The uniformity of mixture in samples 222 to 226 was similar to that of sample 221, and it is believed that these commercial samples also were prepared by the dispersion method.

2.3. Impregnated Bronze

Porous bronze (not oil-impregnated) was impregnated with PTFE suspensoid by subjecting a dry degreased specimen of porous bronze to a vacuum of about 15 mm of mercury for about 10 min. Then PTFE suspension was introduced to cover the specimen before the vacuum was released. The excess suspensoid was wiped from the surface, and the specimen was dried by heating to 400° F. The cycle was repeated several times before finally fusing the plastic at about 700° F. However, stereomicroscopic examination of the broken edge of a 0.19-in. plate showed that the pores near the center were not filled with plastic, the impregnation being complete only near the surface.

Sample 302 of porous bronze, impregnated with graphite, and samples 303 and 304, impregnated with molybdenum disulfide, were obtained commercially. Samples 302 and 303 were prepared by the hot-press method.

2.4. Impregnated Carbon

Samples 401 and 403 were molded carbon-graphite mixtures that had been impregnated with molten silver and with molten babbitt, respectively, by a vacuum-pressure process. Likewise, samples 402 and 404 were electrographitic carbon impregnated with silver and with babbitt, respectively.

2.5. Miscellaneous

The silver amalgam (sample 501) was made from precipitated flowers of silver mixed with mercury with a mortar and pestle. The amalgam was compressed in a steel cylinder at about 10,000 psi to drive out excess mercury. This material was very brittle, and the edges of the hole chipped during the boring and reaming operation. An amalgam of dental-alloy filings (about 70 percent of silver in the alloy) was made similar to the above. This material was less brittle than the silver amalgam, but was not a satisfactory oil-free bearing material; hence the investigation of this type of material was soon discontinued.

Samples 601 (glass), 602 (420 stainless steel), and 604 (sapphire) were used mostly with lubricants for reference purposes. Sample 603 was an electrically anodized coating (essentially a sapphire coating) on an aluminum alloy. Sample 605 was a bearing bronze (in composition similar to SAE Nos. 64 and 660 copper-base casting alloy), and sample 607 was ordinary yellow brass. Sample 606 was a commercial coating material consisting of tungsten, molybdenum disulfide, and a plastic; the coating was applied to the bore of a brass bearing and baked 3 hrs at 400° F, in accordance with the instructions supplied with it. Boron carbide (sample 608) has a hardness between those of sapphire and of diamond (sample 610). Samples 609, 611, and 612 were coatings of PTFCE plus graphite, PTFE one-coat enamel, and PTFE clear finish, respectively, fused on brass.

3. Shaft Materials

The shaft materials tested during this investigation are listed in table 2. The sample number in each case is the same as that used as type designations by the American Iron and Steel Institute (AISI), except for the cases of the cobalt alloy (C40) and the machinery steel (M), which are not listed by the manufacturer as meeting any AISI type.

The 303 steel was a free-machining chromium-nickel austenitic steel not capable of heat treatment, and commonly known as 18–8 steel. This was used chiefly for the wear-test shafts.

The 420 steel was a type used for cutlery, and may be heat-treated to a hardness of about 50 Rockwell C.

TABLE 2. *Shaft materials*

Sample	AISI type	Approximate composition				Hardness, RC
		Carbon	Manganese	Chromium	Nickel	
		%	%	%	%	
303	303	0.15 max	2.0 max	17 to 19	8 to 10	-----
420	420	[a].41	1.0 max	[a]13.7	[a]0.11	50
440C	440C	.95 to 1.2	1.0 max	16 to 18	-------	55
D2	D2	1.50	0.30	12.0	-------	55
D3	D3	2.10	.25	12.5	.50	60
O2	O2	0.90	1.60	-------	-------	60
C40 [b]	-----	.15	2.0	20	15	58
M [c]	-----	.3	(c)	(c)	(c)	24

[a] From analysis; other values from SAE Handbook or from manufacturers type analysis.
[b] 40% cobalt, 7% molybdenum.
[c] A machinery steel described by the manufacturer as a special chrome vanadium alloy with small amounts of nickel and molybdenum.

397105—56——2

The 440C steel is described in various literature as having the greatest quenched hardness and wear resistance upon heat treatment of any corrosion- or heat-resistant steel.

The D2 steel was an air-hardening high-chromium tool steel having some corrosion resistance and good wear resistance in the hardened state. The D3 steel was similar, except that it was the oil-hardening type.

The O2 steel was an oil-hardening, nondeforming type, similar to that used for shafts in lubricated timepieces.

The cobalt-base alloy (C40) was a highly corrosion-resistant material of the type used for mainsprings in watches.

The machinery steel (M) was furnished in the heat-treated condition and recommended as having good wear resistance.

4. Apparatus

The apparatus used in this investigation were selected or designed for making simple comparative tests of the friction and wear characteristics of oil-free bearing materials under conditions simulating those in service. Shafts ¼ in. in diameter were used for friction and wear measurements to give reasonable accuracy under various conditions of speed and load, and still be in the range of application of small oil-free bearings. Wear tests were made with ⅛-in.-diameter oscillating shafts as a compromise between ease of measuring the wear and the smallness of the oscillating shafts in timepieces. For shafts less than ⅛ in. in diameter, timepieces were used for making comparative tests of the more promising materials.

4.1. Static-Friction Machines

An inclined-plane type of apparatus was used for making the static-friction tests. The tangent of the angle with the horizon when a rider on the incline starts to slide is used as a measure of f, the coefficient of friction.

An apparatus of this type available at the start of this project has been described previously [3]. It consists essentially of a hotplate mounted between two journals, with provision for slow tilting. The plate specimen is clamped to the plane surface of the hotplate, which provides for tests at and above room temperature. A pointer indicates the angle of tilt on a calibrated scale.

The rider specimen is loaded by a rectangular yoke, through a point contact. An electric circuit is arranged so that with a slight movement the rider contacts a needle and lights a small signal lamp.

The plate specimens are 7 by 2 by ⅜ in., and the riders are 2 by 1 by ½ in. The riders are undercut to leave a bearing surface 0.125 by 1 in. at each end, and have a cone-shaped depression in the center of the upper surface for contacting the point of the loading yoke.

A similar apparatus, without a hotplate, was constructed on a scale small enough to be operated within an insulated control box at low temperatures. The insulated box was constructed of plywood with a 3-in. thickness of rock-wool insulation between the walls. The front of the box is removable to allow easy access, and windows are provided for readings during tests. An internal compartment contains a sirocco-type blower and space for dry ice or a heater, leaving an available working space 16 by 16 by 12 in.

4.2. Bearing-Friction Test Machines

A small friction-testing machine for use in the temperature-control box was constructed with two support ball bearings for mounting a test shaft with a journal for the test bearing at one end, and provision for driving at the other end. This outboard-test-bearing type of machine facilitates the changing of test bearings and minimizes the damage to the bores of the test bearings when sliding on and off the shaft. Measurements of the frictional torque are obtained from the displacement of a pendulum mounted on the test bearing housing. The load consists of the bearing housing plus the weight of the pendulum and bearing. The pendulum consists of a rod, a small bob, and a pointer that measures displacement from the center line on a suitable scale. The pendulum is calibrated in a horizontal position with the housing on a smooth horizontal surface, as indicated in figure 1. The force, R, necessary to maintain it in a horizontal position is measured by a balance. If the weight of the pendulum acts at its center of gravity so that $Wb=Ra$, then $W=Ra/b$. When the shaft is rotating, the friction torque is given by $Wc=Rac/b$, and $a/b=d/c$. The friction torque, $Wc,=Rd$. The frictional torque may be found from the displacement reading multiplied by R, which is a constant for each pendulum. Likewise,

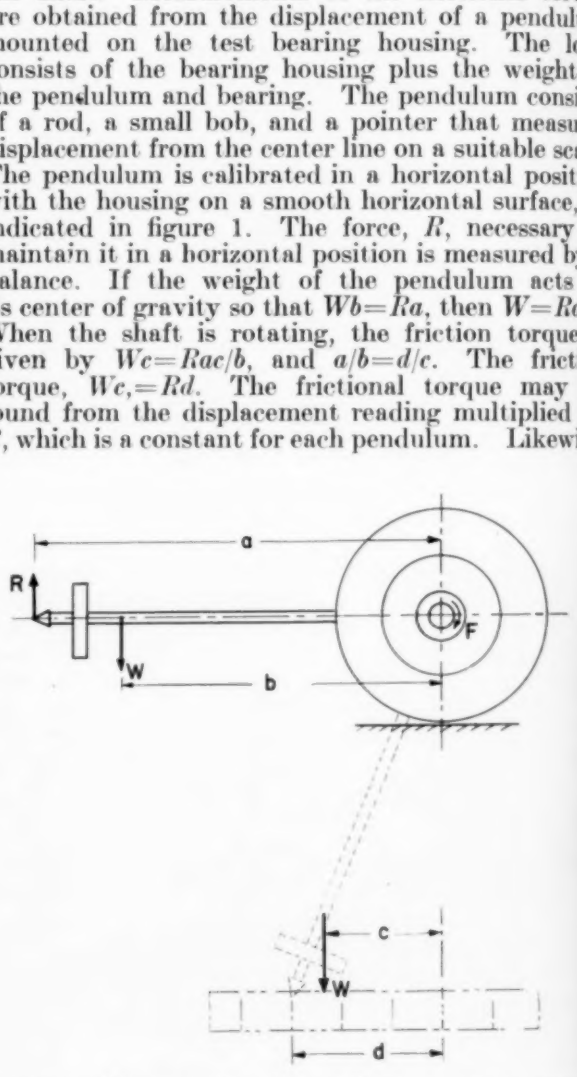

FIGURE 1. *Diagrammatic sketch of friction torque measuring apparatus.*

for a given load and shaft diameter, the coefficient of friction may be computed from the displacement multiplied by the appropriate constant.

4.3. Bearing-Wear Test Machines

Two multiple-shaft speed-reducing units were modified to provide apparatus for studying wear with sleeve bearings on rotating journals. Steel test journals, ¼ in. in diameter, were made and fitted to the ends of the six horizontal output shafts on each unit. Steel housings and weights suspended from flexible wire provide suitable loads on the bearings, and motorized drives are used to obtain the desired speeds. Four shafts of one of these machines are shown on the left half in figure 2. The bearing assembly has been removed from one of the shafts, and is shown disassembled on the table. The collar has been removed from the third shaft from the right to show the end of a test bearing in place.

The wear patterns along the entire lengths of the bearings indicated that the flexible wires attached to the steel housings were suitable for applying the load, and that swivel yokes were not necessary for uniform loading.

For studying wear of sleeve bearings on oscillating journals, oscillating-shaft machines were made by modifying oscillating display motors. One of the oscillating-shaft wear machines is shown in figure 2, clamped to the right end of the support of the above multiple shaft unit. A 2-lb weight attached with a wire plus the other moving parts provide a 1,000-g load on the pair of bearings, which are housed in a yoke made from ⅛-in. by ½-in. brass. One of the bearings may be seen directly above the upper end of the wire supporting the weight. The ⅛-in.-diameter steel shaft passes through two brass collars, which are soldered to the yoke of the oscillating bar; a setscrew in one of the collars engages the shaft so that it oscillates with the oscillating arm. Attached to the outer end of the oscillating arm is a quadrant, which passes through a solenoid. A mercury-in-glass switch attached to the oscillating arm energizes the solenoid at the appropriate time to provide oscillating motion of the shaft-arm-quadrant assembly. Although the static load on the bearings is only 1,000 g, the load during the impulse from the solenoid is considerably greater. The oscillatory surface speed and the impulse loading of the shaft simulate the conditions common to balance-staff journals in timepieces.

An apparatus was designed and built for making thrust-bearing-wear tests with oscillating shafts. This apparatus, designated as an endstone-wear testing machine, is shown in figure 3. A motor-driven connecting rod oscillates a shaft back and forth with a motion of about 87°; and this motion is doubled when transmitted to 4 vertical shafts, each of which has a ⅛-in.-diameter hole and setscrew at each end for attaching test-pin specimens. An endstone specimen in a 1,000-g weight supplies a load on each top pin; a specimen at each lower pin supports the 1,000-g weight plus the weight of the floating shaft and gear, or a total thrust load of 1,240 g. One of the 1,000-g weights has been removed and inverted to show the upper test pin and endstone specimen in the photograph. In operation, each weight is positioned coaxially with its test pin by means of four snug but free-fitting locating pins, and is prevented from rotating by means of a thin flexure spring. No vertical oscillation of the floating shaft was observed, and no effect of vertical forces from the gears was indicated in the test data.

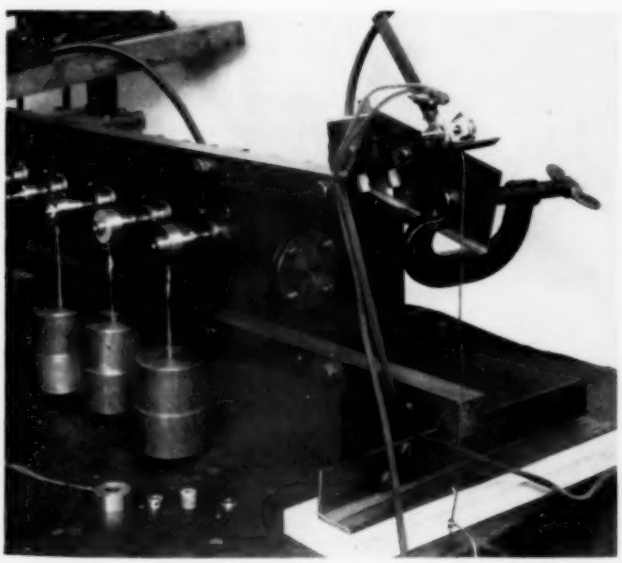

FIGURE 2. *Journal-bearing wear-testing apparatus.*

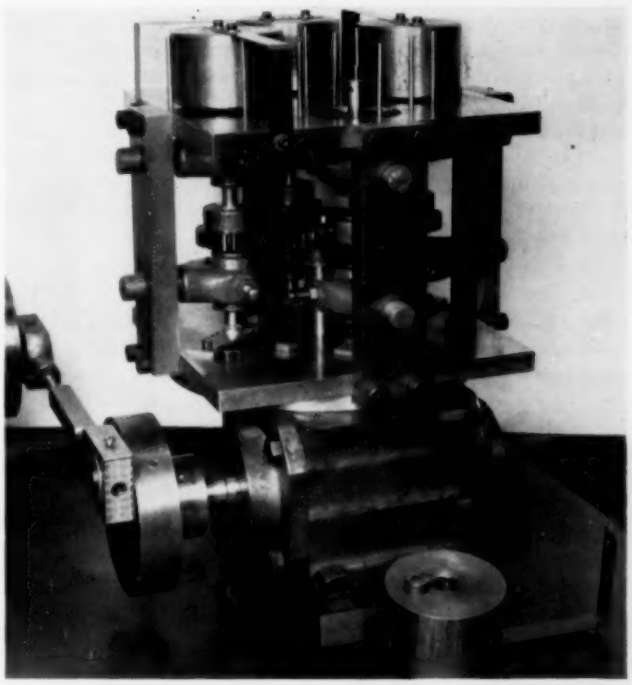

FIGURE 3. *Thrust-bearing (endstone) wear-testing machine.*

4.4. Timepieces

The timepieces used in a study of the suitability of the more promising bearing materials included aircraft clocks, ship clocks, navigation watches (type AN5740), ship chronometers, low-priced pocket watches (no jewels), and automobile electric clocks. Low-temperature tests of the timepieces were made in a commercial subzero chest in which thermostatically controlled temperatures down to −60° C were maintained.

5. Test Procedures

5.1. Static-Friction Tests

The coefficient of static friction between two solids depends largely on the physical and chemical properties of the surfaces [4]. Such factors as different surface finishes and the presence of surface films of oxides, oil, or dirt can seriously affect the reproducibility of friction data during a test program. As these factors vary in practice also, it was believed that in this project no purpose would be served by attempting to approach perfectly smooth and chemically clean surfaces. Instead, it seemed best to try to maintain a certain consistency in these variables, with a reasonable degree of cleanliness.

Accordingly, the surfaces for the static-friction tests were initially washed with soap and water, acetone, and ethyl alcohol; and thereafter, at frequent intervals between tests, wiped with industrial absorbent tissue soaked in ethyl alcohol. As far as possible, the original surface finishes of the specimens were left untouched throughout the tests, but there were a few exceptions, where refinishing was thought advisable.

For a particular set of conditions a friction measurement was taken by placing the rider on the plate and in contact with the needle, applying the load, retracting the needle about 0.004 in., and tilting the plate slowly until the signal lamp lit. This was repeated until a relatively constant value was obtained. Plate temperatures were measured by a thermocouple, and atmospheric temperatures inside the temperature-control box were determined with a liquid-in-glass thermometer.

5.2. Bearing-Friction Tests

Most of the important comparative friction data were obtained with the small outboard-test-bearing machine that was used in the temperature-control box. In general, the test bearings, 0.50 in. long, with bores slightly less than ¼ in., were pressed in a steel housing with a 0.500-in. bore, and then the bearing bore was reamed, burnished, or otherwise smoothly finished to the desired diameter. In these tests, benzene and tissue were used to clean the shafts and bearings, except that no solvent was used on the sintered nylon bearings. To minimize changes of the bearing surface during a test covering a range of temperature, the shaft was not rotated continuously but only for short periods before and while obtaining friction measurements. The air-circulating blower was stopped while the torque was being read, so that the pendulum would not be influenced by the air currents. Observations of the torque were taken at intervals as the temperature near the bearing was reduced from room temperature to −70° C, and as the temperature was increased from room temperature to +70° C, unless excessively high friction resulted before reaching these temperatures. A damping fluid was used around the lower end of the pendulum rod to minimize fluctuations.

In general, the test shafts were ground, honed, or lapped, and polished with 4/0 polishing paper to give a surface finish in the range of 1 to 3 μin.

5.3. Bearing-Storage Tests

For the storage test, three steel shafts, ¼ in. in diameter by 7½ in. long, were supported at the ends, above and parallel to a steel plate, 5 in. by 7½ in. Test bearings, ½-in outside diameter by ½ in. long, were mounted in steel housings weighing 100 g each, and were reamed so that each bearing had a diametral clearance of 0.010 in. Brass collars with setscrews were used to space six bearings on each shaft so that each bearing had ⅛ in. side play for axial movement. The shaft ends were clamped to the supports projecting upward from each end of the steel plate.

In making friction measurements for the beginning of the storage test, the above assembly was mounted on the static friction machine. The plate was tilted backward until all the bearings were touching the brass spacing collars, and then tilted forward until the pointer reading for the tangent of the angle was 0.05. Thereafter, the table was tilted to increase the reading 0.01 at the end of each minute, and a record was made for any bearing that moved axially during each increase in the angle of tilt. During the storage period the assembly was stored on a wooden shelf attached to a brick wall, with the plate tilted about 8 deg to insure that each bearing remained in contact with the appropriate brass spacing collar. The assembly was open to the room air but was protected overhead by another shelf and directly in front by a clear plastic shield, to safeguard against disturbance by falling plaster or wind-blown objects. After 10 months of storage the assembly was mounted on the static-friction machine again to determine the coefficient of starting friction after storage.

5.4. Bearing-Wear Tests

The modified multiple-shaft speed-reducing units were used to obtain the rates of wear with bearings on ¼-in.-diameter journals that were rotated at various speeds, except that for the 1,800-rpm tests the journal was fitted directly to the shaft of an electric motor. The surface finish of the journals at the start of each test was from 1 to 4 μin., except for some special tests with rougher finishes up to 16 μin. The bearings were cleaned, weighed, and pressed in steel housings from which suitable loads were suspended. If rapid wear was evidenced by particles of the bearing material accumulating under

the bearing within a few hours, the bearing was removed and weighed to determine the loss in weight. If no particles from wear were observed beneath the bearing, operation was continued several hundred hours before examination and weighing.

Wear data were obtained from typical oil-free materials on the ⅛-in. oscillating shafts of the modified oscillating display motors. The total angle of motion was about 1 radian (55° to 60°), with about 3 cps, corresponding approximately to simple harmonic motion with an amplitude of 0.5 radian. In each test, a pair of bearings, each 0.25-in. outside diameter by 0.125 in. long with 0.126-in. bore, was fitted to the brass yoke previously described (see fig. 2). The bearings were weighed before and after 60 days of operation. The surface finish of the journals at the start of each test was about 2 μin.

Wear data were obtained with samples of typical materials on the endstone-wear testing machine shown in figure 3. The test pins were ⅛ in. in diameter, with ⅛-in. radius at the ends. Tolerance on the radius was ±0.001 in., with a surface finish of about 2μ in. The total angle of motion was about 3 radians (172° to 175°), with 1 cps, corresponding approximately to simple harmonic motion with an amplitude of 1.5 radians. A dial indicator having a ball point with a radius of about 1/16 in. was mounted over a flat-surface plate and used to measure the depth of wear periodically. When the depth of wear was relatively small, the diameter of the worn spot was measured also with a microscope.

5.5. Timepiece-Bearing Tests

Most of the operation with timepieces was at room temperature (about 25° C). A laboratory oven with a thermostat was used for maintaining the high temperature (75° C), and the subzero chest was used for the low-temperature (mostly −60° C) tests of timepiece operation. The daily rates were determined by comparison with standard NBS time signals available in the laboratory.

At suitable intervals, the oil-free bearings and shafts in the timepieces were examined for evidences of wear and corrosion. Conventional stereomicroscopes and measuring microscopes (10 to 100x) were used for these examinations.

6. Results

6.1. Static-Friction Results

Some preliminary testing was done in order to study reproducibility and the effect of load variation. For the range of pressures from about 10 to 30 psi, the starting friction was practically independent of load, for the materials investigated. A constant load that gave a pressure of 17 psi on the loaded area was used for the subsequent static-friction experiments.

As the cooling of the temperature-control box normally was accomplished by the evaporation of dry ice, the atmosphere inside the box during the low-temperature tests was composed mostly of gaseous carbon dioxide. In order to determine whether or not this influenced the results, some tests were run with a different cooling system. Alcohol was cooled externally by dry ice, and pumped through heat-exchanger elements over which the air in the box was circulated. Although this particular system did not cool the box below −25° C, the results obtained in this range with atmospheric air coincided very well with those from other tests conducted in the carbon dioxide atmosphere.

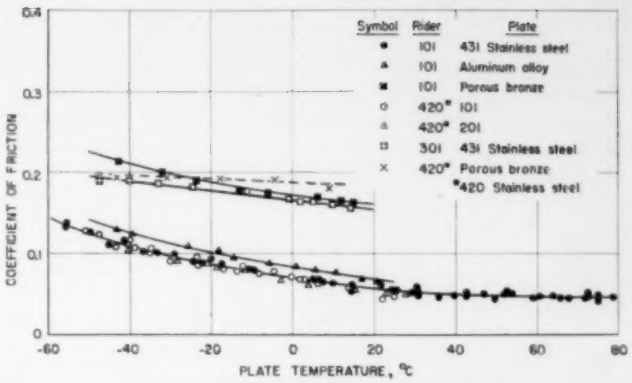

FIGURE 4. *Effect of temperature on the coefficient of static friction.*

The effect of temperature on the static or starting friction for several combinations of different materials is shown in figure 4. The combinations that include PTFE (sample 101) or PTFE with fillers (sample 201) demonstrate an increase in friction with a decrease in temperature. For PTFE sliding on a 431 stainless-steel plate, and for 420 stainless steel sliding on PTFE and on plate 201 (PTFE+ filler), the static friction versus temperature is represented by the lower curve in figure 4; the curve for PTFE sliding on aluminum is slightly higher. For PTFE sliding on dry porous bronze, and for porous bronze impregnated with PTFE (sample 301) sliding on stainless steel, the friction is much higher and is approximately the same as for stainless steel sliding on dry porous bronze. The porous bronze impregnated with PTFE did not have a film of PTFE over its surface, and evidently there was metal-to-metal contact between the bronze and the steel. With a coating of PTFE on the porous bronze, friction data (not shown in fig. 4) was similar to that for solid PTFE.

6.2. Bearing-Friction Results

a. Lubricated Bearings

For reference purposes, the coefficients of friction at speeds from 3 to 600 rpm were determined with a sapphire (not oriented) bearing (½ in. long) on a hardened 420 stainless-steel shaft, at 25° C, with a 643-g load. The diameter of the bore at the largest end was 0.2542 in. and at the smallest part of the bore near the center was 0.2524 in. The results of these tests are shown in figure 5. As would be

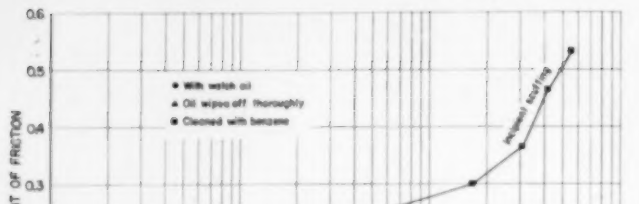

FIGURE 5. *Friction versus speed for a polished sapphire bearing.*

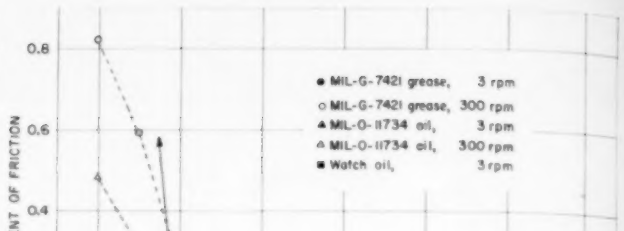

FIGURE 6. *Friction versus temperature for a stainless-steel bearing.*

expected, when fully lubricated with a modern synthetic watch oil, at speeds above 15 rpm (1.0 fpm) the friction was relatively low. When the speed was decreased to about 3 rpm (0.2 fpm), evidently operation was in the thin-film region of lubrication, as there was little difference in friction with abundant oil supply and with a trace of oil left after wiping the shaft and bearing thoroughly with industrial absorbent paper. At higher speeds the inadequate oil supply resulted in higher friction. Removing the traces of oil by washing with benzene resulted in higher friction and incipient scuffing at the higher speeds; the score marks on the journal and the bearing bore were detected with a 20-power stereomicroscope after removing a brown deposit.

In general, when the lubricated jewels in a timepiece were replaced with oil-free bearings, the mainspring, metal bearings, and winding mechanism were lubricated with a low-temperature lubricant. Because of this, and for general information, friction data were obtained with a hardened 420 stainless-steel bearing on a hardened 420 stainless-steel shaft when lubricated with three low-temperature oils. These data, for a 2,200-g load, at 3 speeds, and for a range from −70° to +60° C, are given in table 3. The surface speed at 3 rpm with the ¼-in.-diameter shaft more nearly simulates the surface speeds in timepieces; and, at this speed, the coefficient of friction decreases when the temperature is lowered sufficiently for the increasing viscosity to provide a thicker film of oil for lubrication. The relatively high friction at the higher temperatures indicates operation in the thin-film or boundary region of lubrication, in which oiliness is an important factor; and the lwoer friction with the special silicone fluid under these conditions indicates that it has greater oiliness than that of the other two synthetic oils. The MIL–O–11734 [5] and the MIL–L–17353 [6] lubricants are diester-type synthetic oils containing rust-inhibitor additives, designed for use in mechanical time fuzes and firearm mechanisms respectively. These two oils are not of the nonspreading type, such as watch oils, commonly used for jewel bearings; however, they do not have the extreme spreading tendency common to silicone fluids.

With the 420 stainless-steel bearing and shaft, with a 643-g load, friction data were obtained over a wide range of ambient temperature with MIL–O–11734 oil and MIL–G–7421 (extreme low temperature) [7] grease at 3 and 300 rpm, and with watch oil at 3 rpm. These data are given in figure 6. The relatively high friction with MIL–O–11734 oil at 3 rpm at temperatures above −30° C indicates that this operation is in the thin-film or boundary region.

TABLE 3. *Friction versus temperature for a honed-and-polished hardened 420 stainless-steel bearing, 0.2520-in. bore, cylindrical; with a hardened 420 stainless-steel shaft, 0.2504-in. diameter, with 2,200-g load; lubricated; at three speeds*

Ambient temperature	Coefficient of friction								
	MIL–O–11734 oil			MIL–L–17353 oil			Silicone fluid		
	3 rpm	15 rpm	300 rpm	3 rpm	15 rpm	300 rpm	3 rpm	15 rpm	300 rpm
°C									
60	0.19	0.16	0.01	0.22	0.20	0.03	0.13	0.11	<0.01
40	.18	.15	<.01	.22	.20	.01	.10	.09	<.01
25	.18	.15	<.01	.20	.20	<.01	.10	.09	<.01
0	.18	.15	<.01	.20	.18	<.01	.10	.09	<.01
−20	.15	.17	<.01	.18	.15	<.01	.10	.05	<.01
−40	.11	<.01	.01	.15	.08	<.01	.09	.01	.01
−50	<.01	.01	.06	.12	<.01	<.01	.05	<.01	.02
−60	<.01	.03	.27	<.01	<.01	.04	<.01	<.01	.04
−70	.....	.....	.....	<.01	.01	.09	.....	.....	.....

and the addition of an oiliness agent would be expected to lower the friction under these conditions.

In these and other friction tests, the surface finish of the shafts was kept in the range of 1 to 3 μin. as measured by a profilometer.

b. Oil-Free Bearings

The effects of temperature on kinetic friction for different clearances with various materials were investigated with the small outboard-test-bearing machine with hardened stainless-steel shafts ranging in diameter from 0.2496 in. to 0.2520 in. These tests were run in the temperature-control box, at 300 rpm, with a 643-g load. These data from PTFE are given in figure 7. With a diametral clearance of 0.0024 in., the friction was nearly constant from −65° to +70° C. With a clearance of 0.0016 in. (at room temperature), the friction increased rapidly at about −50° C and at about +50° C, because of binding as the clearance decreased to zero. For the clearances investigated, the friction at 300 rpm was practically independent of clearance, and not greatly affected by temperature, except when binding occurred as a result of dimensional changes caused by the changes in temperature. The coefficient of expansion of PTFE is about 10 times greater than that of steel. At elevated temperatures, the restraint of the steel housing in preventing outward expansion of the plastic causes the bore to become smaller instead of larger. Conversely, as the temperature is lowered, release of the press fit tends to counterbalance the contraction of the bore of the plastic until the temperature is low enough for the bearing to become loose in the steel bore. To prevent movement of the plastic and the filled-plastic types of bearing in the steel housing at low temperatures, a small floating pin was inserted radially through the bearing housing into a matching hole extending $\frac{1}{16}$ in. into the bearing wall.

Typical data showing the effect of speed on friction for several materials are given in figure 8. These data were obtained at 25° C with a 643-g load, using a stainless-steel shaft having a 0.2504-in. diameter.

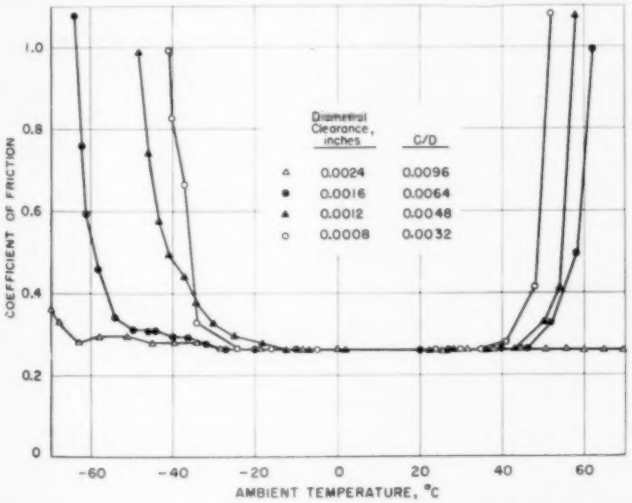

FIGURE 7. *Friction versus temperature for a PTFE bearing, at 300 rpm, with various clearances at room temperature.*

The test of the lapped-and-polished Pyrex-glass bearing lubricated with watch oil was made to obtain comparable data on a hard lubricated material similar to jewels (before the sapphire bearing was obtained). At 15 rpm, where the surface speed is about the maximum encountered in a timepiece bearing, the friction for PTFE is about 60 percent greater than with the lubricated glass, but at 2.5 rpm the friction of this plastic is the same as that of the lubricated glass.

The coefficients of friction at 25° C, using a 643-g load with ¼-in.-diameter stainless-steel shafts at 3, 15, and 300 rpm, for many oil-free materials and for typical lubricated bearings, are given in table 4.

After it became evident that loads greater than 643 g could be tolerated (without excessive wear) with the ¼-in.-bore oil-free bearings, friction data were obtained with a 2,200-g load, and these data are considered more important than the data obtained with the 643-g load. In these tests with the heavier load, friction data were obtained at speeds ranging from 2 to 600 rpm, and then the bearing was run in at 300 rpm to observe changes in friction. Friction data were obtained over the speed range after various amounts of run-in at 300 rpm, to investigate the effect of run-in at the relatively high load and speed. Typical data for these tests with samples 101 and 215 are given in figure 9, which also includes data (dotted curve) for a lubricated stainless steel bearing for comparative purposes. Because of excessive wear with sample 101 (PTFE) under these conditions, run-in with this material was limited to 1 hr and no data were obtained above

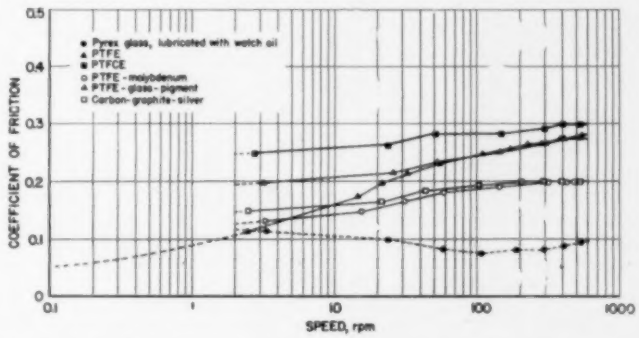

FIGURE 8. *Friction versus speed for various bearing materials, with 643-g load.*

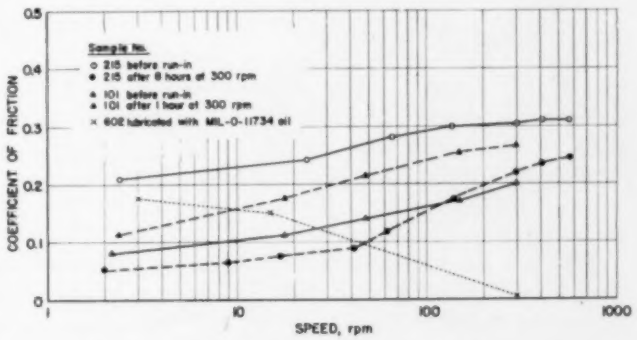
Sample No.
215 before run-in
215 after 8 hours at 300 rpm
101 before run-in
101 after 1 hour at 300 rpm
602 lubricated with MIL-O-11734 oil
COEFFICIENT OF FRICTION
SPEED, rpm

FIGURE 9. *Friction versus speed for typical bearing materials, with 2,200-g load.*

TABLE 4. *Coefficient of friction for various bearing materials, with hardened 420 stainless-steel shafts, ¼-in. diameter, at room temperature, with 643-g load*

Sample	Coefficient of friction		
	3 rpm (0.2 fpm)	15 rpm (1.0 fpm)	300 rpm (20 fpm)
101	0.12	0.18	0.26
102	.25 to .27	.26 to .28	.29 to .45
103	----------	----------	.28 to .35
103a	.22	.20	.28 to .32
103b	.28	.26	.32 to .33
201	.20	.21	.26 to .32
202	.13	.15	.20
202a	.20	.21	.23
202b	.20	.21	.23
202c	.20	.21	.23
203	.27	.26	.23
204	----------	----------	.28
204a	.13	.15	.21
205	.13	.16	.22
206	.13	.18	.28
206a	.26	.28	.31
207	.16 to .25	.18 to .26	.24 to .29
208	.18	.20	.22
208a	.26	.26	.28
209	.11	.13	.18
210	.11	.14	.17
211	.15	.19	.26
212	.16	.18	.23
213	.36	.36	.40
214	.16	.19	.23
215	.22	.22	.26
215a	.28	.26	.23
216	.13	.15	.19
217	.23	.23	.27
218	.26	.26	.26
218a	.26	.26	.27
219	.20	.22	.25
220	.30	.31	.33
220a	.23	.25	.30
221	.15	.16	.19
222	.12	.13	.17
223	.18	.19	.22
224	.13	.15	.20
225	.17	.18	.22
226	.13	.16	.25
227a	.15	.17	.20
228	.22	.23	.25
229	.22	.23	.25
401	.15	.16	.20 to .28
402	.28	.28	.27
403	.21	.22	.23
404	.27	.27	.26
501	.13	.13	.12
602 with MIL-G-7421 grease	.08	.06	.06
602 with MIL-O-11734 oil	.18	.16	.03
602 with watch oil	.12	.06	.04
603 with watch oil	.13	.06	.05
604 with watch oil	.12	.06	.05
604 oil wiped off	.13	.14	.21
604 clean	.18	.20	.36

300 rpm. Even so, rapid wear occurred and the friction increased about 50 percent during the run-in with this bearing. Before run-in, the friction with sample 215 was much higher than with sample 101; but after run-in, the friction with sample 215 was lower than with sample 101.

Friction data obtained with a hardened stainless-steel shaft at 3, 15, and 300 rpm, showing the effect of run-in and the effect of ambient temperature on friction, are given in table 5. With respect to timepieces the coefficient of friction at 3 rpm (0.2 fpm) is considered more significant than the data at higher speeds. Also, the friction after run-in is considered more significant than the initial friction.

For the four samples of PTFE+molybdenum metal powder (samples 202c, 238, 238a, and 238b), after several hours of operation at 300 rpm and then at 3 rpm, at 25° C, the coefficient of friction was in the range 0.18 to 0.26. After continued running at 3 rpm at −60° C the coefficient of friction at −60° C was 0.22 to 0.25. The concentration of molybdenum in these samples ranges from 50 to 75 percent (20 to 42 volume percent); for this range of concentration the coefficient of friction at 3 rpm was not greatly affected by temperature variations in this range from +25° C to −60° C. Likewise, the friction for sample 401 (carbon+graphite+silver) was not greatly affected by temperature.

For the high-density polyethylene (sample 104) and with unlubricated sapphire there was an increase in friction as the temperature was decreased below −20° C.

For the commercial bearing of sintered bronze+molybdenum disulfide (sample 304) the coefficient of friction increased from 0.17 to 0.44 during 12 min of operation at 3 rpm with the 2,200-g load. After turning the bearing 180° in its holder, in another test (not included in the table) with a 643-g load the coefficient of friction increased from 0.17 to 0.60 during 1 hr of operation at 3 rpm.

For the sample of bearing bronze (sample 605) the coefficient of friction increased from 0.13 to 0.44 during an hour of operation at 3 rpm with the 2,200-g load. After turning this bearing 180°, with a 643-g load, the coefficient of friction increased from 0.15 to 0.55 during 2 hr of operation at 3 rpm.

For the sample of commercial coating (sample 606), consisting of tungsten and molybdenum disulfide in a plastic, the coefficient of friction increased from 0.29 to 0.52 during an hour of operation at 3 rpm with a 2,200-g load.

It is of interest to note that under the conditions of these tests, the ordinary bearing bronze (83% copper, 8% tin, 8% lead) was somewhat superior to the bronze containing molybdenum disulfide and also to the commercial plastic coating material containing tungsten and molybdenum disulfide; but each of these samples was inferior to most of the other materials.

For sample 609 (graphite added to PTFCE) the friction was relatively high; above −20° C it was similar to the friction for PTFCE, and at lower temperatures the friction was greater than that of PTFCE.

For PTFCE bearings (at 3 rpm) the friction decreased with a decrease in temperature; but with PTFE or PTFCE containing PTFE as a filler the friction increased with a decrease in temperature in the temperature range from −20° to −60° C. This is illustrated in figure 10, with data for PTFCE, PTFE, and samples of PTFCE resin containing PTFE filler.

Data obtained in England [8], with the apparatus and method of test greatly different from that used at NBS, show no change in friction for PTFE in the range from −55° to −80° C. At temperatures down to −55° C the data are in general agreement with the data obtained at 3 rpm at NBS.

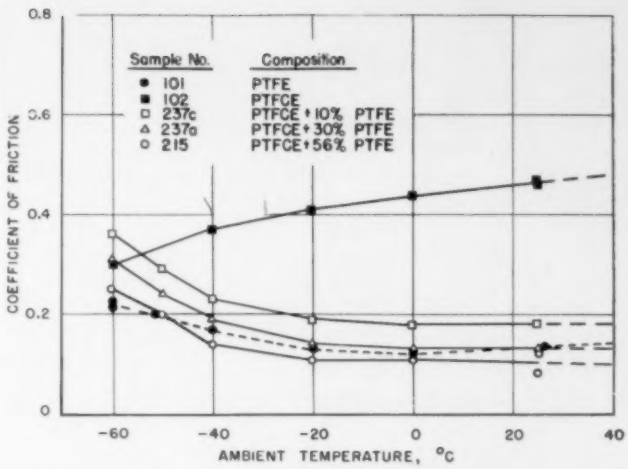

FIGURE 10. *Friction versus temperature for PTFE, PTFCE, and PTFCE plus PTFE bearings.*

TABLE 5. *Effect of run-in and effect of temperature on the coefficient of friction for various bearing materials, with a hardened 420 stainless-steel shaft, ¼-in. diameter*

Sample	Bore condition	Load	Ambient temperature	Coefficient of friction		
				3 rpm	15 rpm	300 rpm
		g	°C			
101	Reamed, C=0.008 in	643	25	0.10	0.13	0.25
	After 1 hr at 300 rpm		25	.10	.13	.23
			0	.10	----	----
			−20	.10	----	----
			−40	.12	----	----
			−50	.15	.18	.23
	After speed range at −50 °C.		−50	.18	----	----
			−60	.22	----	----
	After 5 hr at 3 rpm at −60 °C.		−60	.22	----	----
	After standing overnight		25	.12	----	----
101	Bearing turned 180°	2,200	25	.06	.08	----
	After 1 hr at 3 rpm		25	.14	----	----
			0	.12	----	----
			−20	.13	----	----
			−40	.17	----	----
			−50	.20	.22	----
			−60	.21	----	----
	After 5 hr at 3 rpm at −60 °C.		−60	.23	----	----
	After standing over weekend.		25	.14	.16	----
102	Reamed, C=0.008 in	2,200	25	.19	.22	.35
	After speed range		25	.43	----	.38
	After 0.1 hr at 300 rpm		25	.44	----	.44
	After 7 hr at 3 rpm		25	.48	----	----
	After standing overnight		25	.47	----	----
			0	.44	----	----
			−20	.41	----	----
			−40	.37	----	----
			−50	.33	.31	.34
	After speed range at −50 °C.		−50	.33	----	----
			−60	.30	----	----
	After 6 hr at 3 rpm at −60 °C.		−60	.30	----	----
	After standing overnight		25	.46	----	----
104	Reamed, C=0.008 in	2,200	25	.10	.11	.16
	After speed range		25	.13	----	----
	After 8 hr at 3 rpm		25	.15	----	----
			0	.15	----	----
			−20	.16	----	----
			−40	.23	----	----
			−50	.30	.33	.33
	After speed range at −50 °C.		−50	.28	----	----
			−60	.43	----	----
	After 6 hr at 3 rpm at −60 °C.		−60	.46	----	----
	After standing overnight		25	.15	----	----
202c	Reamed, C=0.008 in	2,200	25	.03	.05	.23
	After 8 hr at 300 rpm		25	.21	.25	.25
	After 8 hr at 3 rpm		25	.22	----	----
	After standing over weekend.		25	.16	----	----
			0	.16	----	----
			−20	.18	----	----
			−40	.20	----	----
			−50	.23	.24	.24
	After speed range at −50 °C.		−50	.22	----	----
			−60	.23	----	----
	After 5 hr at −60 °C		−60	.25	----	----
	After standing overnight		25	.16	.16	.18
214	Reamed, C=0.008 in	2,200	25	.08	.13	.22
	After 7 hr at 300 rpm		25	.22	.25	.28
	After 8 hr at 3 rpm		25	.19	----	----
	After standing overnight		25	.16	----	----
			0	.16	----	----
			−20	.16	----	----
			−40	.16	----	----
			−50	.16	.22	.32
	After speed range at −50 °C.		−50	.22	----	----
			−60	.25	----	----
	After 5 hr at 3 rpm at −60 °C.		−60	.27	----	----
	After standing overnight		25	.11	.13	.22
215	Reamed, C=0.008 in	2,200	25	.05	.08	.24
	After 7 hr at 300 rpm		25	.08	.10	.23
	After 24 hr at 3 rpm		25	.16	----	----
	After standing over weekend.		25	.12	----	----
			0	.11	----	----
			−20	.11	----	----
			−40	.14	----	----
			−50	.20	.25	.31
	After speed range at −50 °C.		−50	.20	----	----
			−60	.25	----	----
	After 5 hr at 3 rpm at −60 °C.		−60	.24	----	----
	After standing overnight		25	.08	.11	.21
219	Reamed, C=0.008 in	2,200	25	.09	.17	.20
	After 7 hr at 300 rpm		25	.09	.11	.22
	After 24 hrs at 3 rpm		25	.15	----	----
	After standing overnight		25	.13	----	----
			0	.13	----	----
			−20	.13	----	----
			−40	.16	----	----
			−50	.20	.25	.34
	After speed range at −50 °C.		−50	.23	----	----
			−60	.28	----	----
	After 5 hr at 3 rpm at −60 °C.		−60	.29	----	----
	After standing 5 days		25	.10	.14	.23
234a	Reamed and burnished, C=0.002 in.	2,200	25	.13	.15	.27
	After 5 hr at 300 rpm		25	.07	.10	.25
	After 3 more hr at 300 rpm		25	.06	.09	.25
	After 54 hr at 3 rpm		25	.11	.13	.26
	After speed range		25	.06	----	----
	After 2 more hr at 3 rpm		25	.08	----	----
			0	.09	----	----
			−20	.11	----	----
			−40	.19	----	----
			−50	.24	.28	.34
	After speed range at −50 °C.		−50	.25	----	----
			−60	.29	----	----
	After 3 hr at 3 rpm at −60 °C.		−60	.32	----	----
	After standing overnight		25	.10	.13	.24
	After 7 more hr at 3 rpm		25	.10	----	----

TABLE 5. *Effect of run-in and effect of temperature on the coefficient of friction for various bearing materials, with a hardened stainless-steel shaft, ¼-in. diameter*—Continued

Sample	Bore condition	Load	Ambient temperature	Coefficient of friction		
				3 rpm	15 rpm	300 rpm
		g	°C			
236	Reamed, C=0.008 in.	2,200	25	0.10	0.11	0.27
	After 7 hr at 300 rpm		25	.10	.12	.23
	After 8 hr at 3 rpm		25	.12	----	----
	After standing overnight		25	.12	----	----
			0	.12	----	----
			−20	.16	----	----
			−40	.23	----	----
			−50	.27	.30	.35
	After speed range at −50 °C.		−50	.29	----	----
			−60	.33	----	----
	After 5 hr at 3 rpm at −60 °C.		−60	.33	----	----
	After standing overnight		25	.12	.15	.24
237	Reamed, C=0.008 in.	2,200	25	.22	.27	.25
	After 6 hr at 300 rpm		25	.12	.14	.24
	After 8 hr at 3 rpm		25	.15	----	----
	After standing overnight		25	.14	----	----
			0	.14	----	----
			−20	.17	----	----
			−40	.22	----	----
			−50	.26	.30	.34
	After speed range at −50° C.		−50	.34	----	----
			−60	.36	----	----
	After 6 hr at 3 rpm at −60° C.		−60	.33	----	----
	After standing overnight		25	.19	.20	.25
237a	Reamed, C=0.008 in.	2,200	25	.13	.18	.23
	After 7 hr at 300 rpm		25	.11	.13	.24
	After 7 hr at 3 rpm		25	.15	----	----
	After standing overnight		25	.13	----	----
			0	.13	----	----
			−20	.14	----	----
			−40	.19	----	----
			−50	.24	.29	.33
	After speed range at −50° C.		−50	.27	----	----
			−60	.31	----	----
	After 6 hr at 3 rpm at −60° C.		−60	.33	----	----
	After standing overnight		25	.13	.14	.23
237b	Reamed, C=0.008 in.	2,200	25	.19	.22	.30
	After 8 hr at 300 rpm		25	.13	.16	.25
	After 8 hr at 3 rpm		25	.13	----	----
	After standing overnight		25	.13	----	----
			0	.13	----	----
			−20	.15	----	----
			−40	.20	----	----
			−50	.24	.27	.31
	After speed range at −50° C.		−50	.26	----	----
			−60	.32	----	----
	After 6 hr at 3 rpm at −60° C.		−60	.34	----	----
	After standing overnight		25	.14	.17	.29
237c	Reamed, C=0.008 in.	2,200	25	.15	.19	.32
	After speed run		25	.22	----	.35
	After 8 hr at 300 rpm		25	.19	.22	.30
	After speed run		25	.16	----	----
	After standing over week-end.		25	.16	----	----
	After 8 hr at 3 rpm		25	.18	----	----
			0	.18	----	----
			−20	.19	----	----
			−40	.23	----	----
			−50	.29	.33	.33
	After speed range at −50° C.		−50	.38	----	----
			−60	.36	----	----
	After 6 hr at 3 rpm at −60° C.		−60	.36	----	----
	After standing overnight		25	.22	----	----
238	Reamed, C=0.008 in.	2,200	25	.08	.13	.19
	After 8 hr at 300 rpm		25	.21	.23	.25
	After 8 hr at 3 rpm		25	.26	----	----
	After standing overnight		25	.18	----	----
			0	.18	----	----
			−20	.18	----	----
			−40	.20	----	----
			−50	.21	.22	.25
	After speed range at −50° C.		−50	.22	----	----
			−60	.22	----	----
	After 6 hr at 3 rpm at −60° C.		−60	.23	----	----
	After standing overnight		25	.19	.19	.20
238a	Reamed, C=0.008 in.	2,200	25	0.06	0.07	0.26
	After 8 hr at 300 rpm		25	.29	.29	.27
	After 7 hr at 3 rpm		25	.25	----	----
	After standing over week-end.		25	.21	----	----
			0	.22	----	----
			−20	.22	----	----
			−40	.23	----	----
			−50	.25	.26	.28
	After speed range at −50° C.		−50	.23	----	----
			−60	.25	----	----
	After 6 hr at 3 rpm at −60° C.		−60	.25	----	----
	After standing overnight		25	.18	.20	.23
238b	Reamed, C=0.008 in.	2,200	25	.10	.15	.17
	After 8 hr at 300 rpm		25	.19	.21	.21
	After 8 hr at 3 rpm		25	.18	----	----
	After standing overnight		25	.15	----	----
			0	.15	----	----
			−20	.16	----	----
			−40	.18	----	----
			−50	.20	.21	.25
	After speed range at −50° C.		−50	.22	----	----
			−60	.18	----	----
	After 6 hr at 3 rpm at −60° C.		−60	.22	----	----
	After standing overnight		25	.22	.22	.20
304	Reamed, C=0.0016 in.	2,200	25	.17	----	----
	After 0.1 hr at 3 rpm		25	.32	----	----
	After 0.2 hr at 3 rpm		25	.44	----	----
401	Reamed and burnished, C=0.002 in.	2,200	25	.16	.18	.23
	After 2 hr at 300 rpm		25	.25	.25	.27
	After 4 more hr at 300 rpm		25	.22	.24	.27
			0	.23	----	----
			−20	.24	----	----
			−40	.26	----	----
			−50	.27	.27	.27
	After speed range at −50° C.		−50	.25	----	----
			−60	.26	----	----
	After 5 hr at 3 rpm at −60° C.		−60	.23	----	----
	After standing overnight		25	.22	.23	.26
604	Polished sapphire, clean, C=0.002 in.	643	25	.18	.22	----
			0	.19	.23	----
			−20	.20	.26	----
			−40	.23	.30	----
			−50	.26	.33	----
			−60	.28	.35	----
605	Reamed, C=0.008 in	2,200	25	.13	.15	----
	After 0.5 hr at 3 rpm		25	.29	----	----
	After 1 hr at 3 rpm		25	.44	----	----
606	Reamed, C=0.008 in.	2,200	25	.29	----	----
	After 0.5 hr at 3 rpm		25	.50	----	----
	After 1 hr at 3 rpm		25	.52	----	----
609	Coating: thickness=0.003 in. C=0.002 in.	2,200	25	.41	.48	.46
	After speed run		25	.44	----	.39
	After 0.1 hr at 300 rpm		25	.38	----	.36
	After 8 hr at 3 rpm		25	.41	----	----
	After standing over holiday		25	.41	----	----
			0	.41	----	----
			−20	.41	----	----
			−40	.41	----	----
			−50	.41	.41	.39
	After speed range at −50° C.		−50	.41	----	----
			−60	.42	----	----
	After 6 hr at 3 rpm at −60° C.		−60	.48	----	----
	After standing overnight		25	.48	----	----
611	Coating: thickness=0.001 in., C=0.008 in.	2,200	25	.03	.04	.21
	After speed run		25	.11	----	.18
	After 0.1 hr at 300 rpm		25	.13	----	.17
	After 8 hr at 3 rpm		25	.15	----	----
	After standing overnight		25	.13	----	----
			0	.13	----	----
			−20	.13	----	----
			−40	.15	----	----
			−50	.18	.22	.24
	After speed range at −50° C.		−50	.19	----	----
			−60	.20	----	----
	After 6 hr at 3 rpm at −60° C.		−60	.18	----	----
			−70	.18	----	----
	After standing overnight		25	.13	----	----

c. Different Shaft Materials With Oil-Free Bearings

To investigate the effect of different shaft materials on friction, data were obtained with 4 typical bearing materials on each of 5 different shaft materials, at 25° C, with a 2,200-g load, during 8 hr of operation at 3 rpm. The data are given in table 6, in chronological order. With the bearing sample containing molybdenum (sample 202c), after 8 hr of operation the coefficient of friction was 0.07 with the cobalt alloy shaft (C40), 0.15 with the hardened 440C stainless-steel shaft, 0.33 with the relatively soft machinery steel (sample M), and 0.22 to 0.25 with the two shafts made of hardened high-chromium tool steels (samples D3 and D2). With each of the other three bearing materials, after 8 hr of operation at 3 rpm on each shaft, the friction was not greatly affected by the shaft material.

Check runs given in table 6 for bearings 101 and 215 give some indication of the reproducibility of the friction data under these conditions. However, in initial tests with bearing 101 and these new shafts there was a progressive increase in friction from 0.06 to 0.28, and a slight brownish glaze was observed on the bearing at its contact area. These test shafts were ground, lapped with diamond dust, and then polished with 4/0 polishing paper. They were cleaned by scrubbing and rinsing with benzene, but it is believed possible that traces of abrasives from the shafts may have been transferred to the bearing. Preliminary operation was continued with occasional cleaning of the bearing with a reamer and with benzene until a colored glaze no longer formed on the bearing and friction data became reasonably reproducible with check runs.

TABLE 6. *Coefficient of friction for typical ¼-in.-diam bearings, with various steel shafts, with 2,200-g load, at 3 rpm, at 25° C*

These data are given in chronological order.

Sample		Coefficient of friction at 3 rpm, after—					
Bearing	Shaft	0 hr	1 hr	2 hr	4 hr	6 hr	8 hr
101	M	0.06	0.09	0.11	0.12	0.12	0.13
	D2	.10	.20	.23	------	------	------
	440C	.10	.13	.14	.15	.15	.15
	D3	.10	.17	.17	.15	.15	.15
	M	.08	.11	.11	.12	.13	.13
	D2	.09	.11	.14	.16	.16	.15
202c	440C	.06	.07	.07	.09	.12	.15
	D3	.08	.10	.10	.12	.15	.22
	M	.07	.19	.27	.32	.32	.33
	D2	.08	.12	.15	.20	.23	.25
215	M	.08	.19	.17	.15	.14	.13
	D2	.16	.19	.18	.15	.13	.13
	440C	.22	.17	.15	.15	----	.17
	D3	.20	.20	.16	.13	.12	.11
	440C	.17	.18	.15	.14	.13	.13
401	D2	.16	.23	.25	.30	.34	.34
	440C	.20	.24	.24	.25	.25	.26
	D3	.20	.27	.28	.29	.30	.30
	M	.24	.29	.33	.36	.36	.34
215 202c 101 401	C40	.04 .03 .06 .22	.10 .09 .07 .25	.11 .09 .08 .26	.13 .06 .10 .27	.14 .06 .11 .27	.13 .07 .11 .27

6.3. Bearing-Storage Results

With the apparatus and procedure previously described, the effect of storage on starting friction and corrosion was investigated with 6 typical oil-free bearing materials on each of 3 different shafts. The shafts were an oil-hardening nondeforming tool steel (O2), an oil-hardening, high-carbon, high-chromium tool steel (D3), and 440C stainless steel; the average values of surface roughness as measured by a profilometer before starting the test were 3, 4, and 1 μin., respectively.

The data for the storage test are given in table 7.

TABLE 7. *Effect of 10 months of storage on the coefficient of static friction, for various bearing and shaft materials*

Sample		Coefficient of static friction		Remarks
Bearing	Shaft	New	After 10 months	
222	O2	0.09	0.15	No rust.
	D3	.12	.17	Do.
	440C	.11	.17	Do.
231	O2	.18	.17	Do.
	D3	.13	.17	Do.
	440C	.12	.17	Do.
237a	O2	.18	.23	Do.
	D3	.18	.23	Do.
	440C	.13	.23	Do.
238	O2	.18	1.7+	Journal badly rusted.
	D3	.12	1.7+	Journal rusted.
	440C	.14	0.90	Do.
401	O2	.17	.17	No rust.
	D3	.18	.20	Do.
	440C	.20	.18	Do.
605	O2	.10	.16	Do.
	D3	.09	.19	Do.
	440C	.10	.22	Do.

With bearing sample 231 on D3 and 440C shafts, and samples 222, 237a, and 238 on each shaft, the static friction increased during the 10 months of storage, the range of increase being from 28 to 77 percent. With sample 231 on shaft O2 and sample 401 on each shaft, within the accuracy of the data, there was no change in friction during storage. With the sample of bearing bronze (No. 605), included for comparative purposes, the increase in friction ranged from 60 to 120 percent. With sample 238 (PTFE+ molybdenum) there was a very great increase in friction, resulting from corrosion on the shafts; in those areas (journals) of the shafts enclosed by this bearing material, the O2 journal was covered with rust and the journals of the other two shafts were spotted with rust. No corrosion was observed on any of the shafts in other bearing positions. There was considerable rust on the steel housings for bearings 238, and a slight amount of rust on the machined faces of the other bearing housings. On the faces in contact with bearings 238 the brass collars were discolored by corrosion. There was no abnormal discoloration on any of the other brass collars.

The sample 238 bearings used in these tests were machined and installed within 2 weeks after the preparation of this sample of material. Strong odors were emitted from the various samples of PTFE plus molybdenum for several weeks after fusing. Previous experience with new bearings in timepieces, and with pieces of steel in sample jars, indicated that freshly prepared samples of this type might cause corrosion. However, after aging several months, samples no longer caused corrosion of the steel in the jars with the samples. It is probable that storage at an elevated temperature would decrease the period of aging that seems necessary to eliminate the corrosive tendency of this type of material.

6.4. Bearing-Wear Results

a. Rotating Journals

Wear data were obtained with 2,000-g loads on bearings that were ½ in. long with ¼ in. bores, corresponding to 35 psi on the projected area. Most of the data were obtained with 303 stainless-steel journals operating at 15 and 150 rpm, but some data were obtained with other types of steel used for the journals and some data were obtained at 700 and 1,800 rpm. These data are given in table 8, in terms of the number of hours of operation for 0.005 in. of radial wear on the loaded side, computed from the wear rates in milligrams per hour and the densities of the samples. An initial diametral clearance of 0.005 in. was assumed in making these computations; and the radial wear of 0.005 in. would increase this to 0.010 in. in the hours given in the table. These computed hours of operation for 0.005 in. of wear should be considered approximations, because the initial clearance in the tests varied from 0.005 in. and the bearing deformation resulting from the load was not considered.

TABLE 8. *Rate of wear for various bearing materials, with ¼-in.-diameter shafts, at room temperature, with 2,000-g load*

Sample		Length of test at 150 rpm	Computed number of hours for 0.005-in. radial wear				Rating[a] at 150 rpm
Shaft	Bearing		15 rpm	150 rpm	700 rpm	1,800 rpm	
		hr	hr	hr	hr	hr	
303	101	5	1,400	25	-----	-----	5
	101	53	-----	91	-----	-----	5
	102	31	1,340	116	-----	-----	4
	102	53	-----	134	-----	-----	4
	103	72	1,440	103	-----	-----	4
303	103a	95	1,160	99	-----	-----	5
	103b	-----	1,570	-----	-----	-----	-----
	104	603	-----	360	-----	27	4
303	201	332	95,400	12,700	-----	-----	2
	202	483	100,000+	100,000+	-----	-----	1
	202a	144	63,400	755	-----	-----	4
	202b	237	54,400	1,550	-----	-----	3
	202c	261	100,000+	1,050	-----	-----	3
303	204a	332	45,700	12,200	-----	-----	2
	205	438	2,230	910	-----	-----	4
	206	166	30,500	480	-----	-----	4
	206a	525	18,200	1,820	-----	-----	3
	207	76	2,050	182	-----	-----	4
303	208	260	8,000	1,280	-----	-----	3
	208a	507	9,690	1,820	-----	-----	3
	209	169	58,100	3,710	1,340	-----	3
	210	378	58,100	6,020	2,050	-----	3
	211	190	19,100	119	-----	-----	4

TABLE 8. *Rate of wear for various bearing materials, with ¼-in.-diameter shafts, at room temperature, with 2,000-g load*—Continued

Sample		Length of test at 150 rpm	Computed number of hours for 0.005-in. radial wear				Rating[a] at 150 rpm
Shaft	Bearing		15 rpm	150 rpm	700 rpm	1,800 rpm	
		hr	hr	hr	hr	hr	
303	212	166	5,790	236	-----	-----	4
	213	166	10,600	2,120	48	-----	3
	214	213	63,100	11,300	286	-----	2
	214	-----	-----	-----	93	-----	-----
	215	385	11,400	8,700	11,400	1,220	3
440C	215	331	-----	1,880	-----	247	3
D3	215	216	-----	1,830	-----	415	3
C40	215	336	-----	3,810	-----	507	3
303	215a	221	1,340	187	-----	-----	4
	216	361	100,000+	24,900	5,170	6,050	2
440C	216	427	-----	30,400	-----	3,860	2
D3	216	234	-----	10,500	-----	1,960	2
303	217	313	18,900	2,070	-----	-----	3
	218	315	26,100	14,000	2,150	-----	2
	218a	334	22,800	12,200	-----	-----	2
303	219	629	31,800	11,900	21	-----	2
	220	335	100,000+	1,630	-----	-----	3
	220a	405	100,000+	8,900	-----	-----	3
	221	331	6,090	2,430	397	-----	3
	222	331	88,600	88,600	-----	-----	2
303	223	602	100,000+	12,000	5,120	1,720	2
	224	599	100,000+	49,800	8,300	3,110	2
	225	600	83,000	35,600	2,490	-----	2
	226	331	20,700	27,600	41,500	6,730	2
D3	226	-----	-----	-----	-----	1,240	-----
303	227a	20	113	35	-----	-----	5
	228	235	60,800	7,020	2,430	962	3
	229	167	60,800	10,100	2,100	704	2
	230	102	13,000	16,600	1,400	-----	2
	231	98	21,500	203	99	-----	4
303	232	102	4,450	1,660	166	-----	3
	233	102	3,380	4,150	553	-----	3
	234	477	-----	4,810	-----	522	3
	234a	576	-----	19,200	-----	1,010	2
	235	449	-----	11,400	-----	2,340	2
D3	235	-----	-----	-----	-----	2	-----
303	236	486	-----	1,010	-----	445	3
D3	236	525	-----	456	-----	237	4
303	236	700	-----	1,830	-----	-----	3
	236	1500	-----	1,010	-----	-----	3
303	236	700	-----	1,070	-----	-----	3
	236	1500	-----	795	-----	-----	4
	236	700	-----	1,520	-----	-----	3
	236	1500	-----	1,010	-----	-----	3
	237	486	-----	507	-----	589	4
303	237a	486	-----	415	-----	760	4
	237b	144	-----	507	-----	570	4
	237c	267	-----	2,220	-----	140	3
440C	237c	458	-----	870	-----	130	4
C40	237c	480	-----	1,220	-----	140	3
303	238	476	-----	26,800	-----	94	2
440C	238	600	-----	1,660	-----	1,510	3
D3	238	312	-----	3,750	-----	1,240	3
C40	238	310	-----	100,000+	-----	21	1
303	238a	478	-----	29,900	-----	30	2
303	238b	390	-----	31,900	-----	42	2
303	304	1	-----	52	-----	-----	5
303	401	597	14,600	13,300	334	-----	2
	402	405	19,400	3,230	-----	-----	3
	403	403	41,500	5,810	-----	-----	3
	404	338	5,740	313	-----	-----	4
303	605	4	-----	50	-----	-----	5
	606	0.8	-----	0.9	-----	-----	5
	609	266	-----	11,600	-----	513	2
	611	170	-----	5,220	-----	166	3
	612	143	-----	630	-----	3	4

[a] 1: 100,000+ hr, excellent.
2: 10,001 to 100,000 hr, very good.
3: 1,001 to 10,000 hr, good.
4: 101 to 1,000 hr, fair.
5: 0 to 100 hr, poor.

In general, the duration of a test was short compared to the hours computed for 0.005-in. radial wear. Included in table 8 are the durations of the tests at 150 rpm. Special tests were made with sample 236 to get indications of the effect of duration of tests and the effect of journal roughness. In these special tests, three bearings (sample 236) with 0.005-in. initial clearance were tested on three 303 stainless-steel journals with roughness values of 2, 8, and 16 μin., as measured with a profilometer. The wear was determined for 700 hr and then for 1,500 hr, after running an additional 800 hr. In this range of roughness, there was no trend for variation of wear with roughness; but there was a trend toward higher rate of wear with the longer period of operation. For these special tests the computed hours of operation for 0.005-in. wear on the loaded side ranged from 795 to 1,830 hr, which may be compared with 1,010 hr computed from a previous test with 486 hr of duration.

In table 8, ratings are given for the wear resistance of the bearing for each test at 150 rpm. Ratings 1 and 2 are given for computed hours of operation above 100,000 and 10,000, and are considered excellent and very good, respectively. Rating 3 is given for operation between 1,001 and 10,000 hr, and is considered good.

TABLE 9. *Wear for various bearing materials, with ½-in. diameter shafts, at room temperature, with 1,000-g load; shafts oscillating, amplitude=0.5 radian, frequency=3 cps*

Sample		Time run	Bearing loss in weight		Condition of journals at end of tests		Rating [a]
Shaft	Bearing		Front	Rear	Front	Rear	
		Days	*mg*	*mg*			
303	101	60	0.8	9.1	Very good	Scored	5
	202c		.0	0.0	Good	Good	1
	209		.0	.4	Fair	Fair	3
	210		.1	.1	do	do	2
	214		.1	.1	do	do	2
303	215	60	.1	.3	Very good	Very good	2
	219		.2	.2	Good	do	2
	221		1.0	.6	Scored	Good	4
	222		0.1	.2	Very good	do	2
	224		.1	.2	Good	Fair	2
303	234	60	.1	.1	Very good	Very good	1
	234a		.1	.0	Good	do	1
	237		.4	.4	Very good	do	3
	401		.6	1.0	Fair	Fair	4
	403		.1	0.2	Good	Good	2
440C	202c	60	.3	.4	Fair	Scored	4
	214		.1	.1	Good	Fair	2
	234a		.1	.1	Very good	Very good	1
	401		.1	.4	Good	Good	3
D3	202c	60	1.9	1.4	Scored	Scored	4
	214		2.5	1.6	do	do	4
	222		0.0	0.1	Good	Very good	1
	401		.2	.1	do	Good	2
C40	202c	60	.6	.3	Fair	do	3
	214		.5	.3	Good	do	3
	401		.0	.0	do	do	1
440C	303	10	5.8	5.8	Worn slightly	Worn slightly	5
	605		23.9	29.0	do	do	5
D3	303	10	12.1	16.3	do	do	5
	605		17.7	16.6	do	Worn and scored.	5

[a] 1: excellent; 2: very good; 3: good; 4: fair; 5: poor.

b. Oscillating Journals

Wear data were obtained with 1,000-g loads on typical paired bearings, each ¼ in. long with ⅛-in. bore, with various steel shafts in the modified oscillating display motors. The pressure during the impulse from the solenoid was considerably greater than the 70 psi corresponding to the 1,000-g static load. These data are given in table 9. In general, the loss in weight of the typical bearings and the condition of the journals after 60 days of operation are given. However, with porous bronze containing molybdenum disulfide (sample 303) and with bearing bronze (sample 605), the friction increased soon after starting the tests to the extent that a much higher voltage had to be applied to the solenoids to maintain operation and one solenoid burned out due to overloading. Because of this and excessive wear, tests with these two materials were stopped at the end of 10 days. It is of interest that the performance with these two bearing materials (samples 303 and 605) in this machine was very much inferior to any of the other oil-free materials that were tested on it. The rating numbers given in table 9 for each test are based on the bearing wear and the condition of the journals at the end of each test. The numbers 1 to 5 correspond to excellent, very good, good, fair, and poor, respectively.

c. Thrus Bearings With Oscillating Pins

With the endstone-wear testing machine, wear data were obtained with typical bearing materials and test pins made of typical shaft materials, with 1,000- and 1,240-g loads. The data obtained with the 440C test pins are given in table 10. For each measured depth of wear (see section 5.4 for method of measuring) the corresponding pressure (pounds per square inch) on the projected area was computed, and these data are included in table 10. At 0.0167 in. of wear the diameter of the wear mark, becomes the same as that of the pin (0.125 in.), so that for greater depths of wear the pressure does not increase. The average rates of wear per bearing, in inches per year, for each period are given in the table also.

With the diamond endstone there was no wear on the diamond or the pin that could be detected by ordinary means. No flat could be detected on the pin when examined with a 20-power stereomicroscope and when examined with a shadowgraph. No roughness was detected on the diamond, but examination with an interferometer indicated a depression about 17 μin. deep near the center of the endstone after the 60-day test. On the basis of this test, diamond is rated as excellent for use as endstones.

With PTFE plus molybdenum (sample 202c) and with PTFCE plus PTFE (sample 215) no measurable wear was detected during the last 20 days of operation, and hence these materials are rated very good for use as endstones.

With samples 222 and 401 the rate of wear was low during the last period of operation, and these materials may be rated as good. The relatively wide spread in the data for the carbon plus graphite

TABLE 10. *Wear data for typical bearing materials, with endstone-wear machine, with 440C hardened steel shafts, ⅛-in. diameter with ⅛-in. radius at ends, at room temperature; shafts oscillating, amplitude=1.5 radians, frequency=1 cps*

Sample	Time run	1,000-g load		1,240-g load		Average rate of wear [b]
		Depth of wear	Pressure [a]	Depth of wear	Pressure [a]	
	Days	*in.*	*psi*	*in.*	*psi*	*in./yr*
101	10	0.0075	385	0.0075	478	0.274
	20	.011	266	.010	363	.110
	40	.016	187	.015	247	.091
	60	.020	180	.020	223	.082
102	10	.005	575	.005	711	.182
	20	.009	323	.0075	478	.119
	40	.013	228	.011	330	.068
	60	.016	187	.014	263	.055
202c	10	.001	2,813	.001	3,490	.036
	20	.0015	1,875	.0015	2,326	.018
	40	.002	1,418	.002	1,758	.009
	60	.002	1,418	.002	1,758	.000
215	10	.0015	1,875	.002	1,758	.064
	20	.002	1,418	.002	1,758	.009
	40	.002	1,418	.002	1,758	.000
	60	.002	1,418	.002	1,758	.000
222	10	.0015	1,875	.0015	2,326	.055
	20	.0015	1,875	.002	1,758	.009
	40	.002	1,418	.002	1,758	.005
	60	.002	1,418	.0025	1,393	.005
401	10	.0015	1,875	.001	3,490	.046
	20	.002	1,418	.0015	2,326	.018
	40	.0035	818	.0015	2,326	.014
	60	.004	715	.0015	2,326	.005
604 (Sapphire)	10	.004 [c]	715	------	------	.146 [c]
	20	.005	574	------	------	.036
	40	.007	412	------	------	.036
	60	.0095	311	------	------	.046
609	10	.010	292	.016	232	.475
610 (Diamond)	10	------	------	.0000	139,300	.000
	20	------	------	.0000	139,300	.000
	40	------	------	.0000	139,300	.000
	60	------	------	.0000	139,300	.000
611	4	.031	180	.027	233	2.65

[a] Computed pressure on the projected area for each measured depth of wear; excepting diamond, in which case pressure was computed from the elastic deformation of the radius on the end of the steel pin.
[b] Computed from average wear during each period of time run.
[c] Wear occurred on end of steel pin instead of on sapphire endstone.

plus silver (sample 401) is believed to be due to a lack of homogeneity in the mixture.

With sapphire (sample 604, unlubricated) a relatively large flat was worn on the end of the test pin, and the rate of wear given in table 10 is for this wear on the pin. However, the sapphire became roughened on part of the rubbing area, and was worn slightly.

With PTFE and with PTFCE the endstone-wear rate was high. With the coatings (samples 609 and 611) the tests were stopped after a few days of operation because of excessive wear.

Results obtained when samples 101, 202c, 215, and 401 were tested with pins made of 303 stainless steel, hardened D3 steel, and C40 alloy were similar to those obtained with 440C stainless-steel pins.

With 303 stainless-steel pins, specimens of tungsten plus molybdenum disulfide plus plastic coating (sample 606) on brass started wearing very rapidly, and the test was stopped at the end of the first day of operation. For comparison, a test with plain brass (sample 607) gave less wear than the coated brass, although wear was excessively great in both cases. Although this coating is advertised as showing no wear when used as a thrust bearing under certain conditions, under the conditions used in these tests its wear resistance was inferior to that of brass.

6.5. Timepiece-Bearing Results

The performance of oil-free bearings was investigated in 18 timepieces, including chronometers, clocks, and watches.

For plastics and plastics with fillers, the coefficients of thermal expansion are such that with ¼-in.-bore bearings subjected to a wide range of temperature, clearances much larger than those commonly used with metallic journal bearings are necessary. However, the percentage of clearance normally used for the relatively small journals in timepieces is such that the above condition presents no problem. Bearings of this type become loose in their housings at low temperature; in order to prevent axial displacement at low temperatures, these bearings were fitted in brass holders having the inner edges crimped inward slightly to retain the bearings.

In general, the amplitude of the motion of the balance wheels in the clocks and watches fitted with oil-free bearings was considerably less than the normal amplitude in oiled-jewel movements at ordinary temperatures. In most cases, heavier mainsprings were installed to increase the torque about 50 percent to provide more normal motion. However, in the chronometers the original mainsprings were not replaced, because they provided sufficient power for normal motion in these timepieces.

On the basis of the experience with timepieces, it appears that for ship chronometers in normal dial-up position the most severe wear is apt to occur at the upper balance-staff endstones, and for clocks operating in the normal 12:00-up position the most severe wear is apt to occur at the bearings for the balance-staff journals. Also, it is probable that the friction at these points is of major importance.

For watches and clocks, the friction and wear at the pallet stones also appears to be of major importance, and no material has been found to be more satisfactory than sapphire for this application. Unlubricated sapphire pallet stone appears to be satisfactory at ordinary temperatures, but at very low temperatures the addition of a film of a suitable low-temperature oil apparently gives less friction than clean sapphire.

Rusting is apt to occur in unlubricated timepieces, especially at the balance-staff pivots, unless precautions are taken to prevent it. Experience with timepieces in this investigation indicates vapor phase inhibitors, such as dicyclohexylammonium nitrite, are effective in preventing rust. Also, rusting may be prevented by the use of corrosion-resistant materials; no rust was observed with cobalt alloy (C40) pivots.

In general, at ordinary temperatures the timekeeping performance of timepieces with conventional

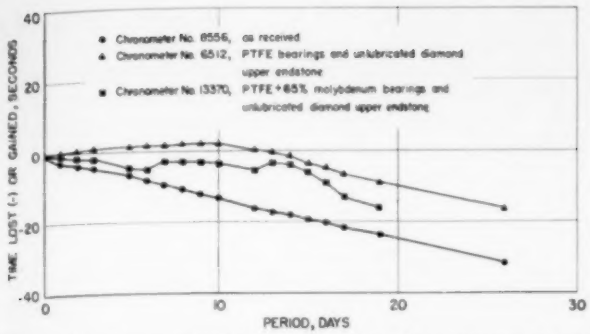
Chronometer No. 6556, as received
Chronometer No. 6512, PTFE bearings and unlubricated diamond upper endstone
Chronometer No. 13370, PTFE+65% molybdenum bearings and unlubricated diamond upper endstone
TIME LOST (-) OR GAINED, SECONDS
PERIOD, DAYS

FIGURE 11. *Representative time error for chronometers, at room temperature.*

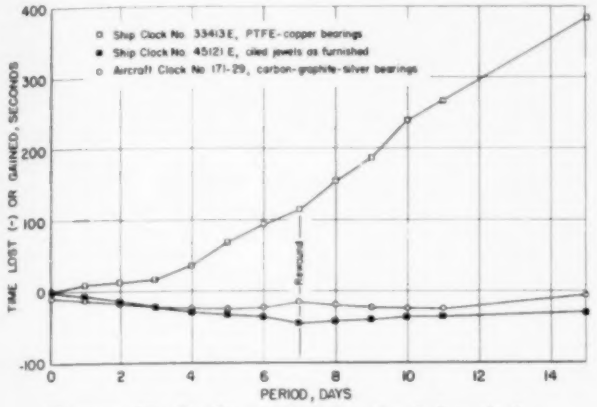
Ship Clock No. 33413E, PTFE-copper bearings
Ship Clock No. 45121E, oiled jewels as furnished
Aircraft Clock No. 171-29, carbon-graphite-silver bearings
Rewound
TIME LOST (-) OR GAINED, SECONDS
PERIOD, DAYS

FIGURE 12. *Isochronism curves for 8-day clocks.*

lubricated jewels was somewhat superior to that of oil-free timepieces. The degree of this superiority is indicated in figure 11, which shows a plot of time errors for a conventional lubricated chronometer and for two chronometers containing oil-free bearings. However, with less accurate timepieces, the difference in accuracy is of less importance. Typical isochronism curves are given in figure 12, for a conventional ship clock, a similar clock fitted with PTFE-plus-copper bearings, and an aircraft clock fitted with carbon-graphite-silver bearings.

Representative data for the performance of six timepieces fitted with oil-free bearings at −60° C, +25° C, and +75° C are given in table 11. The sapphire pallet stones in the watches and clocks and the mainsprings and other metal-to-metal working parts in these timepieces were lubricated with MIL–O–11734 oil. The size of the heavier mainsprings in the ship clocks was such that, because of the lesser free space in the mainspring barrels and the corresponding lesser number of turns in winding, they "ran down" in about 5 days instead of 8 days. This may account for the stoppage of one clock on the fifth day after winding, as it was nearly run down when it stopped. The range of temperature is beyond that ordinarily compensated for in timepieces, and lack of temperature compensation may account for some of the variation in rate with temperature for chronometer 13370 and clock 33413E. Considering the wide range in temperature, the rates for the other timepieces were not greatly affected by temperature variation.

TABLE 11. *Timepiece performance at various ambient temperatures, with oil-free bearings, except for MIL–O–11734 oil on pallet stones, mainsprings, and other metal-to-metal parts*

Timepiece	Oil-free bearings		Gain (+) or loss (−) in 24 hr		
	Sample	Number	−60° C	+25° C	+75° C
			sec	sec	sec
Ship chronometer No. 6512, dial up, wound daily.	101	10 [a]	+17	−1	−40
			+10	−½	−20
			+7	0	−14
			+8	0	−13
			+10	−½	−9
Ship chronometer No. 13370, dial up, wound daily.	202c	10 [a]	−118	+½	+38
			−148	0	+40
			−102	−½	+41
			−112	−1	+47
			−116	−½	+43
Navigation watch No. 995–41, 24:00 up, wound daily.	215	19	−7	+53	+58
			−7	+53	+69
			+51	+55	+60
			+37	+49	+86
			+27	+59	+85
Navigation watch No. 964–42, dial up, wound daily.	202	19	−59	+1	−10
			−33	−3	+20
			−5	−10	+26
			−2	−16	+17
			−31	−4	0
Ship clock No. 33413E, 12:00 up, 1 winding.	205	9	−311	+123	−143
			−334	+2	−35
			−344	−12	−101
			−330	−17	−200
			−354	−23	−200
Ship clock No. 45121E, 12:00 up, 1 winding.	401	9	+9	+52	+10
			+7	+31	+10
			+2	−3	+6
			+12	−15	0
			Stopped	−12	+2

[a] Including 1 diamond and 1 sapphire endstone, unlubricated.

Twelve timepieces fitted with various oil-free bearings were stored in a low-temperature cabinet maintained at −60° C. These were running at the start of this test but were not wound during the storage. After 30 days each timepiece was wound while remaining in the low-temperature cabinet; and if it did not start while winding, it was given quick twists in a manner ordinarily used for starting timepieces. The results of this low-temperature test are given in table 12. The low-priced watch No. 4–52

TABLE 12. *Starting ability of timepieces, after winding, at −60° C, after 30 days of storage at −60° C*

Timepiece	Oil-free bearings		Other parts	Starting ability
	Sample	Number		
Navigation watch 964–42	202	19	(a)	Started.
Ship chronometer 13370	202c	14	(b)	Do.
Ship clock 33413E	205	9	(a)	Do.
Aircraft clock 1	215	8	(a)	Do.
Navigation watch 995–41	215	19	(a)	Do.
Pocket watch 4–52	215	7	(a)	Would not start.
Aircraft clock 93–29	222	12	(a)	Started.
Aircraft clock 88–C–590	234a	12	(a)	Do.
Automobile electric clock KA–494.	234a	4	No oil	Do.
Ship chronometer 6512	237a	16	(b)	Do.
Aircraft clock 171–29	401	12	(a)	Do.
Ship clock 45121E	401	9	(a)	Would not run.

[a] MIL–O–11734 oil applied to pallet stones several months previously.
[b] MIL–G–7421 grease in mainspring barrel to arbor bearing and inside fusee winding assembly.
[c] MIL–O–11734 oil on pallet pins, pallet arbor, and mainspring assembly.

with oil at places noted in the table would not start, and ship clock No. 45121E would not continue running after starting several times. All the other timepieces continued running at −60° C after starting. In the watches and clocks having sapphire pallet stones, the stones had been lubricated with MIL–O–11734 oil several months previously, but this is not a nonspreading type as ordinarily used for this application in timepieces. Some time after the low-temperature starting test, the sapphire pallet stones were examined with a 20-power stereomicroscope; no oil appearing as a liquid could be detected, but various colors appearing on the surface of the sapphire indicated a boundary layer of lubricant was present.

It is believed that MIL–O–11734 oil applied to the sapphire pallet stones will provide boundary lubrication for a period of about 2 years. The oil may be applied to the pallet stones in a few minutes, without the disassembly and time that are required for oiling a timepiece throughout in the conventional manner. For current types of aircraft clocks, by removing the movement from the case the oil may be applied to the pallet stones easily in the conventional manner; or, after practice, with the movement in the case a small wire may be inserted through the regulator screw plug opening to apply the oil to the teeth of the escape wheel in less than a minute.

Near the end of this project, in aircraft clock No. 26169, 6 bearings and 2 endstones, sample 237a, were used to replace 8 sapphire jewels; and 7 PTFCE bearings (sample 102) were installed in other positions; namely, third, center, intermediate, and fourth wheel upper. In figure 10 it may be seen that the coefficients of friction for these two samples are practically the same at −60° C, and that the mean friction for the two samples remains about the same in the temperature range from −60° to +25° C. This combination of bearings of these materials was tried to minimize the effect of temperature on the total friction in the clock. With the original mainspring (0.008 in. thick) the motion was poor; hence a stronger mainspring (0.011 in. thick) was installed to give more normal motion of the balance wheel. Operation at −60° C with the sapphire pallet stones unlubricated was not satisfactory. After the addition of MIL–O–11734 oil to the pallet stones, the motion at −60° C was only slightly less than at room temperature, although the clock lost several minutes per day at −60° C.

7. Conclusions

7.1. Plastics

The wear-test data and experience with PTFE in an aircraft clock and in a chronometer indicate that this material (without additives) is not suitable for general use as a bearing material because of its tendency to wear, but at very low surface speeds and low unit pressures its wear resistance may be adequate for special applications. The increase in friction at temperatures below −20° C detracts from its usefulness at low temperatures.

The high friction common to PTFCE at ordinary temperatures, and the rates of wear obtained with it in bearings, for a clock balance staff and an endstone for a chronometer balance staff, do not recommend its use as an oil-free bearing material for timepieces. However, its decrease in friction with decrease in temperature makes it useful for special applications at low speeds, such as that described in the last paragraph in section 6.5.

Nylon has been used as a bearing material in certain industrial applications. However, its friction is higher than that of some of the other materials investigated, and its relatively large variation in water content and change in size with change in ambient temperature and humidity are not desirable.

The high-density polyethylene is a relatively new type of polyethylene plastic, and was obtained near the end of the project. The friction with this material was somewhat greater than with PTFE, and the increase in friction with decrease in temperature was greater than that of PTFE. However, the rate of wear at 150 rpm with this polyethylene (sample 104) was less than that of any of the other unfilled plastics tested under similar conditions.

7.2. Plastics With Fillers

PTFCE containing 10 to 60 percent of PTFE as a filler is one of the most promising oil-free bearing materials developed during the project. A patent which is pending, covering this type of material, has been assigned to the U. S. Government. This material has some of the hardness characteristics of PTFCE, the frictional characteristics of PTFE, and wear resistance much greater than that of either of these plastics alone. Unfortunately, the fact that its frictional characteristics are similar to those of PTFE detracts from its usefulness at temperatures below −20° C.

With the samples of PTFCE containing graphite and molybdenum disulfide (samples 207 and 213, respectively), the friction and the wear were less than with PTFCE; but these dry lubricant additives did not decrease the friction and wear as much as did the PTFE filler.

PTFE containing molybdenum metal powder as a filler is a promising material also, and a patent (No. 2,715,617) covering this type of material has been assigned to the Government. It has good frictional characteristics and exceptionally good wear resistance under certain conditions.

The commercial preparation of PTFE containing fiber glass and pigment (sample 201) has good wear and friction characteristics when used as oil-free bearings with 0.25-in. bore. However, the relatively large size of some of the glass fibers and the lack of uniformity in the mixture prevent it from being suitable for bearings where the bore is only about 0.005 in.

The addition of graphite, copper powder, or molybdenum disulfide powder to PTFE (samples 204a, 205, and 206) has a similar effect in reducing wear in 0.25-in. bearings. However, these commer-

cial preparations have small pockets of pure plastic similar to those observed in the material with code No. 201.

In general, the addition of a filler to PTFE decreases the wear greatly, but the filler of silver precipitated flowers (sample 203) is an exception. The experience of high wear and high friction at low speeds with a bearing of this material is not understood. It is believed, from microscopic examination, that the silver particles are much less than 1μ in size but have a great tendency to occur in conglomerations larger than 5μ. Because of the conglomerations, it is possible that the PTFE does not surround and bind the individual silver particles; and the breakup of the conglomerations during testing may cause the high wear and high friction. In this connection, molybdenum metal powder is readily available in particle sizes from 0.5 to 5μ, and this range of particle size appears to be especially suitable for fillers in PTFE compositions for small oil-free bearings.

7.3. Impregnated Bronze

Stereomicroscopic examination of the porous bronzes showed some of the pores and the sections of solid bronze to be much larger than the diameters of common balance-staff journals, and this makes the use of impregnated porous bronze impractical for this application. Also, for larger journals, the friction and wear data obtained for porous bronze impregnated with PTFE and with molybdenum disulfide discourage its use for an oil-free bearing composition, under the conditions that were investigated.

7.4. Impregnated Carbon

In general, the metal-impregnated carbon materials that were tested have good friction and wear characteristics. An additional advantage is their low coefficient of thermal expansion, and in some applications their good electrical conductance may be useful. As suggested by the manufacturer, the carbon-graphite-silver material (sample 401) seemed more promising for use in timepieces than other samples (402, 403, and 404) produced by the same company. The spread in data obtained with this material on the endstone-wear testing machine indicates a lack of homogeneity in the sample; this and the relative coarseness of the structure discourage its use for very small bearings (less than 1/16-in. bore).

7.5. Miscellaneous

No material was found to be as satisfactory as diamond for use as a thrust-bearing material under conditions of high load such as occurs at the balance-shaft upper endstone in chronometers. By an X-ray diffraction test for orientation, it was found that the faces of the diamond used in the endstone-wear testing machine and the diamond endstone in chronometer 13370 were within 4° of being parallel to an octahedron (111) face (cleavage plane). The face of the endstone in chronometer 6512 was found to differ about 22° from the octahedral (111) plane. It is considered that each of these diamond endstones was very satisfactory for its intended use as a thrust bearing, even without lubrication.

No material was found to be as satisfactory as sapphire for use as pallet stones in timepieces. Sapphire appeared to be suitable for use as unlubricated endstones when the load was relatively light, especially in timepieces normally operating in an upright position. Unlubricated (clean) sapphire hole bearings (jewels) caused rapid wear or rusting of the conventional balance-staff pivots in timepieces.

Boron carbide without lubrication did not appear to be suitable for use as pallet stones or as a journal-bearing material.

Under the conditions tested, ordinary brass and bearing bronze conventionally used for making small bushings did not appear suitable for this application without lubrication.

In journal bearings, a fused coating of PTFCE plus graphite gave good resistance to wear but the friction was relatively high. A fused coating of PTFE one-coat enamel gave lower friction, but the resistance to wear was somewhat less than with the above coating. Both of these coatings (samples 609 and 611, respectively) wore rapidly when tested as thrust bearings. Because of the thickness of the coatings ordinarily used and the difficulty in making a uniform coating with a good bond on small parts, the use of coatings of this type does not seem practical for journals or bearings less than 1/16 in. in diameter. However, work at the Naval Research Laboratory [9] indicates that PTFE coatings may be useful for some applications.

The silver amalgam (sample 501) gave exceptionally low friction at room temperature. However, this material was very brittle and the edges of the hole chipped badly during the boring and reaming operations. An amalgam of dental alloy filings was also tried; it was less brittle than the silver amalgam, but the bearing gave increasingly high friction at the start of a test and scuffing of the bearing soon occurred.

Other publications that may be of interest deal with dry bearings suitable for textile mills [10], and with the frictional characteristics of plastics with and without lubrication [11].

The experimental work (mostly static friction tests) during the early part of this investigation was conducted by John Young, who left the Government service in September 1952.

8. References

[1] E. I. duPont de Nemours & Co., Tech. Serv. Bul. 13 (1949).

[2] M. W. Kellogg Company, Tech. Bul. 2–10–50.

[3] H. S. White and D. Zei, Static friction tests with various metal combinations and special lubricants, J. Research NBS **46,** 292 (1951) RP2198.

[4] F. P. Bowden and D. Tabor, The friction and lubrication of solids (Oxford Univ. Press, London, 1950).

[5] MIL–O–11734 Military Specification: Oil, lubricating, synthetic (for mechanical time fuzes).

[6] MIL–L–17353 Military Specification: Lubricating-oil, low temperature, special.

[7] MIL–G–7421 Military Specification: Grease; extreme low temperature.

[8] R. F. King and D. Tabor, The effect of temperature on the mechanical properties and the friction of plastics, Proc. Phys. Soc. (London) [B] **66,** 728 (1953).

[9] R. C. Bowers, W. C. Clinton, and W. A. Zisman, Frictional behavior of polyethylene, polytetrafluoroethylene, and halogenated derivatives, Lubrication Eng. **9,** 204 (1953).

[10] S. Ricklin and R. R. Miller, Filled Teflon for dry bearings, Materials & Methods **40,** 112 (October 1954).

[11] W. C. Milz and L. B. Sargent, Jr., Frictional characteristics of plastics, Lubrication Eng. **11,** 313 (1955).

WASHINGTON, January 31, 1956.

Journal of Research of the National Bureau of Standards Vol. 57, No. 4, October 1956 Research Paper 2710

Preliminary Spectroradiometric Measurements of the Solar Constant[1]

Ralph Stair and Russell G. Johnston

Spectroradiometric measurements of the distribution of direct solar radiation at Sunspot, New Mexico (altitude 9,200 feet), in June 1955 are described. Detailed spectral data were obtained within the spectral range of 299 to 535 millimicrons for different air masses. At longer wavelengths radiant-energy evaluations were made only for selected points between the water-absorption bands.

From these data, supplemented by other measurements and estimates for radiant-energy intensities for very short and very long wavelengths, a preliminary spectral integration of the total solar intensity yields a solar constant in general agreement with the best published values.

1. Introduction

Recent scientific advances in many fields have reached the stage where a higher accuracy in the knowledge of the intensity of the radiant energy from the sun is required. The present research has been carried out with the idea of obtaining a value of the solar constant by a method that is different from previous determinations.

During the past 30 years the Astrophysical Observatory of the Smithsonian Institution has accumulated a tremendous amount of spectral solar radiant energy data at a number of stations scattered over the world. These measurements have recently been supplemented by rocket data, which have extended the spectrum essentially to the ultraviolet cutoff of solar emission [1,2].[2]

The Smithsonian data are obtained by a method that requires a number of corrections. There is some question as to the precise value of some of these corrections [3,4,5,6,7]. Many of them result from the particular method employed in obtaining and evaluating the data [8].

In the Smithsonian work [9] the solar beam was reflected into a spectroradiometer by a metal-coated mirror whose reflectivity was subject to change with age. In measurements by this method the optical characteristics of the spectroradiometer would need to be evaluated for light reflected from various angles. It is difficult to obtain this correction with a high precision. Because an image of the solar disk was focused upon the entrance slit of the spectrometer, any attempt to evaluate the data in terms of an average value for the complete disk would be subject to doubt.

In addition, an attempt to integrate the data for the complete spectrum in absolute value was made by employing a pyrheliometer in the measurement of the total radiant energy coming through the atmosphere. This involved a number of corrections because of water vapor and other absorptions in the atmosphere, as well as assumptions regarding the spectral limits of the two instruments. Something of the magnitude of these difficulties has been indicated in the literature [4,7,10].

When we speak of the solar constant we really are discussing a variable quantity, as it is generally recognized that solar emissions vary from time to time. However, for all practical purposes, the solar constant is the mean rate at which solar radiant energy (ultraviolet, luminous, and infrared) is present (per unit area) in free space at mean solar distance. Expressed mathematically, it is the total solar radiant energy received in gram-calories per square centimeter (langleys) per minute at the earth's mean distance from the sun. The accurate measurement of this constant, as well as the evaluation of any variations[3] that may occur in its value, has great significance in many fields.

The sun is a gaseous mass having a mean surface temperature of approximately 6,000° K. To the unaided eye it appears as a smooth circular disk. Magnified, the surface appears highly granulated and surrounded by a gaseous envelope, which, when examined under suitable conditions, is found to undergo much turmoil. In any case, this outer gaseous envelope produces the Fraunhofer absorption spectrum, which modifies markedly the visible and ultraviolet spectra of the solar emission. As a result, the effective radiating layer of the sun varies with wavelength (frequency of emitted radiation). That is, the effective solar temperature may be considerably below 6,000° K in the ultraviolet, whereas it may be significantly different in the infrared. A value near 7,000° K has been estimated for the far infrared at about 24 μ [12,13]. Hence sunspots, flares, or other disturbances in the solar surface may be expected to affect significantly not only the relative spectral emission from the sun, but also the total emission—the value of the solar constant.

No mention has been made of the radio emissions from the sun. Although such exist and indicate an effective solar temperature of around 1,000,000° K [14, 15], the energies involved are insignificant when compared with the normal blackbody radiation in the heat spectrum

[1] This work was supported by the Geophysics Research Directorate of Air Force Cambridge Research Center.

[2] Figures in brackets indicate the literature references at the end of this paper.

[3] Measurements in the visible spectrum by Hardy and Giclas over a 5-year period indicated variations not exceeding 1.0 percent [11].

2. Instruments and Method

The instrumental setup (see fig. 1) employed in this work has resulted from experiences gained in connection with the measurement of the spectral distribution of the radiant energy from the sun at Washington and elsewhere during the past 5 years [16, 17, 18]. It consists primarily of a Carl Leiss double quartz-prism spectrometer mounted on a polar axis driven by a synchronous motor to follow (approximately) the path of the sun across the sky.

The use of this spectroradiometer mounted directly on a polar axis eliminates corrections previously required because of polarization effects introduced by reflections at variable angles from the heliostat mirrors and the faces of the optical components of the spectrometer. Also, optical errors introduced by improper adjustment of the heliostat or by solar declination change are no longer present. The spectrometer is simply aimed directly at the sun, which it then follows closely for hours without significant readjustment. Any departure due to changes in solar declination or to atmospheric refraction effects are detected by a photoelectric detector (also a visual indicator in the form of a directed light spot) and are corrected manually.

This spectroradiometer employs two 30-deg quartz prisms, through each of which the radiant energy makes a double pass. The collimating mirrors are spherical and coated with aluminum. The three slits are manually adjustable. The first and second slits were set for a mechanical opening of about 0.15 mm, and the third slit at 0.50 mm, for most of the data reported in the present case. With this instrument, changes in wavelength are accomplished by prism rotation, with a synchronous-motor drive attached to the wavelength drum. This unit permits recording at any one of three speeds, forward or reverse. A built-in clutch allows quick resetting of the wavelength drum, so that any part of the spectrum can be repeated at will.

The light beam was modulated at 510 cps by means of a sector disk mounted on a synchronous motor, and the output of the phototube was fed into a tuned amplifier. A strip recorder was used to register automatically the spectral data. A 935, emission-type phototube was employed as the detector in the ultraviolet and visible spectra to about 550 mμ. An Eastman lead sulfide photoconducting cell was employed at longer wavelengths, extending to about 2.6 μ, where water vapor rendered the terrestrial atmosphere opaque to solar radiation.

All principal components of the setup are commercially available, except the tuned amplifier. This was built especially with an 11-step sensitivity-control (really a 33-step control because each of the three controls is separately adjustable) so as to cover a wide range of solar intensities. Fundamentally, the circuit layout is the same as that of an instrument previously described [19]. Experience has suggested several modifications, however, that have adapted its use more closely to the present work. Chief among these are the incorporation of the special 11-step sensitivity controls, the addition of a switch to adapt the amplifier for use with lead sulfide cells, a change in grid-bias voltage of the second amplifier stage to increase linearity in response, and additional filtering in the power supply to improve plate-voltage regulation. The revised circuit diagram is given in figure 2.

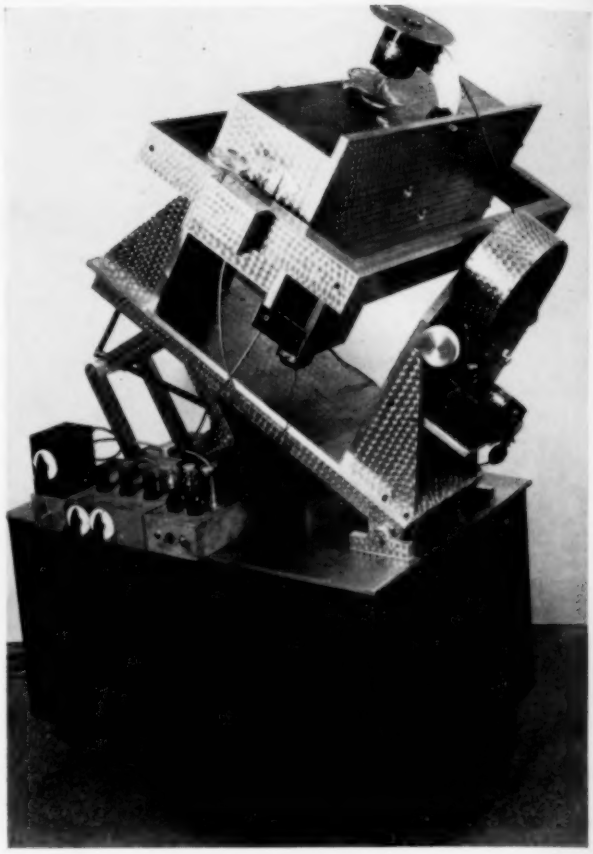

FIGURE 1. *Photograph of the spectroradiometer mounted on a polar axis.*

The instrument was set up outdoors, with the axis in a north-south direction as determined by the position of the sun at solar noon. Leveling screws at each corner of the instrument base (not shown in the photograph) made possible the precise placing of the instrument in a horizontal position. The instrument base thus furnished a level surface on which solar air-mass determinations could be made easily in terms of the shadow lengths of a cylindrical bar [20].

The operation of an instrument of this type on a polar axis is unusual but not entirely new [21]. The construction of this double monochromator lends itself to relatively satisfactory mounting in this manner, with only minor instrumental revisions, principally of increasing the spring tension holding the prisms in place. Slight flexing of the larger mirror mounts may be reduced by added adjustable bracing. The larger opening of the third slit eliminated most of the wavelength drift resulting from instrumental distortion as the spectroradiometer was rotated in following the sun.

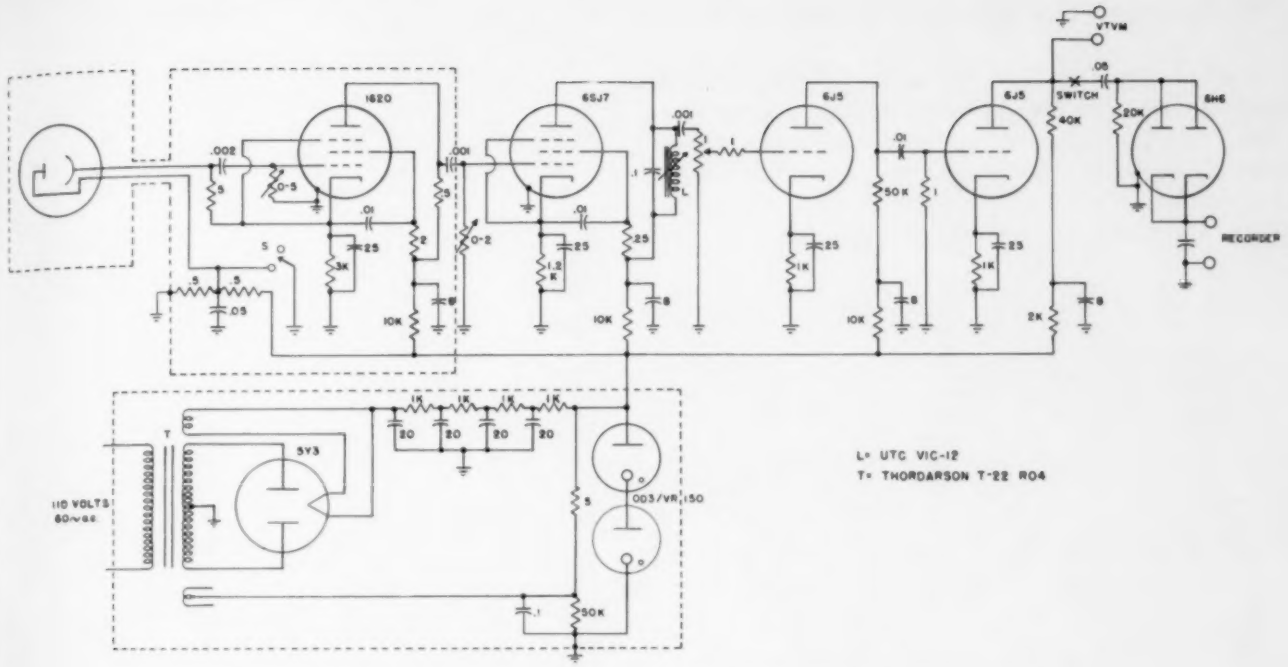

FIGURE 2. *Electronic circuit employed in 510-cycle-per-second tuned amplifier.*

Resistances in megohms and capacitances in microfarads except as otherwise noted.

Effects of instrumental temperature change were closely controlled through 24-hour operation of heating coils and a thermostat for keeping the spectrometer at a temperature near the highest point that would normally be approached in midafternoon. A housing of heavy aluminum, insulated inside with asbestos and outside with cork (not shown in the illustration), simplified temperature-variation problems. An auxiliary unit controlled the temperature of the PbS cell. No refrigeration was employed.

The wavelength scale was calibrated with a mercury-vapor lamp for the ultraviolet and visible spectra [19]. Water vapor, oxygen, and carbon-dioxide atmospheric absorption bands were employed in the infrared. The solar Fraunhofer bands furnished secondary wavelength standards and became the working wavelength references not only in recording but in the evaluation of the data.

A special tungsten-ribbon-filament-in-quartz lamp was employed in the spectral radiant-energy calibration of the entire spectroradiometer, including all the optical and electronic parts, as well as the recorder. This new lamp was more intense and more compact but otherwise similar to the standard lamps previously employed [17, 19]. The greater compactness of the lamp, together with the elimination of the heliostat, permitted the placing of the standard much closer to the entrance slit of the spectrometer, so that the calibrating intensities were increased by a factor of 10 or more above that previously possible.

Furthermore, for the spectral region of wavelengths between 296.7 and 435.8 mμ, a mercury-arc lamp was employed as a supplementary standard of radiant intensity. The relative intensities of the mercury lines from this source are known in this spectral region from laboratory measurements. The response of the spectroradiometer was calibrated from these mercury lines by normalizing their intensities against the tungsten continuum at 404.5 and 435.8 mμ.

The spectral distribution of the radiant energy of the tungsten-ribbon-filament-in-quartz lamp was established in terms of its color temperature (measured by the Colorimetry Section of the Bureau), the spectral emissivity of tungsten [4] as determined by DeVos [22], and the absolute radiant-energy output for selected wavelengths in terms of an NBS standard of thermal radiation [23, 24]. The first step of this evaluation involved the determination of the true temperature of the tungsten filament in terms of the color temperature (2,854°K, C_2=14,380) and the spectral emissivity of tungsten. A value of 2,790°K resulted from this calculation. Next, by employing blackbody data for this temperature and the spectral emissivities of tungsten (taken from the DeVos data), a relative spectral-energy curve for the tungsten-ribbon-filament was calculated. Finally, through the use of color filters the absolute radiant energy for the tungsten lamp was determined radiometrically for a number of selected spectral regions within the vicinity of some of the stronger mercury emission lines, which served as secondary radiant-intensity standards in carrying over the calibration from the thermal carbon-filament standards.

[4] It is realized that the published values of tungsten emissivity may not be precisely employed in the standardization of the particular tungsten-ribbon lamp used in this work. However, variations between different available lamps are small.

3. Spectral Solar-Energy Distribution

Most of the details relating to the reduction of the spectral distribution of the solar radiant energy (see table 1 and fig. 3) are omitted from this report. However, the methods were similar to those described in previous reports [16,17,18], for the ultraviolet and part of the visible portions of the spectrum.[5]

TABLE 1. *Spectral distribution of radiant energy from the sun for selected air masses, Sunspot, N. Mex.*

Altitude 9,200 feet. Mean for 4 days in June 1955. Radiant energy in microwatts per square centimeter per 10 mμ (corrected for mean solar distance). The M_0 factor in column 7 is the reciprocal of the atmospheric transmittance. The data in column 6, at wavelengths for which there are no entries in columns 2 to 5, are interpolations.

1	2	3	4	5	6	7	8
Wavelength	June 3 Air mass 1.00	June 4 Air mass 1.00	June 6 Air mass 1.00	June 7 Air mass 1.00	Mean Air mass 1.00	M_0 factor	I_0 Air mass 0
mμ							
299.5					5.3	45	241
300.7					11.1	34	377
302.5	16.3			16.7	16.5	18.5	306
304	40.0	36.5	42.9	43.2	40.6	11.6	472
305.5					64.3	9.00	579
306	60.0	56.2	62.7	65.6	61.1	8.20	501
309.2					112	5.39	602
310	101	98	108	105	103	4.97	514
311.3					194	4.40	852
312	180	177	190	183	182	4.13	752
314					233	3.62	843
314.9					225	3.43	772
315.8					245	3.22	789
316.5	209	213	214	208	211	3.11	658
317.9					319	2.88	920
318.5	275	272	284	274	276	2.78	769
319.8					303	2.60	788
321.1					374	2.46	921
321.7					342	2.40	821
322.8					351	2.31	811
323.5	320	320	328	321	322	2.25	725
325.5					404	2.15	867
327.5					548	2.08	1,141
328.5	524	520	526	517	522	2.06	1,075
330.3					640	2.00	1,278
331.5	588	584	579	572	581	1.96	1,139
332.9					585	1.93	1,129
333.6					573	1.91	1,094
335.3					612	1.88	1,151
337	544	543	543	534	541	1.85	1,001
340.8					686	1.78	1,220
341.7					653	1.77	1,156
343.5					696	1.745	1,214
344.1	587	586	585	577	584	1.73	1,010
348.5					666	1.69	1,125
351.5					760	1.66	1,261
352.6					710	1.65	1,171
355.1					845	1.625	1,373
358.1	597	600	608	590	599	1.60	958
360					801	1.585	1,269
360.9	739	606	751	734	730	1.575	1,150
363.6					814	1.555	1,265
366.4					987	1.53	1,509
367.8					928	1.52	1,411
370					974	1.51	1,471
373.5	769	774	778	758	770	1.48	1,139
378.2					1,085	1.46	1,583
380					968	1.45	1,403
382.3					966	1.44	1,392
384					653	1.43	932

[5] Briefly, the effect of atmospheric attenuation on solar radiation was removed by assuming the validity of Beer's law and assuming that the thickness of the atmosphere is proportional to the secant of the zenith angle, z. The "Optical Air Mass" is defined as sec z, and the data for various angles z are plotted as log I versus sec z, and the resulting straight lines are extrapolated to $z=0$, or zero air mass.

TABLE 1. *Spectral distribution of radiant energy from the sun for selected air masses, Sunspot, N. Mex.*—Continued

1	2	3	4	5	6	7	8
Wavelength	June 3 Air mass 1.00	June 4 Air mass 1.00	June 6 Air mass 1.00	June 7 Air mass 1.00	Mean Air mass 1.00	M_0 factor	I_0 Air mass 0
mμ							
387					846	1.42	1,202
391					1,086	1.40	1,521
393.4	683	689	688	680	685	1.39	952
396					955	1.375	1,314
396.9					805	1.37	1,103
403.5					1,514	1.34	2,029
406.4	1,414	1,434	1,424	1,395	1,417	1.33	1,884
410.2					1,426	1.31	1,868
416.7					1,495	1.295	1,937
420.7					1,500	1.28	1,920
423.5					1,429	1.27	1,815
427.2	1,182	1,201	1,196	1,177	1,189	1.26	1,498
432.5					1,361	1.25	1,701
438.3	1,454	1,454	1,448	1,431	1,447	1.24	1,794
440.5					1,610	1.23	1,980
450.8	1,732	1,743	1,732	1,711	1,730	1.22	2,110
455.6					1,732	1.205	2,087
465	1,725	1,740	1,709	1,694	1,717	1.19	2,043
482					1,843	1.18	2,175
487	1,702	1,711	1,694	1,675	1,695	1.175	1,992
497					1,871	1.17	2,188
500	1,851	1,856	1,843	1,813	1,841	1.17	2,154
509					1,900	1.16	2,204
518	* 1,778	1,781	1,778	1,742	1,770	1.155	2,044
527					1,892	1.15	2,175
530	1,932	1,959	1,950	1,913	1,938	1.15	2,229
535					1,865	1.15	2,145

For the spectral region from about 540 mμ to 2.5 μ covered by the lead sulfide-cell measurements a slightly different technique was required in the determination of the spectral radiant-energy emission of the sun. Although the lead sulfide cell was enclosed in a sealed brass box (constructed of massive material of thicknesses ranging from ¼ to ⅜ in.) and thermostatically controlled so that temperature and humidity conditions were relatively constant, large changes in sensitivity occurred from time to time, so that direct standard-lamp calibrations (although made several times each day) could not be relied upon. Hence, measurements at two wavelengths in the visible spectrum (428 and 487 mμ), which were repeatedly scanned every few minutes along with the infrared spectrum, were employed in establishing the energy levels throughout the infrared spectrum. In doing this it was assumed that the solar intensity at these key wavelengths remained the same during the time the work was in progress (June 3 to 19). This assumption is probably true within the limits of the experimental data [11]. Reference to table 1 indicates the small spread found in the observed intensity at these wavelengths for the 4 days upon which the infrared data are based.

Furthermore, within the infrared spectrum a number of intense water-vapor bands exist. The principal ones near 942, 1,135, 1,379, and 1,872 mμ extend over relatively wide spectral regions and have intense absorption, so that the usual variations occurring in the concentration of water vapor in the atmosphere above the Sacramento Mountains prohibited the use of any wavelengths within the immediate vicinity of these regions in the evaluation

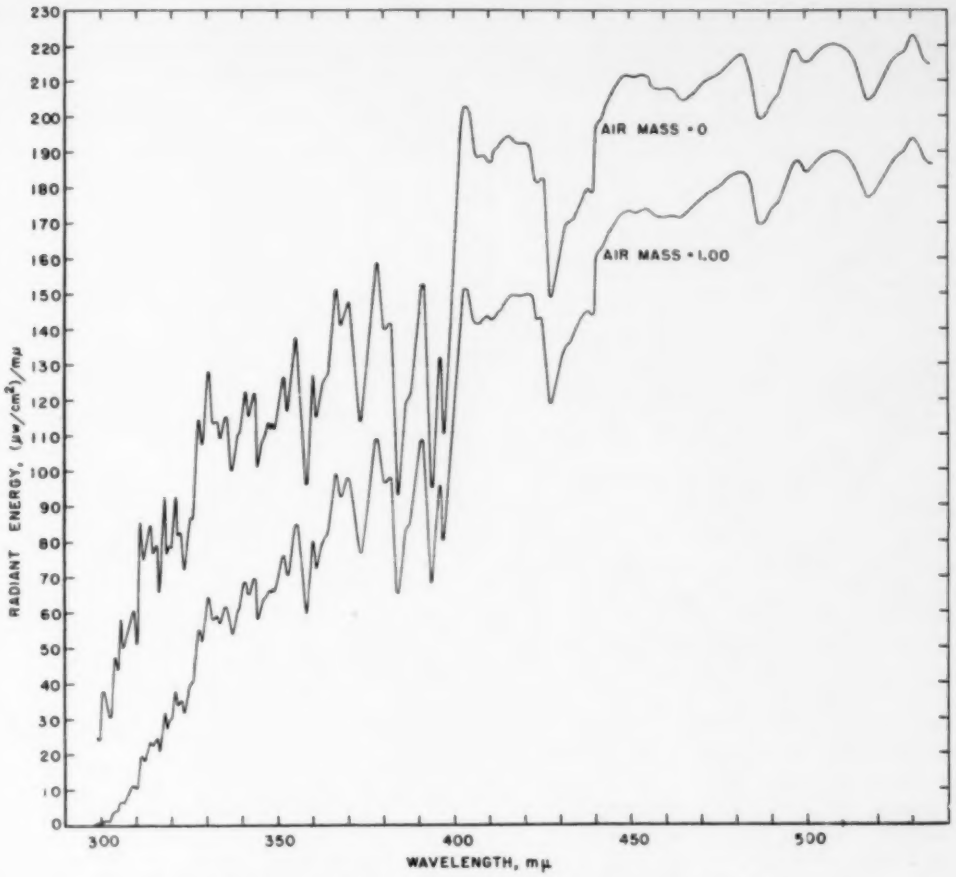

FIGURE 3. *Spectral distribution of the radiant energy from the sun.*
Sunspot, N. Mex., June 1955. (Mean of 4 days.)

of the data. Hence, it was necessary to choose a group of wavelengths that was little affected by water vapor in the extrapolations and calculations of the spectral solar radiant energy in the infrared region between the visible and 2.5 μ. Although the 4 days (June 16, 17, 18, and 19) for which the data were reduced were exceptionally dry for the location, the water-vapor absorption was very intense and therefore very sensitive to small changes in the total water content of the atmosphere. This high sensitivity to small changes in atmospheric water content has been recognized in the development of absolute humidity meters [25].

4. Atmospheric Transmittance and Ozone

The atmospheric transmission curve calculated on the basis of the data for the 4 days (June 3, 4, 6, and 7) is given in figure 4. In this illustration the logarithm of the observed transmittances of unit atmosphere has been plotted against a function of the wavelength. In order to obtain a straight line within those spectral regions in which there is no atmospheric absorption, the wavelength scale has been expanded according to the function $-(\mu-1)^2\lambda^{-4}$ of Rayleigh's law of molecular scattering [26].

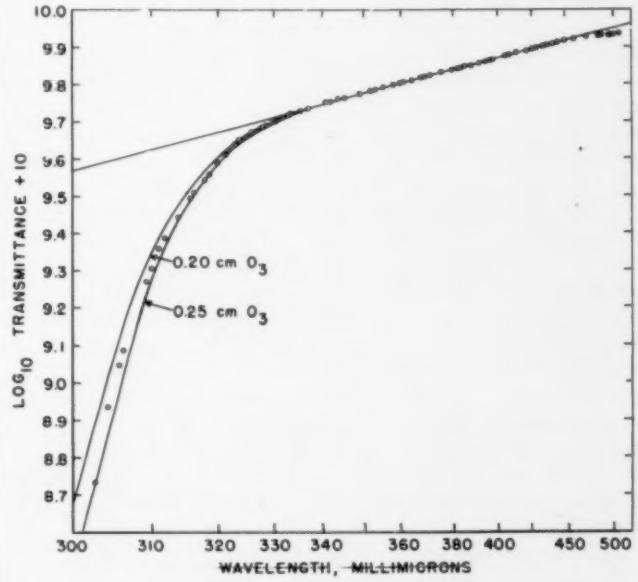

FIGURE 4. *Atmospheric transmittance at Sunspot, N. Mex., altitude 9,200 feet; also determination of total ozone above the observing station.*

Upper curve, scattering; lower curves, ozone; circles, atmospheric transmittance; air mass, 1.00; wave length scale as a function of $-(\mu-1)^2\lambda^{-4}$.

The selective absorption at wavelengths shorter than about 340 mμ is assumed to result from ozone. The amount of absorption is hence a measure of the total ozone concentration in the upper atmosphere.

In order to translate the specific absorption data in the wavelength region below 340 mμ into precise amounts of ozone, the absorption coefficients for the pure gas reported by Fabry and Buisson have been employed [27] in the calculations of the two curves (fig. 4) representing the amounts of ozone required for a similar amount of optical absorption. On the basis of these data, about 0.22 to 0.23 cm of ozone (ntp) was present at the time this investigation was in progress. This is in close agreement with previous measurements at this station for this season of the year [18, 28].

5. Evaluation of the Solar Constant

The spectral range covered in this work includes most of the solar radiant energy reaching the earth's surface. Its use in an integration of the solar emission, calculated for outside the terrestrial atmosphere for mean solar distance (per unit area), results in a radiant-energy value known as the solar constant, Q, when defined in terms of gram-calories per square centimeter (langleys) per minute.

The evaluation of Q requires three steps; first an integration of the data recorded herein (see fig. 3) for air mass 0, that is, outside the atmosphere within the limits of observation—300 to 2,500 mμ; second, a correction for mean solar distance; and third, corrections for unmeasured ultraviolet and infrared radiant energy of wavelengths shorter than 300 mμ and longer than 2,500 mμ.

The integrated values resulting as the mean for 4 days wherein measurements were made through the spectral region of 300 to 540 mμ and for the 4 days wherein measurements were made through the spectral region of about 320 to 2,600 mμ are given in table 2. These values have been increased already by 2.94 percent, the amount to correct them for mean solar distance. The correction in the ultraviolet for wavelengths below 300 has been made by arbitrarily extrapolating the solar energy curve to zero within the spectral region of about 200 to 220 mμ.[6] The infrared correction of 0.06 gram-calories per square centimeter per minute has been added as the probable value of solar radiant energy for wavelengths longer than 2.5 μ [5] based on a blackbody curve at the solar temperature. This results in a value of 2.05 gram-calories per square centimeter per minute as a preliminary measured value of the solar constant, Q, by this method. This value is probably correct to less than 5 percent and is in general agreement with recent estimates [4, 5, 18], being a little higher than those usually reported by the Smithsonian Institution.

[6] Rocket data were examined [1, 2] and guided somewhat the extent of this small correction.

TABLE 2. *Integrated spectral distribution of solar radiant energy for air mass 0*

Center of wavelength interval	Radiant energy	Center of wavelength interval	Radiant energy	Center of wavelength interval	Radiant energy
mμ	μw/cm²	mμ	μw/cm²	mμ	μw/cm²
300	1, 857	497. 5	1, 089	865	1, 005
302. 5	200	502. 5	1, 084	875	985
307. 5	279	507. 5	1, 100	885	968
312. 5	378	512. 5	1, 096	895	948
317. 5	388	517. 5	1, 043	905	930
322. 5	410	522. 5	1, 050	915	911
327. 5	521	527. 5	1, 097	925	894
332. 5	578	535	2, 113	935	876
337. 5	548	545	2, 138	945	859
342. 5	586	555	2, 113	955	842
347. 5	551	565	2, 086	965	826
352. 5	621	575	2, 053	975	809
357. 5	585	585	2, 018	985	793
362. 5	613	595	1, 982	995	778
367. 5	624	605	1, 994	1, 005	762
372. 5	665	615	1, 906	1, 015	746
377. 5	691	625	1, 868	1, 025	732
382. 5	666	635	1, 829	1, 035	718
387. 5	592	645	1, 790	1, 045	703
392. 5	623	655	1, 754	1, 055	689
397. 5	606	665	1, 707	1, 065	675
402. 5	1, 009	675	1, 662	1, 075	661
407. 5	940	685	1, 614	1, 085	646
412. 5	947	695	1, 564	1, 095	632
417. 5	972	705	1, 513	1, 150	5, 707
422. 5	929	715	1, 463	1, 250	4, 715
427. 5	818	725	1, 415	1, 350	3, 916
432. 5	869	735	1, 367	1, 450	3, 194
437. 5	923	745	1, 321	1, 550	2, 541
442. 5	1, 021	755	1, 278	1, 650	1, 951
447. 5	1, 058	765	1, 242	1, 750	1, 446
452. 5	1, 054	775	1, 213	1, 850	1, 102
457. 5	1, 049	785	1, 187	1, 950	947
462. 5	1, 050	795	1, 164	2, 050	830
467. 5	1, 027	805	1, 139	2, 150	711
472. 5	1, 035	815	1, 115	2, 250	653
477. 5	1, 061	825	1, 093	2, 350	593
482. 5	1, 072	835	1, 069	2, 450	558
487. 5	1, 000	845	1, 047		
492. 5	1, 055	855	1, 025		

Total μw/cm² for wavelengths shorter than 2,500 mμ=139,164
Total gram-calories cm⁻²/min for wavelengths shorter than 2,500 mμ=1.99
Correction for wavelengths longer than 2,500 mμ=0.06
Total value of solar constant, Q=2.05

6. Discussion of the Data

This work is a continuation of that previously initiated and has offered an opportunity to test the merits of certain changes in the original equipment [16, 17, 18]. Although on many days clouds or dust interfered with the work, there were 8 days (4 when the ultraviolet phototube was set up and 4 when the lead sulfide cell was employed) on which little interference resulted from dust or clouds. Only the data obtained on these days have been used in the reductions for the spectral-energy distributions and for the integration of the value of the solar constant, Q. This work involves radiant-energy evaluations of a highly complicated nature, so that there are numerous points at which errors or uncertainties may enter. Hence, the accuracy cannot be claimed to be better than plus or minus a few percent. However, the preliminary evaluation of the solar constant by this method indicates something of the possibilities that exist in this field. Improvements of the equipment

no doubt account for certain variations between the data recorded herein and those previously reported at Climax [17] and at Sacramento Peak [18]. Others possibly result from solar changes within the interval. Future measurements of a still higher accuracy should furnish much valuable information on the character of the solar radiation and the magnitude of its variations.

The spectral-energy values, as well as the integrated total (solar Q) intensities, are dependent very much upon the adopted values for the spectral emissivity of tungsten. Hence, if it is later found that erroneous values for the spectral emissivity of tungsten have been employed in this work, a correction to the data recorded herein will be required. Basic to the comparison of Smithsonian value of the solar constant and that here derived is the comparison of the radiometric standards used by the Bureau and the Smithsonian Scale of Pyrheliometry.

The authors express their sincere appreciation to the Geophysics Research Directorate of Air Force Cambridge Research Center for supporting this project; to members of that organization, in particular to P. R. Gast for helpful advice and other assistance; and to John W. Evans, Capt. Lewis B. C. Logan, and other members of the Upper Air Research Observatory, who made available the facilities of the Observatory and otherwise rendered valuable assistance.

7. References

[1] E. O. Hulburt, The upper atmosphere of the earth, J. Opt. Soc. Am. **37,** 405 (1947).
[2] J. L. Greenstein, H. E. Clearman, and E. Durand, Upper atmosphere studied from rockets, G. P. Kuiper, ed., The atmospheres of the earth and planets (Univ. of Chicago Press, Chicago, Ill., 1949).
[3] L. B. Aldrich and W. H. Hoover, The solar constant, Science **116,** 3 (Dec. 12, 1952).
[4] Francis S. Johnson, The solar constant, J. Meteorol. **11,** No. 6, 431 (1954).
[5] M. Nicolet, Sur le probléme de la constante solaire, Ann. astrophys. **14,** 249 (1951).
[6] C. G. Abbot, A revised analysis of solar-constant values, Smithsonian Inst. Misc. Publs. No. 3902 (1947).
[7] Evry Schatzman, Sur la valeur de la constante solaire, Ann. astrophys. **12,** 305 (1949).
[8] C. G. Abbot and L. B. Aldrich, Ann. Astrophysical Observatory of the Smithsonian Inst. **3,** 21, 73 (1913).
[9] C. G. Abbot, Ann. Astrophysical Observatory of the Smithsonian Inst. **4,** 99 (1922).
[10] M. Minnaert, The photosphere, G. P. Kuiper, ed., The Sun (Univ. Chicago Press, Chicago, Ill., 1953).
[11] R. H. Hardie and H. L. Giclas, A search for solar variation, Astrophys. J. **122,** 460 (1955).
[12] A. Adel, Selected topics in infrared spectroscopy of the solar system, G. P. Kuiper, ed., The atmospheres of the earth and planets (Univ. Chicago Press, Chicago, Ill., 1949).
[13] R. Peyturaux, Contribution a l'étude du fond continu du spectre solaire dans le Proche infra-rouge, Ann. Astrophys. **15,** 302 (1952).
[14] S. K. Mitra, The upper atmosphere (The Asiatic Society, Calcutta, 1948).
[15] A. V. Haeff, On the origin of solar radio noise, Phys. Rev. **75,** 1546 (1949).
[16] Ralph Stair, Ultraviolet spectral distribution of radiant energy from the sun, J. Research NBS **46,** 353 (1951) RP2206.
[17] Ralph Stair, Ultraviolet radiant energy from the sun observed at 11,190 feet, J. Research NBS **49,** 227 (1952) RP2357.
[18] Ralph Stair, Russell G. Johnston, and Thomas C. Bagg, Spectral distribution of energy from the sun, J. Research NBS **53,** 113 (1954) RP2523.
[19] Ralph Stair, Photoelectric spectroradiometry and its application to the measurement of fluorescent lamps, J. Research NBS **46,** 437 (1951) RP2212.
[20] Ralph Stair, The spectral radiant energy from the sun through varying degrees of smog at Los Angeles (Proceedings of the third Air Pollution Symposium, Pasadena, California, April 1955).
[21] W. W. Coblentz and H. Kahler, A new spectropyrheliometer and measurements of the component radiations from the sun and from a quartz mercury vapor lamp, BS Sci. Papers **16,** 233 (1920) S378.
[22] J. C. DeVos, The emissivity of tungsten ribbon. The tungsten striplamp as a standard source of radiation (Thesis, Univ. Amsterdam, 1953); see also, Physica **20,** 690 and 715 (1954).
[23] W. W. Coblentz, Measurements on standards of radiation in absolute value, Bul. BS **11,** 87 (1915) S227.
[24] Ralph Stair and Russell G. Johnston, Effects of recent knowledge of atomic constants and of humidity on the calibrations of the National Bureau of Standards thermal-radiation standards, J. Research NBS **53,** 211 (1954) RP2535.
[25] L. W. Foskett, N. B. Foster, W. R. Thickstun, and R. C. Wood, Infrared absorption hygrometer, Monthly Weather Rev. **81,** 267 (1953).
[26] Edison Pettit, Spectral energy-curve of the sun in the ultraviolet, Astrophys. J. **91,** 159 (1940).
[27] C. Fabry and H. Buisson, Data on ozone absorption, Compt. rend. **192,** 457 (1931).
[28] Ralph Stair, Filter radiometry and some of its applications, J. Opt. Soc. Am. **43,** 971 (1953).

WASHINGTON, April 20, 1956.

Journal of Research of the National Bureau of Standards Vol. 57, No. 4, October 1956 Research Paper 2711

Infrared Spectrum of Acetylene[1]

Harry C. Allen, Jr., Eugene D. Tidwell, and Earle K. Plyler

The spectrum of acetylene has been observed and measured under high resolution from 1,900 to 8,500 cm^{-1}. Many of the bands observed have been analyzed and precise values obtained for ν_0 and $B'-B''$. A good value of B_0 (1.17684 $\pm$ 0.00016) has been obtained by combining the results of the present work with previous data in the photographic infrared. The vibrational-energy problem is discussed.

1. Introduction

The photographic region of the infrared spectrum of acetylene was studied many years ago [1].[2] More recently, high-resolution work has been reported [2] for the region below 4,000 cm^{-1}, and in a short note [3] the band centers for many of the bands from 4,000 to 8,000 cm^{-1} have been reported. Many of the latter band centers were reported only to the nearest wave number, and no attempt was made to evaluate the constants in the vibrational-energy expression. Present spectrometers and measuring techniques make it possible to get better data and hence more precise band centers. The present investigation was undertaken in order to obtain these more precise band centers and to attempt to evaluate the constants in the expression for the vibrational energy as a function of the vibrational quantum numbers.

2. Experimental Procedure

The bands in the spectral region from 1,900 to 8,500 cm^{-1} were observed by the use of two spectrometers [4], one having a grating with 15,000 lines/in. and a lead sulfide cell as the detector, and the other instrument having a grating with 7,500 lines/in. and a cooled lead-telluride cell as the detector. In the region from 4,000 to 8,500 cm^{-1} a resolution of about 0.1 cm^{-1} was obtained, and from 1,900 to 3,500 cm^{-1} the resolution was about 0.2 cm^{-1} when a cell of 1 m was used. With a 10-m multiple-reflection cell the resolution was reduced by a factor of two. This resolution was ample to bring out all the main lines of the band and in some cases to resolve the lines of overlapping hot bands.

Examples of the spectra obtained are shown in figures 1 and 2. The figures are photographs of the recorder paper, which were obtained when the instrument was scanned over the band. The wavelengths of the lines were determined by making measurements from the superimposed fringe system and standard atomic lines. These are not shown in the figures, but details of the method of measurement have been given in a previous paper [5].

Figure 1 represents the absorption spectra in the region from 4,600 to 4,770 cm^{-1} of acetylene at a pressure of 1 atm and with a 10-m cell. Two bands have been analyzed from the rotational structure, and the assignments of the lines are shown below the spectra. The centers of the two bands occur at 4673.38 and 4722.72 cm^{-1}. Figure 2 represents the absorption spectra in the region from 5,750 to 6,000 cm^{-1}. Although the cell length was 10 m and the pressure was 1 atm, the bands are weak. There are several bands in this region, but the rotational structure was only of sufficient intensity to allow an assignment of the rotational lines for two bands. The centers of these two bands occur at 5,850.75 and 5,944.40 cm^{-1}.

3. Analysis

The bands were analyzed by the method of combinations and differences. Values of ν_0 and $B'-B''$ for each band were obtained from the expression,

$$R(J+1)+P(J)=2\nu_0+2(B'-B'')J^2.$$

As many combinations as possible were set up for each band, and the resulting equations were solved by the method of least squares. The results of these calculations for the various bands are given in table 1.

Values for B_0 and D_0 were obtained in the same manner from the expression,

$$\Delta F_2=R(J-1)-P(J+1)=4B(J+\tfrac{1}{2})-8D(J+\tfrac{1}{2})^3.$$

The value of B_0 obtained in this manner varied somewhat from band to band because of the strong overlapping of bands in all spectral regions. In order to minimize this effect, the ΔF_2 values for the six best bands were averaged, omitting all differences that depended on absorption peaks that were obviously the blend of two or more transitions. The value of B_0 determined in this manner agrees very well with the value obtained from photographic infrared bands [6]. Because the earlier workers reduced their data graphically, their results were reworked in the manner described above. The uncertainty in the B_0 value was further reduced by averaging the ΔF_2 values of Herzberg and Spinks with the values obtained in this work. These three values are compared in table 2. The uncertainties given are one standard deviation. Because of the large uncertainties and the fact that the values of $J>25$ were not used in the ground-state calculations, very little significance can be attached to the values of D_0 given in table 2.

[1] This work was supported by the Atomic Energy Commission.
[2] Figures in brackets indicate the literature references at the end of this paper.

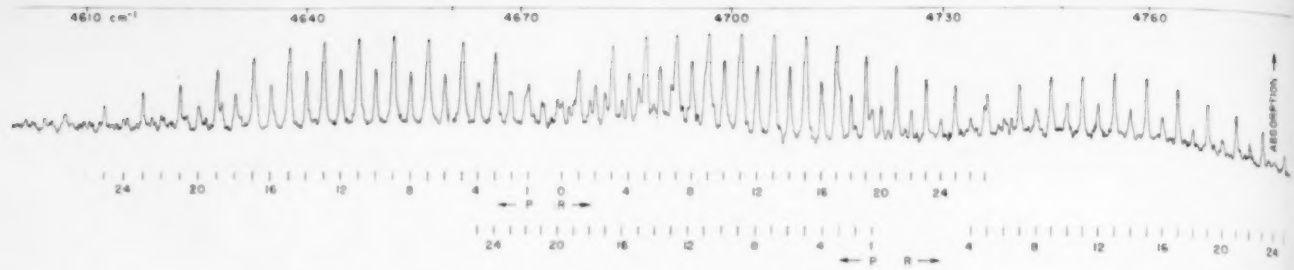

FIGURE 1. *Acetylene absorption bands at 4673.38 and 4722.72 cm⁻¹.*

The cell length was 10 m and the gas pressure was 1 atm.

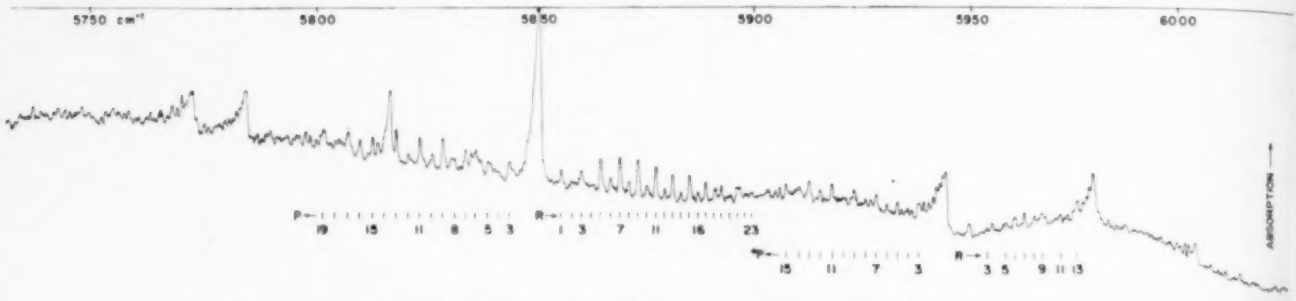

FIGURE 2. *Absorption spectrum of acetylene in the region from 5,750 to 6,000 cm⁻¹.*

The two bands with the most intense rotational structures occur at 5850.75 and 5944.40 cm⁻¹. The cell length was 10 m and the gas pressure was 1 atm.

TABLE 1. *Assignments of the observed bands of acetylene*

Observed	Calculated	D. D. Resonance	Excited v_1	v_2	v_3	v_4^l	v_5^l	Lower v_1	v_2	v_3	v_4^l	v_5^l	$B'-B''$
cm^{-1}	cm^{-1}												
	611.58					1^1							
	729.25						1^1						
1328.18 [a]	1328.18					1^1	1^1						
1940.11	1940.07					2^0	1^1						−0.00090
1973.8 [b]	1973.8			1									
2169.24	2169.15						3^1						−.00171
2560.51	2560.52					3^1	1^1						−.00892
2644.58	2644.45		1									1^1	−.01134
2670.35	2670.27				1						1^1		−.00903
2683.38	2683.42			1		1^1	1^1				1^1		−.00003
2690.78	2690.97			1			2^0					1^1	−.00329
2702.20	2702.20			1			1^1						−.00658
3281.85	3281.93				1								−.00529
3294.96	3294.98			1		1^1	1^1						−.00534
3373.7 [b]	3373.7		1										
4062.00	4062.11		1			1^1	1^1				1^1		−.00243
4068.57	4069.93		1				2^0					1^1	−.00194
4080.3	4079.89		1				2^0					1^1	−.0015
4091.20	4091.20		1				1^1						−.00704
4138.82	4138.81			1			3^1						
4673.68	4673.67		1			1^1	1^1						−.00372
4722.72	4719.45				1		2^0						−.00154
5772.99	5783.23	5771.61			2							1^1	*Q* only.
5850.75	5850.64			1	1	1^1							−.01286
5944.40	5945.06		1		1						1^1		*Q* only.
5979.37	5969.99	5981.61	2									1^1	*Q* only.
6530.00	6531.10		1		1	1^1					1^1		−.01590
6556.62	6556.62		1		1								−.01286
6623.33	6623.53		1	1		1^1	1^1						−.00924
7141.22	7142.66		1		1	1^1							−.01072
7217.6	7230.27	7217.95			2		1^1						*Q* only.
7416.51	7404.99	7417.31	2				1^1						−.01396
8512.09	8512.10		1	1	1								−.01872

[a] From reference [2]. [b] Raman lines from reference [1].

TABLE 2. *Values of B_0 and D_0 for acetylene*

	B_0	D_0
	cm^{-1}	
This work	1.17665±0.00024	$2.12\pm1.1\times10^{-4}$
Herzberg and Spinks	1.17684±0.00021	1.75±1.1
Combination of both	1.17684±0.00016	2.19±0.85

In addition to the bands for which P and R structure was observed, several Q branches were observed without P and R structure. These bands are appropriately marked in table 1. For all perpendicular-type bands, the $B'-B''$ values refer only to the effective inertial constant from the P and R branches. No Q branches were sufficiently resolved to enable the other effective inertial constant to be determined for the state involved.

4. Vibrational Energy

It is customary to express the vibrational energy in terms of the vibrational quantum numbers as

$$E_{v'}-E_0=\sum_i \omega_i^0+\sum_{ik} X_{ik}V_iV_k+\sum_i\sum_k g_{ik}l_il_k.$$

For the acetylene molecule, if there are no vibrational interactions, there are 22 constants to be evaluated. Herzberg [1] has suggested that, as in the water-vapor spectrum, states described by the quantum numbers $(v_1,v_2,v_3,v_4^l,v_5^l)$ $(v_1+2,v_2v_3-2,v_4^lv_5)$ enter into a second-order Fermi resonance. This has been investigated [7] and shown to exist. Such a resonance introduces another constant, γ, to be evaluated.

Attempts were made to evaluate these 23 constants from the observed band centers. No set of 23 constants was found that would predict all the observed bands precisely. This is not surprising because in the case of water vapor [8] it was found that one constant, γ, would not predict the correct splitting for all the resonating states. Likewise it seems likely that states characterized by the quantum numbers, $[v_1,\ v_2,\ v_3,\ v_4^l,\ v_5^l]$ and $[v_1,\ v_2,\ v_3,\ (v_4+2)^l,\ (v_5+2)^l]$, also interact resonance-wise. All these complications make it quite difficult to get a unique set of constants for the energy expression. The set given in table 3 predicts the bands below 8,500 cm^{-1} as shown in table 1. No claim is made that these are unique, for several other sets are nearly as good. These constants do not predict the photographic bands nearly as well. The values of ω_4^0, X_{44}, g_{44} do not agree well with those found in the ultraviolet [9].

From the several difference bands observed, values of ν_4^1 and ν_5^1 have been obtained. The frequency for $\nu_4^1+\nu_5^1$ used to evaluate these constants was obtained from reference [2] and the Raman frequencies from reference [1].

Because of the serious problem of overlapping bands, one cannot place too much faith in the $B'-B''$ values obtained from the analyses. As a result, no α values are given.

TABLE 3. *Vibrational constants of acetylene (cm^{-1})*

ω_1^0=3397.78	$X_{11}=-24.08$	$X_{12}=-16.94$	$X_{13}=-99.01$	$X_{14}=-16.46$
ω_2^0=1981.72	$X_{22}=-7.92$	$X_{23}=-1.38$	$X_{24}=-6.15$	$X_{25}=-0.85$
ω_3^0=3307.62	$X_{33}=-25.69$	$X_{34}=-9.06$	$X_{35}=-5.73$	$X_{15}=-11.75$
ω_4^0= 607.28	$X_{44}=5.38$	$X_{45}=-12.65$	$g_{44}=1.10$	$g_{55}=2.49$
ω_5^0= 729.03	$X_{55}=-2.27$	$\gamma=49$		

Several regions could not be investigated because of atmospheric absorption. Several important bands could thus not be observed. It is felt that when these bands are available some improvement can be made in the vibrational constants.

The authors thank Joseph Cameron for carrying out the least-squares reductions on SEAC.

5. References

[1] For comprehensive review of early work, see G. Herzberg, Infrared and Raman spectra of polyatomic molecules (D. Van Nostrand Co., Inc., New York, N. Y., 1945).
[2] E. E. Bell and H. N. Nielsen, J. Chem. Phys. **18,** 1382 (1950).
[3] R. M. Talley and A. H. Nielsen, J. Chem. Phys. **18,** 680 (1950).
[4] Earle K. Plyler, L. R. Blaine, and W. S. Connor, J. Opt. Soc. Amer. **45,** 102 (1955).
[5] Earle K. Plyler, L. R. Blaine, and Eugene D. Tidwell, J. Research NBS **55,** 279 (1955) RP2630.
[6] G. Herzberg and J. W. T. Spinks, Z. Physik **91,** 386 (1934).
[7] N. M. Nordin and R. N. H. Haslam, Can. J. Res. [A] **26,** 279 (1948).
[8] W. S. Benedict, N. Gailar, and Earle K. Plyler, J. Chem. Phys. **24,** 1139 (1956).
[9] K. K. Innes, J. Chem. Phys. **22,** 863 (1944).

WASHINGTON, April 20, 1956.

Journal of Research of the National Bureau of Standards Vol. 57, No. 4, October 1956 Research Paper 2712

Variation of Peak Temperature With Heating Rate in Differential Thermal Analysis

Homer E. Kissinger

In differential thermal analysis, the temperature at which the maximum deflection is observed varies with heating rate for certain types of reactions. An expression can be derived relating this variation with the kinetics of the reaction. By making a number of differential thermal patterns at different heating rates, the kinetic constants can be obtained directly from the differential thermal data.

Measurements of the variation of peak temperature with heating rate have been made for several minerals of the kaolin group, the values of the kinetic constants determined, and these values compared with corresponding values obtained for both the same samples and similar material by conventional isothermal techniques. Some factors affecting the results are discussed.

1. Introduction

The method of differential thermal analysis (DTA) has been universally accepted by mineralogical laboratories as a rapid and convenient means for recording the thermal effects that occur as a sample is heated. Changes in heat content of the active sample are indicated by deflections shown by a line representing the differential temperature. It is conventional to represent an endothermic effect by a negative deflection and an exothermic effect by a positive deflection. The deflections, whether positive or negative, are called peaks.

The factors responsible for the size, shape, and position of the resulting peaks are not well understood. Often the temperature of maximum deflection, or peak temperature, is considerably higher than the known transition or decomposition temperature of the substance. The peak temperature is also markedly affected by changes in technique [1].[1] Only in the case of crystalline inversions (transitions occurring instantaneously at a fixed temperature), has there been a satisfactory explanation of the DTA peaks [2].

The work of Murray and White [3, 4, 5] on the kinetics of decomposition of clay minerals can be applied to the interpretation of the DTA patterns of these materials. These workers measured the rates of isothermal dehydration of clays, calculated the kinetic constants of the materials, and from these data constructed curves of reaction rate versus time for constant heating rates. These artificial curves were similar in shape to DTA curves, the temperatures of maximum reaction rate were very close to the peak temperatures observed in DTA, and these temperatures varied in the same manner with heating rate for both the calculated and the observed curves. Later Sewell [6] found that the peak temperatures of DTA patterns made at different heating rates were predicted fairly closely by the equation of Murray and White.

According to the equation derived by Murray and White, the temperature of maximum deflection is defined by the kinetic constants of the material and the heating rate. The assumption that the peak temperature occurs when the reaction rate is a maximum is supported by the experimental work described above. It should then be possible to calculate the kinetic constants directly from DTA data by making a number of patterns at different heating rates. The series of experiments to be described was performed to verify the equation of Murray and White and to apply it to the determination of kinetic constants from DTA data.

[1] Figures in brackets indicate the literature references at the end of this paper.

2. Preliminary Theory

Murray and White [3] and Vaughan [7] reported that the thermal decomposition of clays obeyed a first-order law. At constant temperature,

$$\left(\frac{\partial x}{\partial t}\right)_T = k_T(1-x), \tag{1}$$

where x is the fraction of material decomposed. The magnitude of the rate constant, k_T, is determined by the temperature and is given by the Arrhenius equation

$$k_T = Ae^{-\frac{E}{RT}}, \tag{2}$$

where R is the gas constant, T is the Kelvin temperature, and A and E are constants that are properties of the material. The constant E, called the activation energy, is often interpreted as the energy barrier opposing the reaction. The constant A, most often called the frequency factor, is a measure of the probability that a molecule having energy E will participate in a reaction.

When the temperature is changing with time, the reaction rate is

$$\frac{dx}{dt} = \left(\frac{\partial x}{\partial t}\right)_T + \left(\frac{\partial x}{\partial T}\right)_t \frac{dT}{dt}. \tag{3}$$

The rate of change of x with temperature, with the time coordinate fixed, $(\partial X/\partial T)_t$ is zero, because fixing the time also fixes the number and position of the

particles constituting the system. The only effect of an instantaneous change in temperature is in the velocity of thermal motion of the particles. The total rate of reaction may then be expressed,

$$\frac{dx}{dt}=A(1-x)e^{-\frac{E}{RT}}. \tag{4}$$

This expression holds for any value of T, whether constant or variable, so long as x and T are measured at the same instant.

When the reaction rate is a maximum, its derivative with respect to time is zero. Solving eq (4) for $(d/dt)(dx/dt)$:

$$\frac{d}{dt}\left(\frac{dx}{dt}\right)=\frac{dx}{dt}\left(\frac{E}{RT^2}\frac{dT}{dt}=Ae^{-\frac{E}{RT}}\right). \tag{5}$$

The maximum value of dx/dt occurs at temperature T_m, defined by

$$Ae^{-\frac{E}{RT_m}}=\frac{E}{RT_m^2}\frac{dT}{dt}. \tag{6}$$

This is the equation derived by Murray and White [5].

From eq (6) it is easily seen that

$$\frac{d\left(\ln\frac{\phi}{T_m^2}\right)}{d\left(\frac{1}{T_m}\right)}=-\frac{E}{R}, \tag{7}$$

where $\phi=dT/dt$, the heating rate.

3. Experimental Procedure

3.1. Materials

The clay minerals of the kaolin group have been the predominant materials used in previous studies of the relation of chemical kinetics and DTA. For this reason, this group has been used in the present study.

Three kaolinite samples, designated A, B, and C, were chosen. Kaolinite A was a Florida kaolinite, whereas B and C were from Georgia. Examination with the electron microscope showed that kaolinites B and C consisted of well formed hexagonal plates with sharply defined edges. The particles of kaolinite A were smaller, thicker in proportion to their breadth, and less well defined in outline. Impurities were almost nonexistent in all three kaolinites. X-ray examination showed all three to be well crystallized, with very little *b*-axis disorder of the type described by Brindley and Robinson [8].

Two samples of halloysite were chosen, one from Eureka, Utah, and one from Bedford, Ind. These materials were described by Kerr and Kulp [9]. The Indiana material was designated by the symbol H–12, the Eureka material by H–13. This identification was retained for the present study. Both halloysites contained appreciable amounts of impurities, principally gibbsite and quartz.

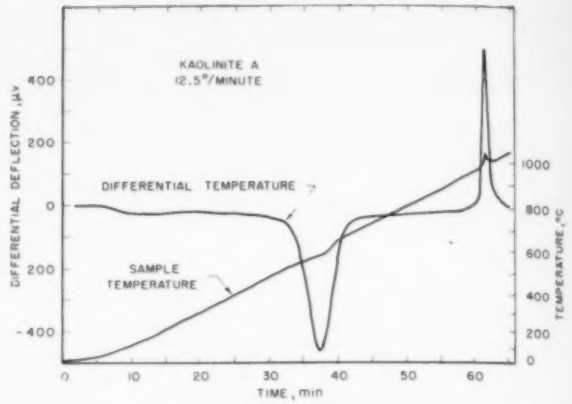

FIGURE 1. *A typical differential-thermal-analysis pattern of a kaolinite clay.*

The endothermic peak in the region 500° to 700° C results from the loss of hydroxyl groups from the structure. The position, and the height, of the peak vary with heating rate.

3.2. Apparatus and Procedure

The differential-thermal-analysis apparatus used in this work consists of a vertical platinum-wound furnace and the associated controlling and recording equipment. Specimen holders are platinum tubes, made of 20-mil Pt sheet. Two sizes of specimen holders are available, one pair being ⅜ in. in diameter by 1¼ in. long, the other ⅛ in. in diameter and ½ in. long. Platinum-platinum 10-percent-rhodium thermocouples made of 15-mil wire are used.

The furnace temperature is controlled by a cam-driven program controller. A current interrupter in the cam-motor circuit allows any heating rate up to about 25 deg C/min to be selected by the operator.

The differential temperature is measured between the centers of the active and the reference sample. The reference material is α-aluminum oxide. The sample temperature and the differential temperature are recorded on the same chart by a multipoint recorder. A typical pattern is shown in figure 1.

Each of the five sample materials was run in DTA in the ⅜-in. holders at about 3, 4.5, 6, 10, 12.5, and 20 deg C/min. The 20 deg/min rate was not used with the ⅛-in. holders.

Isothermal weight-loss determinations were made with the NBS recording analytical balance [10]. A platinum crucible, suspended in the furnace from one side of the balance, contains the sample. The loss in weight is recorded continuously while the furnace temperature is held constant. In the present study, weight-loss determinations were made at 450°, 500°, 550°, and 600° C for each material. Approximately 1 g of sample was used for each determination. Reaction-rate constants were calculated at each temperature by the method described by Murray and White [3]. Kinetic constants were then calculated by graphical solution of eq (2).

4. Results and Discussion

The isothermal weight-loss data verified the first-order law (eq 1) for the three kaolinites. The halloysite decomposition did not obey the first-order

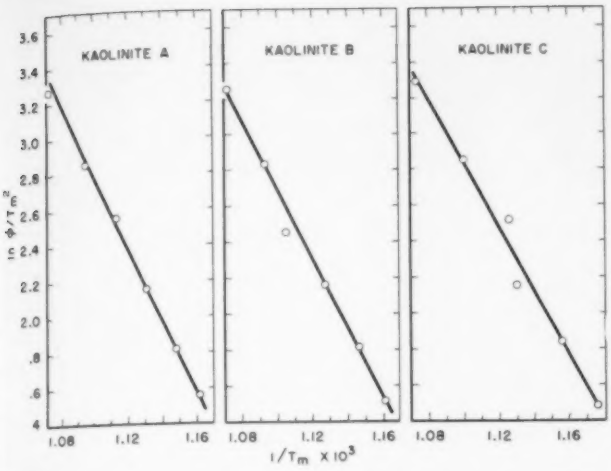

FIGURE 2. *Differential-thermal-analysis data obtained for the kaolinites in the ⅜-in. specimen holder, plotted to determine E/R.*

equation at the higher temperatures. Although other workers [3, 7] have reported that halloysite decomposes according to the first-order law, the present work indicates that this is true only at low temperatures and low reaction rates. Trial-and-error attempts to determine the reaction order were but partially successful, indicating that the order became less than unity at more rapid reaction rates.

Activation energies and frequency factors were calculated for the kaolinites from the isothermal data. It was not possible to obtain these constants from the data for the halloysites. The values of A and E for the kaolinites are given in table 1. Some values reported by other workers are shown for comparison.

The values of A and E for kaolinite vary from sample to sample. In general, the well-crystallized kaolinites have activation energies in the range 38 to 45 kcal/mole, whereas the less well ordered forms, the fireclays, give values of E down to 30 kcal/mole or less. Halloysite, with the same composition and only slightly different in structure from kaolinite, is reported [3, 7] to have activation energies slightly lower than those of well-crystallized kaolinites.

TABLE 1. *Values of activation energy E and frequency factor A determined isothermally for kaolin minerals*

Source	Material	E	$\log_{10} A$
		kcal/mole	
Present work	Kaolinite A	42.06	8.66
	Kaolinite B	37.20	6.86
	Kaolinite C	38.81	7.10
Murray and White [4]	Supreme kaolin	44.83	9.07
	K. plastic kaolin	36.69	6.96
	Newton Abbot	40.66	7.98
	Raw bottle clay	38.99	7.56
	Eureka halloysite	36.74	6.90
Vaughan [7]	China clay 1	40.61	9.83
	China clay 2	38.10	9.26
	Fireclay 1	25.75	6.01
	Fireclay 2	26.30	6.26
	Halloysite	34.90	8.45

In differential thermal analysis, the temperature at which the peak deflection occurs for a given heating rate is determined by both A and E (eq 6). If the heating rate is changed, the peak temperature is changed. The variation of peak temperature with heating rate is governed only by the activation energy, E (eq 7). Plotting $\ln \phi/T_m^2$ versus $1/T_m$, as indicated by eq (7), should give a straight line of slope $-E/R$.

The results of the DTA experiments with the ⅜-in. holders are given in table 2, a. It was found that reproducibility of peak temperatures at a given heating rate was improved by loading the sample loosely into the holder, with no packing other than gentle tapping around the outside of the holder. The standard deviation of an individual measurement was found to be 2.6 deg C, calculated from 25 pairs of duplicate determinations [11]. The data for the three kaolinites, plotted as indicated by eq (7), is shown in figure 2.

The slope of the line and the standard deviation of the points about the line are readily calculated [11]. For purposes of calculation, $1/T_m$ was taken as the dependent variable. The standard deviation in $1/T_m$ was converted to a standard deviation in T_m by the relation $\Delta(1/T)=\Delta T/T^2$, taking T as 800° K. The standard deviations of the observed peak temperatures from the predicted temperatures are: for kaolinite A, 2.2 deg C; kaolinite B, 2.0 deg C; kaolinite C, 3.7 deg C; halloysite H–12, 1.3 deg C and halloysite H–13, 1.0 deg C. These values are equal within acceptable limits to the standard deviation of a single determination, 2.6 deg C.

The slopes of the lines are used to determine the energy of activation, E. When E is known, A can be calculated from eq (6). The values of A and E determined in this manner are given in table 3.

The values of E determined by this method are from 3 to 8 percent lower than those determined isothermally. The values of $\log_{10} A$ are also lower.

TABLE 2. *Differential-thermal-analysis measurements*

Heating rate,[a] ϕ	Peak temperature				
	A	B	C	H–12	H–13
a. ⅜-in. holders					
deg C/min	°C	°C	°C	°C	°C
20	660	665	659	641	640
12.5	640	642	635	629	629
10	625	632	615	616	614
6	611	614	611	603	597
4.5	598	599	592	588	583
3	588	584	574	582	568
b. ⅛-in. holders					
12.5	557	563	544	553	553
10	549	553	530	547	542
6	537	538	520	530	533
4.5	525	528	511	519	517
3	514	523	499	512	508

[a] Heating rates given are nominal values. The actual rates were measured individually for each pattern and varied slightly from pattern to pattern.

TABLE 3. *Values of activation energy E and frequency factor A determined by differential-thermal-analysis method*

Material	In ⅜-in. holder		In ⅛-in. holder	
	E	$\log_{10} A$	E	$\log_{10} A$
	kcal/mole		*kcal/mole*	
Kaolinite A	38.83	7.05	40.91	8.54
Kaolinite B	36.00	6.28	35.98	7.14
Kaolinite C	34.97	6.11	35.79	7.33
Halloysite H-12	38.01	6.91	38.07	7.82
Halloysite H-13	36.10	6.49	35.85	7.22

This discrepancy may be due to the temperature gradient across the sample. The thermocouple at the center of the sample indicates a temperature different from that of the bulk of the sample. To reduce this temperature difference to a minimum, samples of the kaolinites were diluted 1:4 with α-Al_2O_3. When the DTA results were plotted, it was found that in some cases the points fitted a straight line, but that activation energies much larger than those found for the undiluted samples were indicated. For kaolinite C, figure 3, the standard deviation of the points from a straight line was 11 deg C, much too large to be accounted for by the experimental error.

In a further attempt to reduce the temperature difference between the center and the bulk of the sample, the experiments were repeated with undiluted samples, using the ⅛-in. specimen holders. Reproducibility was about the same as for the larger

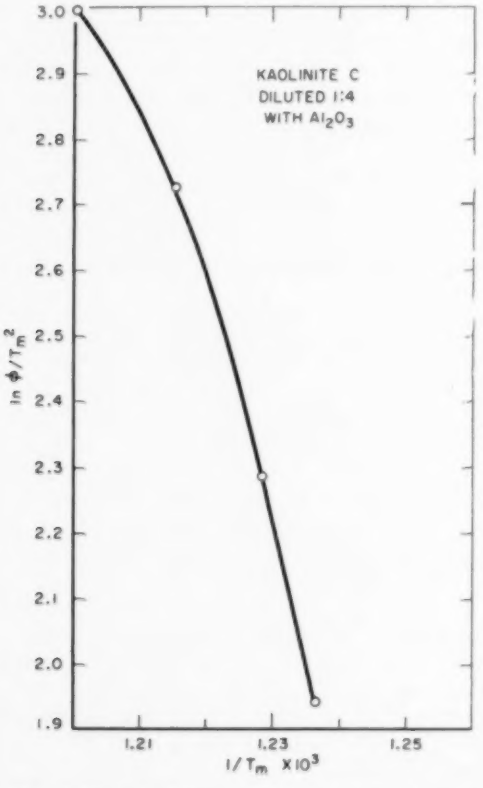

FIGURE 3. *Differential-thermal data for a specimen containing a 1:4 mixture of clay and alumina.*

holders, the standard deviation being 2.2 deg C. The results obtained at the 20 deg C/min rate were occasionally erratic, the decomposition proceeding so rapidly that some of the powdered sample was forced from the holder. This was not observed to occur with the larger holders.

Results of DTA measurements using the smaller holders are given in table 2,b. The peak temperatures are from 60 to 80 deg C lower than those obtained at corresponding heating rates in the large holders. An undetermined part of this difference is the result of the modifications to the thermocouple assembly necessary to accommodate the smaller holders. Calculated as before, the standard deviations were, for the five samples, 1.2, 1.9, 1.6, 2.5, and 2.4 deg C. The values of E and A obtained from these data are given in table 3.

In table 3 it can be seen that the values of E are only slightly different, for data obtained with the two specimen-holder sizes. The values of E obtained by the DTA method are somewhat lower than those determined isothermally, however, whereas the values of $\log_{10} A$ obtained with the ⅛-in. holder are virtually identical with the isothermal values.

The approximate precision of the DTA method can be calculated. In the present case, the standard deviation of a single measurement is 2.2 deg C. The order of magnitude of the quantities encountered is 40 kcal for E and 800° K for T_m. For the five heating rates used with the ⅛-in. holders (table 2), the standard deviation in E is about 2.4 kcal. The value of $\log_{10} A$ depends on the magnitude of the peak temperature, which varies with the technique used.

Setting confidence limits equal to twice the standard deviation, this method of determining E should give values within ± 5 kcal, or about 12 percent, for five heating rates between 3 and 12½ deg C/min. Considering the narrow range of temperature that is used, it is not surprising that this method is no more precise. The agreement of the DTA results with the isothermal results, within the limits of precision, is considered confirmation that, for reactions that proceed at a rate varying with temperature, eq (7) correctly describes the variation of peak temperature with heating rate in differential thermal analysis. The lack of agreement in the case of diluted samples can not be explained. The same effect was observed by Sewell [6], who attributed the discrepancy to variations in the partial pressure of the evolved gas within the reacting sample.

5. References

[1] J. A. Pask and M. F. Warner, Differential thermal analysis methods and techniques, Bul. Am. Ceram. Soc. **33,** 168–175 (1954).

[2] H. T. Smyth, Temperature distribution during mineral inversion and its significance in differential thermal analysis, J. Am. Ceram. Soc. **34,** 221–224 (1951).

[3] P. Murray and J. White, Kinetics of the thermal dehydration of clays, Trans. Brit. Ceram. Soc. **48,** 187–203 (1949).

[4] P. Murray and J. White, Kinetics of the thermal decomposition of clay. 2. Isothermal decomposition of clay minerals, Trans. Brit. Ceram. Soc. **54,** 151–187 (1955).

[5] P. Murray and J. White, Kinetics of the thermal decomposition of clay. 4. Interpretation of the differential thermal analysis of clays, Trans. Brit. Ceram. Soc. **54,** 204–237 (1955).
[6] E. C. Sewell, The consequences for differential thermal analysis of assuming a reaction to be first order, Clay Minerals Bul. **2,** 233–241 (1955).
[7] F. Vaughan, Energy changes when kaolin minerals are heated, Clay Minerals Bul. **2,** 265–274 (1955).
[8] G. W. Brindley and K. Robinson, Randomness in the structures of kaolinitic clay minerals, Trans. Faraday Soc. **42***b*, 198–205 (1945).
[9] P. F. Kerr and J. L. Kulp, Reference clay localities: United States, Prelim. Rep. No. 2, Am. Petroleum Inst. Proj. 49, Columbia Univ. (1949).
[10] F. A. Mauer, An analytical balance for recording rapid changes in weight, Rev. Sci. Inst. **25,** 598–602 (1954).
[11] W. J. Youden, Statistical methods for chemists, p. 45 (John Wiley & Sons, Inc., New York, N. Y., 1951).

WASHINGTON, June 8, 1956.

Journal of Research of the National Bureau of Standards Vol. 57, No. 4, October 1956 Research Paper 2713

Mass Spectrum of Sulfur Vapor

Paul Bradt, Fred L. Mohler, and Vernon H. Dibeler

The mass spectrum of sulfur vapor has been measured by evaporating sulfur from a heated tube directly into the ionization chamber of a mass spectrometer. Ions S_x^+ with x ranging from 1 to 8 are observed with S_2^+ most abundant. Isotope abundances were computed from the S_x^+ ions. The appearance potentials of S_8^+ and S_2^+ are respectively 8.9 ± 0.2 and 8.3 ± 0.2 electron volts. This suggests that the vapor in the ionization chamber is a mixture of molecules containing S_2 and S_8 and possibly other molecules.

1. Introduction

The mass spectrum of sulfur vapor has been studied in connection with a program to establish reference samples of natural isotopic abundance [1].[1] While one objective of this study was to check the isotope ratios and the chemical purity of the reference sample, the mass spectrum and the appearance potentials are of research interest. The molecular weight of sulfur vapor indicates that the vapor in equilibrium with sulfur at 175° C is predominantly S_8 [2]. This is a relatively unstable configuration, and in the presence of an electric discharge an S_2 band spectrum is observed [3]. The vibration series and predissociation spectra give with some uncertainty a value of 4.4 ev for the S_2 bond energy, indicating that S_2 is quite stable.

2. Experimental Procedure

The sulfur from the reference-sample stock is virgin sulfur from a dome in Wharton County, Tex. The sulfur-vapor pressure is too small to measure the mass spectrum at room temperature, and the measurements were made by evaporating the sulfur from a heated tube into the ionization chamber of a 60° mass spectrometer. A few milligrams of coarse powder were held in a capillary tube with a thermocouple in contact with the tube. This in turn was in a 6-mm tube, which extended about 2 cm to the entrance port of the ionization chamber. The ionization chamber reached a temperature of 186° C during operation, and the sample attained a steady temperature of 94° C by heat conduction and radiation. This proved to be a convenient temperature for recording the spectrum.

Sulfur dioxide was made by burning the sulfur in air, and the mass spectrum of SO_2 and the air oxygen was measured with a 180° gas-analysis mass spectrometer. This is the conventional method of measuring sulfur-isotope abundances.

[1] Figures in brackets indicate the literature references at the end of this paper.

3. Results

3.1. Mass Spectrum

Table 1 gives the principal ions observed in the mass spectrum of sulfur vapor. Column 3 gives the relative abundance of the ions S_x^{32}, whereas column 4 gives the monoisotopic spectrum. It is the sum of the isotope peaks in each S_x group relative to the S_2 ions taken as 100. The rather complicated isotope structure identifies all these ions as predominantly singly charged ions, except for the following: Mass 16 from S^{++} was 0.05 percent of the 64 peak in a spectrum where O^+ from O_2 and CO_2 was negligible. Mass 32½ from $S^{32}S^{33++}$ was 0.06 percent of the 64 peak, and is about 4 percent of the 65 peak. Hence, doubly charged ions of mass 64 contribute 4 percent to the 32 peak. A peak at mass 80 from S_5^{++} is 0.06 percent of the 64 peak.

Impurities that can be ascribed to the sulfur rather than the mass-spectrometer background are volatile gases, which decrease with time. H_2S^+ ranged from 1.2 to 0.15 percent of the 64 peak, and CS_2^+ was 0.13 to 0.07 percent. A 48 peak ranging from 0.17 to 0.02 percent may be SO^+ from SO_2. The molecule ion masked by S_2^+ would be about twice the SO^+ peak.

TABLE 1. *Mass spectrum of sulfur vapor*

m/e	Ion	Relative intensity	Monoisotopic spectrum
32	S^{32}	13. 5	12. 8
64	S_2^{32}	100. 0	100. 0
96	S_3^{32}	4. 7	5. 0
128	S_4^{32}	8. 1	9. 0
160	S_5^{32}	5. 2	6. 1
192	S_6^{32}	3. 2	3. 9
224	S_7^{32}	0. 33	0. 43
256	S_8^{32}	5. 4	7. 3

3.2. Isotope Ratios

Sulfur has four isotopes of abundance S^{32}, 95.0; S^{33}, 0.76; S^{34}, 4.2; S^{36}, 0.014 (see table 2). The relative intensity of the isotope peaks in a molecule containing x atoms can be expressed formally by means of the x power of the expression,

$$S^{32}+a_1S^{33}+a_2S^{34}+a_3S^{36},$$

where the a's are abundances relative to that of S^{32} as unity, but the S terms are chemical symbols, not algebraic terms. Thus the isotopes of S_2 give the terms:

$$S^{32}S^{32}+2a_1S^{32}S^{33}+2a_2S^{32}S^{34}+a_1^2S^{33}S^{33}+2a_1a_2S^{33}S^{35}+$$

$$2a_3S^{32}S^{36}+a_2^2S^{34}S^{34}+2a_1a_3S^{33}S^{36}+2a_2a_3S^{34}S^{36}+a_3^2S^{36}S^{36}.$$

Collecting terms of equal-mass numbers gives the relative intensities of the S_2 ions as listed in column 2 of table 2. Because of intensity and resolution, the S_2 ions are best adapted to deriving isotope ratios, and mass peaks 64, 65, 66, and 68 were used to determine a_1, a_2, and a_3. Five successive slow scans of the S_2 peaks under steady conditions gave the relative intensities listed in column 3, where uncertainties listed are the maximum spread of the data. In these measurements the 64 peak was about 5,600 scale divisions on the most sensitive scale, and a small drift in the 64-peak height was corrected by a linear interpolation to the positions of the measured peaks on the record. The fourth column gives the derived relative abundances.

TABLE 2. *Isotope abundances and relative intensities of S_2 ions*

m/e	Relative intensities	Observed intensities	Derived ralative abundances
64	1	1	
65	$2a_1$	0.01596 ± 7	$a_1=0.00798\pm4$
66	$2a_2+a_1^2$	$.08897\pm20$	$a_2=0.04445\pm20$
67	$2a_1a_2$		
68	$2a_3+a_2^2$	$.00228\pm2$	$a_3=0.00015$
69	$2a_1a_3$		
70	$2a_2a_3$		
72	a_3^2		

Table 3 gives percentage abundances from data of table 2 and values derived from the mass spectrum of SO_2 made from this sulfur. The correction for O_2 isotopes was based on measurements of the air oxygen used in making SO_2. The table also includes published values from SO_2 spectra.

The S_2 ions are not favorable for the computation of a_3, for the contribution of $2a_3$ to the 68 peak is only 15 percent of the a_2^2 term. A source of uncertainty in evaluating a_1 from the 65 peak arises from the possibility that a trace of $S_3^{32}S^{34++}$ may be present. The comparative values of table 2 give no evidence of this.

TABLE 3. *Sulfur-isotope abundances*

	Mass number			
	32	33	34	36
S_2^+(sulfur vapor)	95.0	0.76±0.004	4.22±0.01	0.014
SO_2 (same sulfur)	95.0	.77±.01	4.23±.07	
Nier [5]	95.1	.74±.02	4.20±.1	.016±.0016
Thode [6] sulfur from same region			4.293	

3.3. Appearance Potentials

Some measurements of appearance potentials were made to see whether or not S_2^+ was a fragment ion from S_8 ionization. The experimental conditions were not well adapted to accurate measurements. The ion-repeller voltage was kept rather high to maintain sensitivity, and there were irregularities in the current-voltage curves that may come from surface charges on adsorbed sulfur. Mercury vapor was introduced with the sulfur vapor, and the appearance potentials of sulfur ions were measured relative to that of Hg^+ (spectroscopic value 10.34 ev) [4]. Measurements are based on semilog plots, with current plotted on a scale to make the ion current at 50 v unity. Values of the appearance potentials at an ordinate of 0.003 of the current at 50 v are: S_8^+ 8.9±0.2 ev and S_2^+ 8.3±0.2 ev. Variations in the slopes of the current-voltage curves give some added uncertainty. Some measurements on S^+ indicate an appearance potential roughly 2 v higher than S_2^+ and S_8^+. A search for negative ions gave negative results, but there was no basis to appraise the sensitivity for negative-ion detection.

4. Discussion

The fact that the appearance potential of S_2^+ is somewhat less than that of S_8^+ suggests that S_2 molecules are present and 8.3 ev is the ionization potential of S_2. Ionization resulting in a pair of positive and negative ions could give fragment ions at an appearance potential less than the ionization potential of the S_8 molecule, but there is no evidence that this occurs. As vapor in the ionization chamber is at a pressure less than 10^{-4} mm and at a temperature of 186° C, dissociation of S_8 into the relatively stable S_2 molecule is not unexpected. The mass spectrum of sulfur vapor given in table 1 is probably to be interpreted as the spectrum of a mixture of molecules.

The appearance potentials are unexpectedly low. Smyth and Blewett [7] reported an appearance potential of 10.7±0.3 ev for S_2^+ from thermally dissociated CS_2, as compared with 8.3 ev found in this work. An ionization potential of S_2 lower than that observed by Smyth and Blewett is suggested by analogy with O_2. The ionization potential of O is 13.61 ev [4] and that of O_2 is 12.2 ev [8]. As the ionization potential of S is 10.36 ev [4], the ionization potential of S_2 is expected to be considerably lower than this, not slightly higher as reported by Smyth and Blewett.

The isotope ratios of sulfur are fairly consistent with published values, as is evident in table 2, but there is considerable variation in isotope abundances of sulfur. Thode and his colleagues [6] have made an intensive survey of relative abundances of S^{34} in sulfur from various sources and find values ranging from 4.39 to 4.19 percent, with a value of about 4.29 percent reported for native sulfur from the same region as the reference sample.

WASHINGTON, May 9, 1956.

5. References

[1] F. L. Mohler, Science **122,** 334 (1955).
[2] G. B. Guthrie, Jr., D. W. Scott, and G. Waddington, J. Am. Chem. Soc. **76,** 1488 (1954).
[3] A. G. Gaydon, Dissociation energies and spectra of diatomic molecules (John Wiley & Sons, Inc., New York, N. Y., 1947).
[4] Charlotte E. Moore, Atomic energy levels I, NBS Circ. 467 (1949).
[5] A. O. C. Nier, Phys. Rev. **53,** 282 (1938).
[6] H. G. Thode, R. K. Wanless, and R. Wallouch, Geochim. et Cosmochim. Acta **5,** 286 (1954).
[7] H. D. Smyth and J. P. Blewett, Phys. Rev. **46,** 276 (1934).
[8] T. M. Sugden and W. C. Price, Trans. Faraday Soc. **44,** 116 (1948).

Journal of Research of the National Bureau of Standards Vol. 57, No. 4, October 1956 Research Paper 2714

Calibration of Vibration Pickups by the Reciprocity Method

Samuel Levy and Raymond R. Bouche

The reciprocity theory for the relationship between mechanical force and velocity and electric current and voltage is presented for a linear electrodynamic vibration-pickup calibrator having a driving coil, a velocity-sensing coil, and a mounting table. The theory takes account of flexibility in the calibrator structure and in the coils, electric coupling between different parts of the same coil and between parts of one coil and parts of the other, and flexibility in the magnet structure. The theory shows what measurements are required in using a linear electrodynamic calibrator for the absolute calibration of vibration pickups.

A description is given of the mechanical arrangement and electric circuitry used at the National Bureau of Standards in calibrating calibrators by the reciprocity method. A typical velocity-sensing-coil calibration curve is presented showing the effect of pickup mass on the calibration factor. Typical examples of measurement of calibration factor and mechanical impedance of pickups are also presented.

Practical limitations of the reciprocity method due to nonlinearity resulting from lack of tightness of mechanical joints, resonance effects, amplitude effects, etc., are discussed.

1. Introduction

An early application of the reciprocity method to the measurement of mechanical quantities was that by R. K. Cook [1] [1] in 1940. He applied the method to the absolute calibration of microphones. This was followed in 1948 with papers by H. M. Trent [2] and A. London [3], who showed how the reciprocity method could be used for the absolute calibration of vibration pickups. The reciprocity method was applied to the calibration of electrodynamic transducers in 1948 by S. P. Thompson [4] and to the calibration of piezoelectric accelerometers in 1952 by M. Harrison, A. O. Sykes, and P. G. Marcotte [5].

Commercially available calibrators for vibration pickups have a mounting table that is connected by a relatively rigid internal structure to a driving coil and to a velocity-sensing coil. This internal structure is supported from the frame by flexure springs or guide wires. John C. Camm, formerly of NBS, in 1953 showed how the reciprocity method could be applied to the calibration of the velocity-sensing coil of such a calibrator in connection with work for the Office of Naval Research. In 1955 the authors of the present report, in connection with work for the Diamond Ordnance Fuze Laboratories, extended Camm's theory to take account of pickup mass and flexibility in the internal structure for the frequently occurring case where the driving coil, sensing coil, and mounting table are mechanically joined at a point.

The present report gives a broader basis for the application of the reciprocity method to the calibration of the velocity-sensing coil of calibrators, by considering both the internal structure and the magnet to be flexible and by taking account of electric-coupling effects. It also shows how the calibrator, once its velocity-sensing coil has been calibrated by the reciprocity method, can be used to determine the calibration factor and to measure the mechanical impedance of vibration pickups.

2. Reciprocity Theory for Flexible Vibration-Pickup Calibrators

In the appendix the general reciprocity theory for a calibrator is presented. This theory is applicable to a calibrator operating in any frequency or amplitude range in which it can be considered to be a linear system. Neither the internal structure nor the magnet structure need be considered rigid. The theory is applicable, for example, not only at low frequencies and at frequencies near certain resonances, but also at frequencies above axial resonance where

[1] Figures in brackets indicate the literature references at the end of this paper.

397105—56——5

the driving coil and mounting table move in opposite directions. The theory is also applicable where there is electric coupling between different parts of the same coil and between parts of one coil and parts of the other.

The positive terminals of the driving and sensing coils are designated as those having positive voltages when the mounting table is moving inward. Conversely, positive current in the coils produces outward velocity at the mounting table.

When the calibrator is energized with current in the driving coil at any particular frequency, the calibration factor, F, is defined as the ratio of the voltage in volts in the velocity-sensing coil to the velocity in inches per second at the surface of the mounting table. It is shown in the appendix that

$$F=a+bY_p \tag{1}$$

where Y_p is the pickup mechanical impedance (lb-sec/in.), and all the symbols represent complex numbers in the manner commonly used for alternating-current electrical theory. The calibrator constants, a and b, are determined by the following two experiments and computational procedure.

Experiment 1: The equipment is shown in figure 1 (a). Attach weights to the mounting table and measure for each weight the transfer admittance in amperes per volt, G, between the driving and sensing coils:

$$G=\frac{I_o^D}{E_o^S} \tag{2}$$

where

I_o^D = current in driving coil.

E_o^S = voltage generated in open-circuited sensing coil. (It is permissible to leave a voltmeter permanently connected to the sensing coil. If this is done, the open-circuit condition is obtained when no other connection is made to the sensing coil.)

Experiment 2: The equipment is shown in figure 1 (b). Couple a second vibration exciter to the calibrator being calibrated at the mounting table, and measure the ratio, R, of open-circuited voltages generated in the sensing and driving coils:

$$R=E_o^S/E_o^D. \tag{3}$$

Computational Procedure: Determine the ordinate intercept, J, and the slope, Q, of the function $W/(G-G_o)$ when plotted against the weight, W, attached to the mounting table in experiment 1, where G_o is the value of G when $W=0$. Constants a and b in eq (1) are then given by

$$a=0.01711\sqrt{j\omega JR}, \qquad b=6.601Q\sqrt{R/(j\omega J)}, \tag{4}$$

where ω is the frequency in radians per second, and j is the unit imaginary vector.

It is shown in the appendix that the vibration-pickup calibrator calibrated by the reciprocity method can be used to determine the mechanical impedance, Y_p, of a pickup by measuring the admittance, G_p, eq (2), with the pickup attached to the mounting table, and the admittance, G_o, when nothing is attached to the table, by use of the relationship

$$Y_p=j\left(\frac{\omega}{386}\right)\left(\frac{J(G_p-G_o)}{1-Q(G_p-G_o)}\right). \tag{5}$$

To carry out the calibration of a pickup the following procedure is used: The driving coil of the calibrator is energized at the desired frequency and the value of Y_p is determined. The

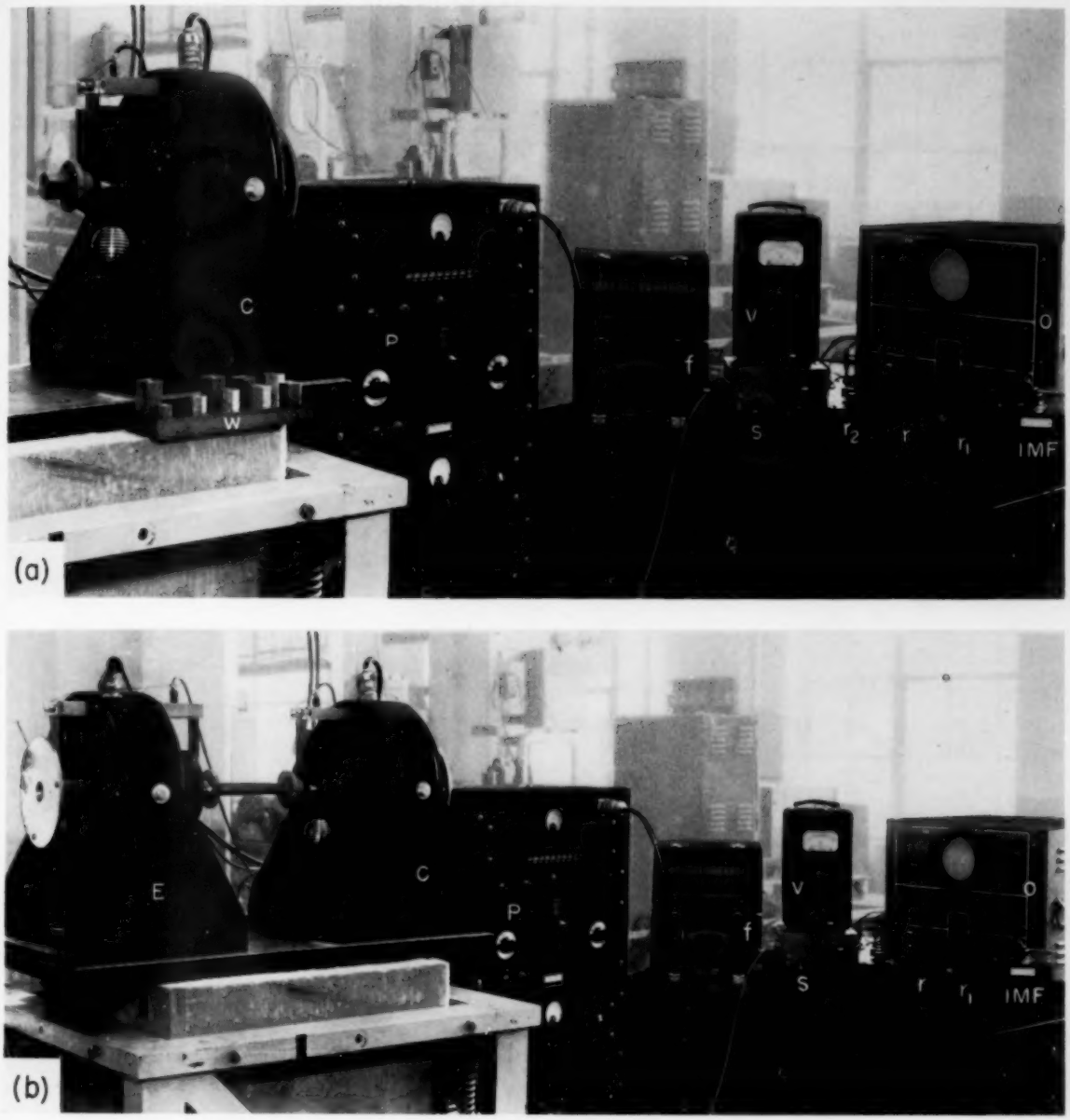

FIGURE 1. *Measurement of constants of vibration-pickup calibrator.*

(a) Weights, *W*, are attached to mounting table of calibrator, *C*, in experiment 1. (b) External vibration exciter, *E*, is required to provide sinusoidal motion to calibrator, *C*, in experiment 2.

calibrator is then driven at the desired amplitude as indicated by the voltage, E_o^s, in the sensing coil, and then the velocity is given by

$$v = E_o^s / F, \tag{6}$$

where F is obtained by substituting Y_p in eq (1). The output of the pickup corresponding to this excitation is then measured. Ordinarily the term bY_p in eq (1) for F is negligibly small, except at frequencies high enough to cause relative displacements between the mounting table and the sensing coil. Where it is known that bY_p is negligibly small, the determination of Y_p may be omitted from the calibration procedure.

3. Measurement of Constants

3.1. Accuracy of Weights

The weights attached to the table in carrying out experiment 1 at the Bureau are shown at W in figure 1 (a). The weights increase in 0.1-lb steps from 0 to 1 lb. They vary less than 0.1 percent from their rated values. Their attachment surface has a stud that engages the mounting table and a contacting ring, ⅛ in. wide, which provides a connection of high rigidity. A film of oil is wiped on this ring before engagement to eliminate air in the contact surface.

3.2. Accuracy of Frequency Measurements

The frequency was measured with a calibrated electronic frequency meter. The indicated audio oscillator frequency did not differ from the measured frequency by more than 0.2 percent.

3.3. Measurement of Transfer Admittance

The circuit shown in figure 2 (a) is used to measure the transfer admittance. With the switch in the "up" position, the values of r and r_1 are adjusted until the voltage drops $|E_{12}|$ across terminals 1 and 2, and $|E_{13}|$ across terminals 1 and 3, are equal as measured on a high-impedance voltmeter. The magnitude of G is then given by

$$|G|=\frac{r+r_1+r_2}{rr_2}. \tag{7}$$

The accuracy of $|G|$ determined in this manner depends only on the accuracy of the circuit elements and the repeatability of the voltmeter reading, but not on the accuracy of the voltmeter. Values of the resistances are chosen to load the amplifier suitably. Typical values for this calibrator are r_2, equal to 10 ohms, and $r+r_1$, approximately 1,000 times greater than r_2.

Voltage $|E_{23}|$ across terminals 2 and 3 is then read from the voltmeter. The switch is lowered to the "down" position. The value of r_1 is adjusted until $|E_{14}|$ equals $|E_{13}|$, and voltages $|E_{13}|$ and $|E_{43}|$ are read on the voltmeter. The phase angle, ϕ_G, of the transfer admittance, G, is the phase angle of I_o^D with respect to E_o^S. Because the currents in r, r_1, and r_2 are in phase with I_o^D, phase angle ϕ_G can be determined from a construction of a polygon of voltages as

$$\phi_G=\cos^{-1}\left(1-\frac{1}{2}\frac{|E_{23}^2|}{|E_{13}^2|}\right). \tag{8}$$

A suitable value of r_2 is used so that $r_1\omega 10^{-6}$ is greater than 100; then the approximate value of

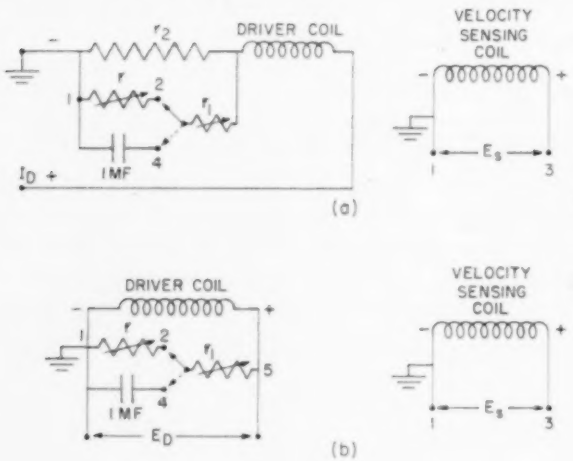

FIGURE 2. *Circuits used in the measurement of constants of vibration-pickup calibrator.*

(a) Measurement of transfer admittance. (b) Measurement of voltage ratio.

ϕ_G can be determined from

$$(\phi_G)\ \text{approx}=90°-\cos^{-1}\left(1-\frac{1}{2}\frac{|E_{34}^2|}{|E_{13}^2|}\right). \tag{9}$$

The use of both eq (8) and (9) determines the magnitude and quadrant for ϕ_G. It happens, though, except near certain resonances, that ϕ_G is near $\pm 90°$. Small errors in $|E_{43}|$ or $|E_{13}|$ result in large changes in the angle

$$\cos^{-1}\left(1-\frac{1}{2}\frac{|E_{43}^2|}{|E_{13}^2|}\right)$$

when ϕ_G is near $-90°$. Difficulty in measuring the small value of $|E_{43}|$ results in error when ϕ_G is near 90°. Therefore, eq (8) is used to determine the magnitude of ϕ_G and (9) its quadrant.

3.4. Measurement of Voltage Ratio

The circuit shown in figure 2(b) is used to measure the ratio of the open-circuit voltages of the driving and sensing coils when the calibrator being calibrated is driven by an external vibration exciter. With the switch in the "up" position and with r_1 set at 10,000 ohms, resistor r is adjusted until the voltages across terminals 1 and 2 and terminals 1 and 3 are equal. The magnitude of the voltage ratio, R, is then given by

$$|R|=\frac{r}{10{,}000+r}. \tag{10}$$

(In the case of a calibrator for which 10,000 ohms is not effectively an infinite impedance across the driving coil, r_1 in figure 2(b) should be increased to an adequate value and eq (10) correspondingly modified.)

To determine the phase angle of R, $|E_{13}|$ and $|E_{23}|$ are measured. The switch is then put in the "down" position, r_1 is adjusted until $|E_{14}|$ equals $|E_{13}|$, and $|E_{43}|$ is measured. Then from a construction of a polygon of voltages

$$\phi_R=\cos^{-1}\left(1-\frac{1}{2}\frac{|E_{23}^2|}{|E_{13}^2|}\right), \tag{11}$$

and

$$\phi_R=\cos^{-1}\left(1-\frac{1}{2}\frac{|E_{43}^2|}{|E_{13}^2|}\right)-\cos^{-1}(|R|). \tag{12}$$

It happens that ϕ_R is near either 0° or 180°. Equation (11) is insensitive for these angles, either because $|E_{23}|$ is very small for ϕ_R near 0° or because the cosine is insensitive to small changes in $|E_{23}|$ near 180°. Therefore, eq (12) is used to determine the magnitude of ϕ_R and eq (11) only its quadrant.

4. Typical Results

4.1. Calibration of Sensing Coil

Results obtained in the calibration of the sensing coil of a typical calibrator having a nominal 50-lb driving-force rating are now presented. All measurements were made after thermal equilibrium was approached. The positive terminals of the driving and sensing coils were determined as those having positive voltage when the mounting table had inward velocity. Positive velocity is then outward.

First, the transfer admittance, G, experiment 1, was measured for a sequence of weights, W, on the mounting table at each frequency for which a calibration was desired. Typical results at frequencies of 900 and 5,000 cps are presented in figure 3. In figure 4 are the corresponding plots of $W/(G-G_o)$ against W. The data were fitted by a weighted least-squares procedure for a straight line. The weighting as determined by a consideration of the expected error in $1/(G-G_o)$ was 1, 2, 3, . . ., 10 for W=0.1, 0.2, 0.3, . . ., 1.0 lb. Intercepts J and

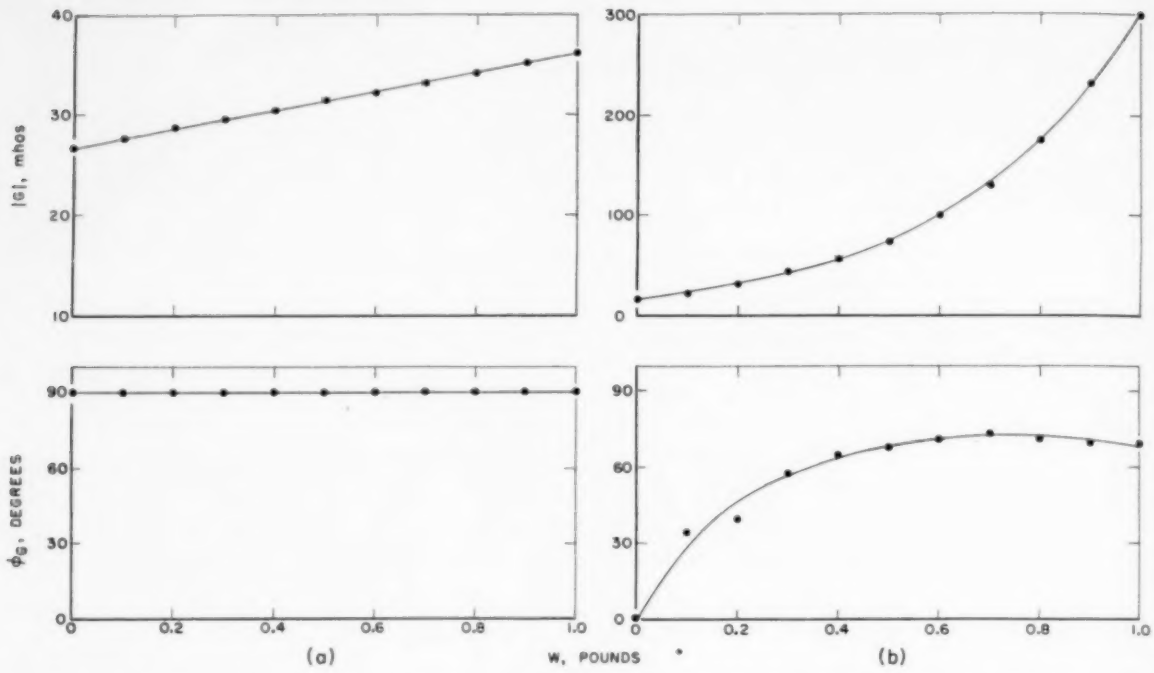

FIGURE 3. *Variation of transfer admittance, G, with weight, W, on the mounting table for a typical vibration pickup calibrator at frequencies of (a) 900 cps and (b) 5,000 cps.*

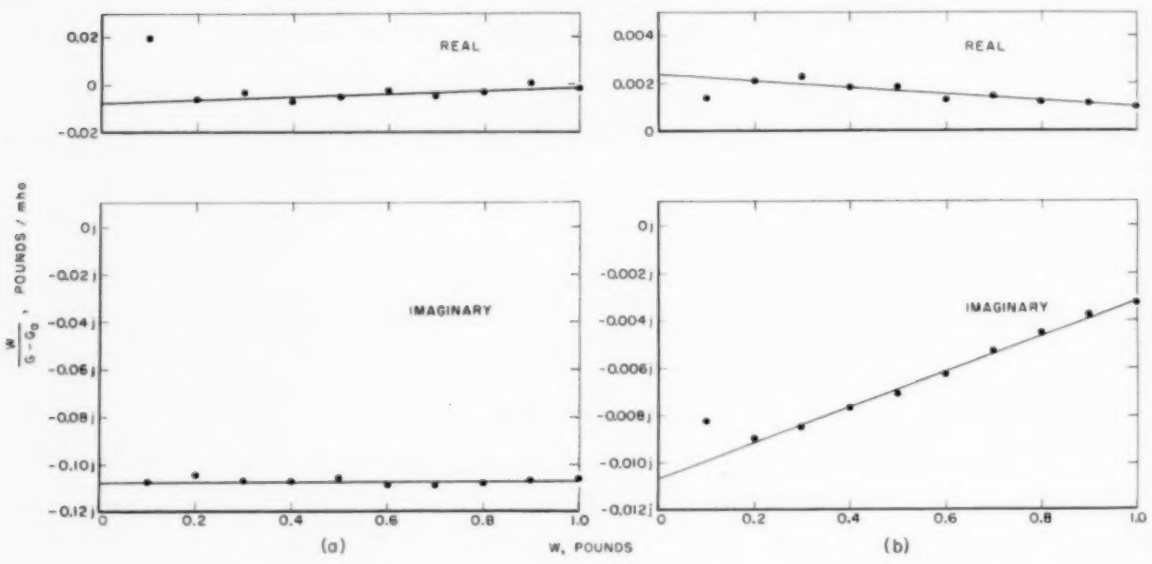

FIGURE 4. *Plot of $W/(G-G_a)$ as a function of W for a typical vibration pickup calibrator at frequencies of (a) 900 cps and (b) 5,000 cps.*

slopes Q, determined by this procedure, are at 900 cps $J=0.1089/\underline{-94.2°}$ lb-ohm, and $Q=0.00767/\underline{11.8°}$ ohm, and at 5,000 cps, $J=0.01094/\underline{-77.4°}$ lb-ohm, and $Q=0.00765/\underline{100.4°}$ ohm.

The voltage ratio, R, when driven by an external vibration exciter, experiment 2, was then determined as $R=0.1090/\underline{-2.6°}$ at 900 cps and $R=0.2495/\underline{-2.0°}$ at 5,000 cps. Next the constants a and b in eq (4) were computed. Substituting their values in eq (1) gave calibration factors of the sensing coil with a pickup of mechanical impedance Y_p on the mounting table,

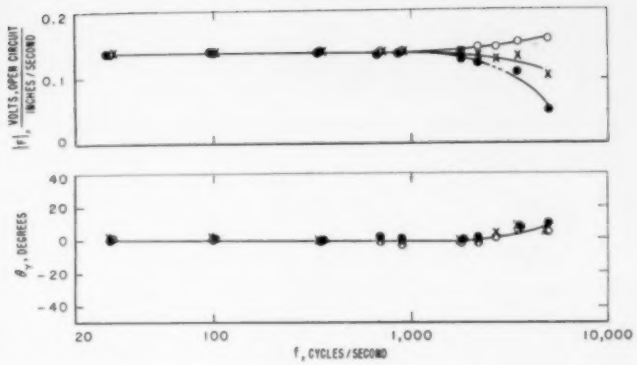

FIGURE 5. *Variation of calibration factor of velocity-sensing coil with frequency and pickup weight for a typical vibration pickup calibrator.*

○=0 lb, ×=½ lb, ●=1 lb.

at 900 cps, $F=0.1402/\underline{-3.4^\circ}+0.000674/\underline{12.6^\circ}\ Y_p$ v-sec/in., and at 5,000 cps, $F=0.1584/\underline{5.5^\circ}+0.001360/\underline{93.1^\circ}\ Y_p$ v-sec/in.

In figure 5 are shown the magnitude and phase angle of the calibration factor of the velocity-sensing coil of this typical vibration-pickup calibrator as a function of frequency for pickups having a mechanical impedance Y_p corresponding to weights W of 0, 0.5, and 1.0 lb ($Y_p=j\omega W/386$). It is evident that, for this particular vibration-pickup calibrator, the calibration factor of the velocity-sensing coil is nearly independent of frequency and pickup weight up to 900 cps. The curve for 1 lb is dotted in the vicinity of 2,700 cps because the plot similar to that shown in figure 4 was not linear beyond 0.5 lb. The source of this nonlinearity could not be localized. This nonlinearity has not been found in other calibrators of the same make and model number calibrated at the same frequency.

4.2. Calibration of a Variable-Resistance-Type Accelerometer and a Piezoelectric-Type Accelerometer

Results obtained in the calibration of a variable-resistance-type accelerometer and piezoelectric-type accelerometer are now presented. In these calibrations the circuit shown in figure 2 (a) was used with the pickup terminals designated 6 and 7, in place of velocity-sensing-coil terminals 1 and 3. The method given in section 3.3 was then used for the measurement of G_p, the value of G with the pickup attached to the mounting table.

For the piezoelectric pickup, the value of G_p obtained at 900 cps was $G_p=I_o^D/E_o^S=28.51/\underline{91.8^\circ}$ mhos, and at 5,000 cps, $G_p=37.9/\underline{43.6^\circ}$ mhos. With terminal 6 grounded and terminal 7 replacing terminal 3, the same procedure gave, at 900 cps, $I_o^D/E_p=16.35/\underline{2.5^\circ}$ mhos, and at 5,000 cps, $I_o^D/E_p=3.201/\underline{-44.6^\circ}$ mhos, where E_p is the output voltage of the pickup. From eq (5), the mechanical impedance, Y_p, of the pickup was computed by using, at 900 cps, $G_o=26.81/\underline{92.0^\circ}$ mhos, and at 5,000 cps, $G_o=16.51/\underline{18.1^\circ}$ mhos, and the values of J and Q obtained in section 4.1. This gave, at 900 cps, $Y_p=2.712/\underline{83.3^\circ}$ lb-sec/in. and at 5,000 cps, $Y_p=18.23/\underline{70.5^\circ}$ lb-sec/in. Using these values of Y_p in eq (1), the velocity sensing-coil calibration factors at 900 cps and 5,000 cps, respectively, are $F=0.1399/\underline{-2.7^\circ}$ v-sec/in. and $F=0.1357/\underline{9.2^\circ}$ v-sec/in. The pickup acceleration calibration factor, F_p, is

$$F_p=\frac{(I_o^D/E_o^S)}{(I_o^D/E_p)}\frac{Fg}{j\omega} \tag{13}$$

where $Fg/(j\omega)$ is the acceleration calibration factor of the sensing coil. Using this equation, at 900 cps, $F_p=0.0166/\underline{-3.4^\circ}$ v/g, and at 5,000 cps, $F_p=0.0197/\underline{6.5^\circ}$ v/g. Figure 6 shows the complete calibration of the piezoelectric-type accelerometer.

The calibration of the variable-resistance-type accelerometer, which was performed in a similar manner, is shown in figure 7. To compute the results on the variable-resistance

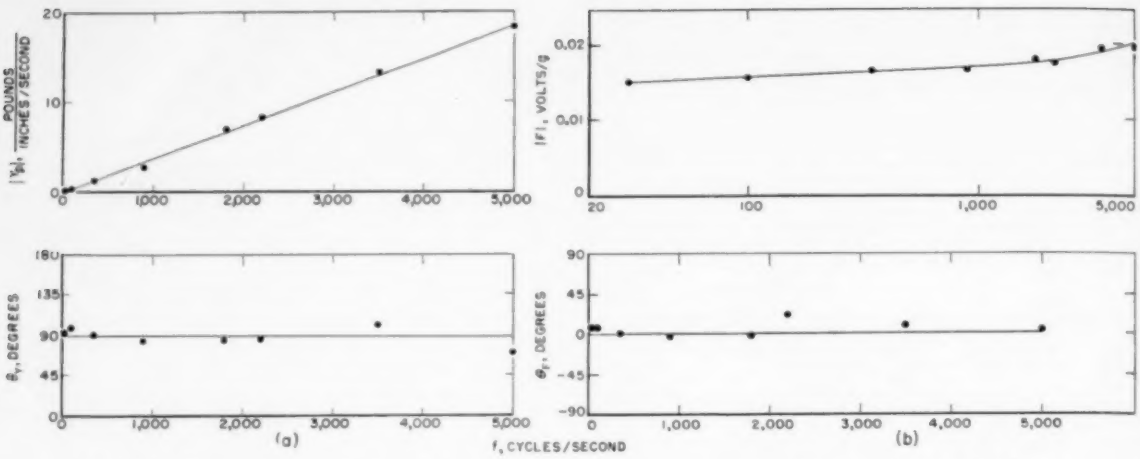

FIGURE 6. *Calibration of piezoelectric-type accelerometer at a nominal acceleration level of 2 g.*

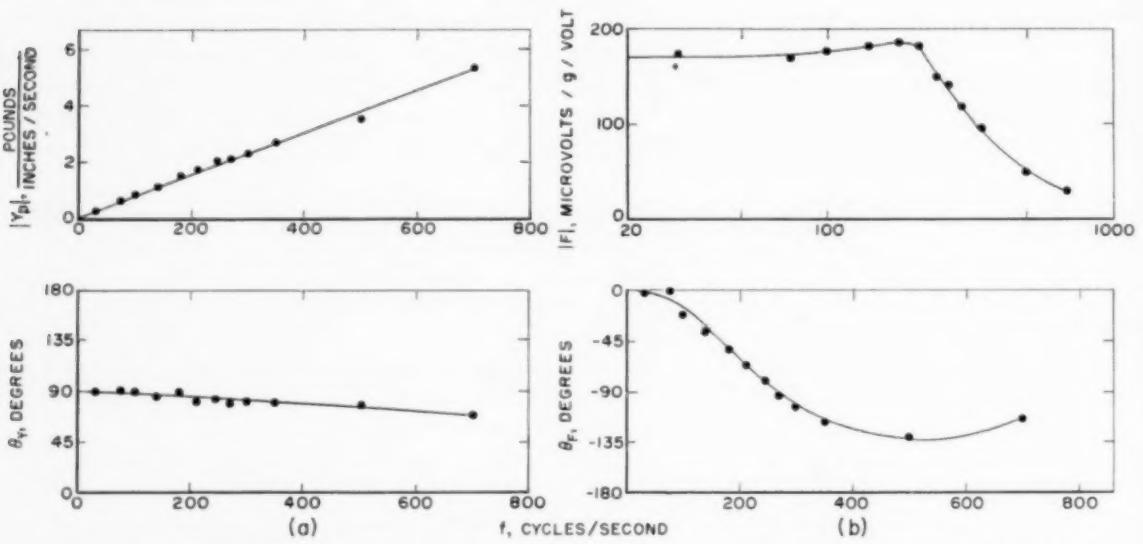

FIGURE 7. *Calibration of variable-resistance-type accelerometer at a nominal acceleration level of 2 g.*

pickup at frequencies other than those at which the vibration-pickup calibrator was calibrated, it was necessary to interpolate suitably for a, b, R, and Q, and compute J from eq 4. This interpolation was only used at frequencies below 900 cps. In this frequency range, such interpolation results in no appreciable error for this calibrator when the resonant frequencies of the flexures are avoided. The frequencies used for the pickup calibration were not those at which flexure resonance was present.

5. Effects of Calibrator Construction on Accuracy

Inaccuracy in the reciprocity method, exclusive of electrical measurements, arises primarily from deviations from true linearity in the calibrator performance. The more important forms of nonlinearity are discussed below.

5.1. Resonance Effects

Resonance accentuates inaccuracy due to nonlinearity because relatively small changes in the calibrator constants, which are caused by very small changes in the structure of the calibrator and small changes in the exciting frequency, can cause large changes in the amplitude of vibration. Even when such changes do not occur, the large amplitudes associated with resonance may exceed the linear range. The resonance of the driving coil relative to the velocity-sensing coil reduces the accuracy of the reciprocity calibration over a small frequency range because $|R|$ is very small and therefore difficult to measure, and because the large amplitude of the driver coil may exceed its linear range. Operation of the calibrator near resonance frequencies should therefore be avoided. Some common resonance conditions in their usual order of appearance with increasing frequency follow:

a. Resonance of mounting table and coils as a rigid body on the guiding flexures.
b. Local resonance in the flexures.
c. Transverse vibration of the shaft connecting mounting table and driving coil.
d. Longitudinal resonance of shaft connecting mounting table and driving coil.
e. Local resonance in table or coils.

5.2. Transverse Motion

Transverse motion from any source invalidates the reciprocity method, which requires the mounting table to have uniaxial motion. Transverse motion occurs at the resonance frequencies of the flexures and at the transverse resonance frequencies of the shaft on which the moving parts are mounted. At resonance, the amplitude will vary substantially for small changes in frequency and the resonance may occur at a frequency that is a harmonic of the driving frequency. Flexures can be detuned by attaching small weights to them.

5.3. Tightness of Mechanical Joints

The tightness of the mechanical joints in a calibrator will have little effect on its performance at low frequencies, where the moving assembly of mounting table and coils acts as a "rigid body." At frequencies approaching those for internal resonance in the assembly, looseness in the joints can affect behavior by, for example, changing the structural stiffness or by introducing coulomb friction. At very high frequencies, joints normally thought to be tight may be a source of erratic behavior, which is difficult to eliminate as tightness will ordinarily vary with temperature and time. Coating all joints with oil improves their rigidity.

5.4. Amplitude Effects

The nonuniformity of the magnetic fields surrounding the coils is a primary source of nonlinearity. This effect tends to be greatest at low frequencies, where the displacement amplitude is large for a given acceleration. At high frequencies, the displacement amplitude is relatively small, and this effect is negligible. The change in equilibrium position of the moving assembly of a calibrator, when its orientation is changed, may cause a change in calibration factor due to change in the effective field strength.

The structure of a calibrator will ordinarily experience small deformations in its linear range at permissible current intensities. At resonance, the deformations are larger. Little is known about the linearity of structural damping for a structure as complicated as a calibrator; however, so long as the damping is small, its possible lack of linearity would affect only the resonant response.

5.5. Temperature Effects

Changes in temperature cause moderate changes in elastic constants and in the tightness of joints, and in this way can affect the calibrator performance near resonance. Changes in temperature may also affect the field flux density, and thus the electrical characteristics of the driving coil, but should not ordinarily affect the calibration factor of the velocity-sensing coil.

5.6. Purity of Electric-Power Sources

If the magnets are excited by direct current containing an alternating-current ripple, this ripple may appear in the velocity output of the calibrator owing to currents included in the driving coil by transformer action from the field. Such a disturbance can readily be detected by exciting the field and observing the velocity of the mounting table with the driving coil short-circuited.

Any harmonic content in the power supply to the driving coil will excite the calibrator at the harmonic frequencies, as well as at the primary frequency. The techniques described in this paper are applicable only for excitation at a single frequency.

6. Conclusions

It is concluded that the reciprocity methods described can be used for the accurate calibration of vibration pickups and calibrators having linear response. The accuracy is limited primarily by the accuracy of electrical measurement, by deviations from true linearity in construction, and by impurities in power supplies to the field and driving coils. The frequency range is limited theoretically only to frequencies for which the mechanical impedance of the weights attached to the mounting table can be computed. Ordinarily this limits the range to that at which the weights act as though they were rigid bodies. Practically, the calibrator used as an example in this report is most suited for use at frequencies of 900 cps and below, where its calibration factor is not affected by the mechanical impedance of most vibration pickups that would be attached to its mounting table. The calibrator is suited for use above 900 cps, however, with some loss in precision primarily due to the electromechanical properties of the calibrator being less constant with respect to field-coil temperature than they are at lower frequencies. The upper acceleration range of most calibrators, when resonance is avoided, is below 50 g. This would be the limit for calibrating by the reciprocity method.

7. Appendix. General Reciprocity Theory

7.1. Reciprocity for Electric Circuit

If a complicated electric circuit is considered to be made up of a number of meshes, the almost trivial fact that the common impedance between meshes i and k, for example, is the same as that between k and i is the basis for the proof of the reciprocity theorem. This proof is elegantly presented by Guillemin on page 152 of reference [6]. Guillemin states on page 276 that the reciprocity theorem can be proved for both transient and steady-state performance. This means, for example, that if we impress a voltage in mesh 5 of a given network and measure the current, say in mesh 2, and then place the voltage in mesh 2 instead of in mesh 5 and measure the current in mesh 5, we will find the current exactly the same in the two cases, both in magnitude and phase.

7.2. Reciprocity for Mechanical System

If a complicated mechanical system can be replaced by an equivalent system having discrete mass-points joined by springs and dashpots, the fact that the spring and dashpot connecting points i and k is the same as that connecting points k and i makes possible a proof of the reciprocity theorem for mechanical systems completely analogous with that for electric circuits. (Reference [7] gives a proof of this theorem for conservative systems.) In other words, this reciprocity theorem states, for example, that if we impress a force on point 5 of a given system and measure the velocity, say at point 2, we will find the same velocity in magnitude and phase when we place the force at point 2 instead of at point 5 and measure the velocity at point 5. It should be mentioned that it is possible to have a mechanical system consisting of discrete elements that is not reciprocal, for example, if it contains gyroscopic elements.

7.3. Reciprocity for Combined System

In developing the reciprocity theorem for the combined electric-mechanical system of a calibrator, we will use matrix notation. This will permit us to consider the coils as flexible bodies and take account of electric coupling between coils, as well as deformation in the field and movable structure. The notation and theorems given by Frazer, Duncan, and Collar [8] will be used.

Currents and voltages in the velocity-sensing coil will be indicated by S and in the driving coil by D. We will consider the coils subdivided into a sufficient number of segments so each moves as a rigid body and number them consecutively in the two coils. The subscript o will indicate terminal values. Complex notation used in alternating-current electrical theory will be used throughout. All symbols represent vector quantities, unless otherwise noted. An English system of units (inches, pounds, and seconds) will be used.

Current I_o^S at the terminals of the sensing coil is given by

$$I_o^S=\frac{E_o^S}{z_{oo}^{SS}}+\frac{E_o^D}{z_{oo}^{SD}}+[z^S]\{E\}, \tag{A1}$$

where

E_o^S = voltage at terminals of coil S.

E_o^D = voltage at terminals of coil D.

z_{oo}^{SS} = impedance at terminals of coil S.

z_{oo}^{SD} = transfer impedance from terminals of coil S to terminals of coil D.

$[z^S]=\begin{bmatrix}\frac{1}{z_{o1}^S} & \frac{1}{z_{o2}^S} & \cdots & \frac{1}{z_{on}^S}\end{bmatrix}$, where z_{on}^S is the transfer impedance from segment n to the terminals of coil S.

$\{E\}=\begin{bmatrix}E_1\\E_2\\\cdot\\\cdot\\\cdot\\E_n\end{bmatrix}$, E_n is the voltage generated in segment n.

A similar expression can be written for I_o^D. Both of these expressions can be expressed as

$$\{I_o\}=[z_o]\{E_o\}+[z]\{E\}, \tag{A1a}$$

where

$$\{I_o\}=\begin{bmatrix}I_o^S\\I_o^D\end{bmatrix};\quad \{E_o\}=\begin{bmatrix}E_o^S\\E_o^D\end{bmatrix}$$

$$[z_o]=\begin{bmatrix}\frac{1}{z_{oo}^{SS}} & \frac{1}{z_{oo}^{SD}}\\ \frac{1}{z_{oo}^{DS}} & \frac{1}{z_{oo}^{DD}}\end{bmatrix}$$

$$[z]=\begin{bmatrix}\frac{1}{z_{o1}^S} & \frac{1}{z_{o2}^S} & \cdots & \frac{1}{z_{on}^S}\\ \frac{1}{z_{o1}^D} & \frac{1}{z_{o2}^D} & \cdots & \frac{1}{z_{on}^D}\end{bmatrix}.$$

The current in any segment is given by

$$\{I\}=[z]'\{E_o\}+[Z]\{E\}, \tag{A2}$$

where

$\{I\}=\begin{bmatrix} I_1 \\ I_2 \\ . \\ . \\ . \\ I_n \end{bmatrix}$, I_n is the current in segment n,

$[Z]=\begin{bmatrix} \frac{1}{z_{11}} & \frac{1}{z_{12}} & \cdots & \frac{1}{z_{1n}} \\ \frac{1}{z_{21}} & \frac{1}{z_{22}} & \cdots & \frac{1}{z_{2n}} \\ . & . & & . \\ . & . & & . \\ . & . & & . \\ \frac{1}{z_{m1}} & \frac{1}{z_{m2}} & \cdots & \frac{1}{z_{mn}} \end{bmatrix}$, z_{mn} is the transfer impedance from segment m to segment n,

$[z]'$=transpose of $[z]$.

Velocity v_o at the mounting table, taken positive outward, is given by

$$v_o=\frac{F_o}{Y_{oo}}+L_1[y][k]\{I\}, \tag{A3}$$

where

F_o=the force at the mounting table.

Y_{oo}=the mechanical impedance at the mounting table.

$L_1=2.249\times10^{-7}$, a conversion factor.

$[y]=\begin{bmatrix} \frac{1}{y_{o1}} & \frac{1}{y_{o2}} & \cdots & \frac{1}{y_{on}} \end{bmatrix}$, where y_{on} is the transfer mechanical impedance from the mounting table to segment n.

$[k]=\begin{bmatrix} B_1l_1 & 0 & 0 & \cdots & 0 \\ 0 & B_2l_2 & 0 & \cdots & 0 \\ 0 & 0 & B_3l_3 & \cdots & 0 \\ . & . & . & & . \\ . & . & . & & . \\ . & . & . & & . \\ 0 & 0 & 0 & \cdots & B_nl_n \end{bmatrix}$, where B_n is the flux density, and l_n is the length for segment n.

In eq (A3), the product $L_1 B_n l_n I_n$ gives the force, in pounds, at segment n when I_n is the current, in amperes. The velocity of the various segments is given by

$$\{v\} = [y]' F_o + L_1 [Y][k]\{I\}, \tag{A4}$$

where

$\{v\} = \begin{bmatrix} v_1 \\ v_2 \\ . \\ . \\ . \\ v_n \end{bmatrix}$, v_n is the velocity of segment n.

$[y]'$ = transpose of $[y]$.

$[Y] = \begin{bmatrix} \frac{1}{y_{11}} & \frac{1}{y_{12}} & \cdots & \frac{1}{y_{1n}} \\ \frac{1}{y_{21}} & \frac{1}{y_{22}} & \cdots & \frac{1}{y_{2n}} \\ . & . & & . \\ . & . & & . \\ . & . & & . \\ \frac{1}{y_{m1}} & \frac{1}{y_{m2}} & \cdots & \frac{1}{y_{mn}} \end{bmatrix}$, y_{mn} is the transfer mechanical impedance from segment m to segment n.

The corresponding velocity in the magnetic field at the various segments is given by

$$\{v^M\} = L_1 [Y^M][k]\{I\} + [y^M]' F_o, \tag{A4a}$$

where

$\{v^M\} = \begin{bmatrix} v_1^M \\ v_2^M \\ . \\ . \\ . \\ v_n^M \end{bmatrix}$, v_n^M is the velocity of the magnetic field at segment n.

$[Y^M] = \begin{bmatrix} \frac{1}{y_{11}^M} & \frac{1}{y_{12}^M} & \cdots & \frac{1}{y_{1n}^M} \\ \frac{1}{y_{21}^M} & \frac{1}{y_{22}^M} & \cdots & \frac{1}{y_{2n}^M} \\ . & . & & . \\ . & . & & . \\ . & . & & . \\ \frac{1}{y_{m1}^M} & \frac{1}{y_{m2}^M} & \cdots & \frac{1}{y_{mn}^M} \end{bmatrix}$, y_{mn}^M is the transfer mechanical impedance from the location of segment m to that of segment n in the magnetic field.

$[y^M]'=\begin{bmatrix} \frac{1}{y^M_{o1}} \\ \frac{1}{y^M_{o2}} \\ \cdot \\ \cdot \\ \cdot \\ \frac{1}{y^M_{on}} \end{bmatrix}$, y^M_{on} is the transfer mechanical impedance from the mounting table to the magnetic structure opposite segment n.

The voltage generated in each segment is

$$\{E\}=-L_2[k]\{v\}+L_2[k]\{v^M\}, \tag{A5}$$

where $L_2=2.540\times10^{-8}$, a conversion factor. In eq (A5), $-L_2B_nl_n(v_n-v_n^M)$ is the electromotive force generated in segment n, in volts, when the relative velocity between segment n and the magnetic field, in inches per second, is $(v_n-v_n^M)$. Substituting (A2) into (A4) and (A4a), and substituting the results into (A5) gives

$$\{E\}=-F_oL_2[k][y-y^M]'-L_1L_2[K][z]'\{E_o\}-L_1L_2[K][Z]\{E\}, \tag{A6}$$

where

$$[K]=[k][Y][k]-[k][Y^M][k]. \tag{A7}$$

Letting

$$[V^{-1}]=[1]+L_1L_2[K][Z], \tag{A8}$$

where

$[1]=\begin{bmatrix} 1 & 0 & 0 & \cdot & \cdot & \cdot & 0 \\ 0 & 1 & 0 & \cdot & \cdot & \cdot & 0 \\ 0 & 0 & 1 & \cdot & \cdot & \cdot & 0 \\ \cdot & \cdot & \cdot & & & & \cdot \\ \cdot & \cdot & \cdot & & & & \cdot \\ \cdot & \cdot & \cdot & & & & \cdot \\ 0 & 0 & 0 & \cdot & \cdot & \cdot & 1 \end{bmatrix}$, the unit matrix,

$[V^{-1}]$ = inverse of $[V]$.

$$\{E\}=-F_oL_2[V][k][y-y^M]'-L_1L_2[V][K][z]'\{E_o\}. \tag{A9}$$

Substituting (A9) into (A1a),

$$\{I_o\}=[z_o]\{E_o\}-F_oL_2[z][V][k][y-y^M]'-L_1L_2[z][V][K][z]'\{E_o\}. \tag{A10}$$

Substituting (A9) in (A2) and the result in (A3) gives

$$v_o=\frac{F_o}{Y_{oo}}-L_1L_2F_o[y-y^M][k][Z][V][k][y-y^M]'+L_1[y-y^M][k][V]'[z]'\{E_o\}, \tag{A11}$$

using

$$[V]'=[1]-L_1L_2[Z][V][K]. \tag{A12}$$

The proof of eq (A12) is obtained as follows: By using (A8),

$$\begin{aligned}[1]-L_1L_2[Z][V][K]&=[K^{-1}]([K]-L_1L_2[K][Z][V][K])\\&=[K^{-1}]([K]+(1-[V^{-1}])[V][K])\\&=[K^{-1}][V][K].\end{aligned}\tag{A13}$$

Also, premultiplying both sides of (A8) by $[K^{-1}]$,

$$[K^{-1}][V^{-1}]=[K^{-1}]+L_1L_2[Z].\tag{A14}$$

As $[K]$ is symmetric, $[K^{-1}]$ is symmetric. As $[Z]$ is also symmetric, $[K^{-1}][V^{-1}]$ is symmetric. Its inverse $[V][K]$ is therefore also symmetric. The transpose of a symmetric matrix is itself or

$$[V][K]=[K]'[V]'=[K][V]'.\tag{A15}$$

Substituting (A15) in (A13) gives (A12).

The current in the velocity-sensing coil is always zero,

$$I_o^S=[1\ 0]\{I_o\}=0.\tag{A16}$$

Substituting (A10) into (A16) and solving for E_o^S gives

$$E_o^S=\frac{F_oL_2z_{oo}^{SS}[z^S][V][k][y-y^M]'-E_o^D\left(\frac{z_{oo}^{SS}}{z_{oo}^{SD}}-L_1L_2z_{oo}^{SS}[z^S][V][K][z^D]'\right)}{1-L_1L_2z_{oo}^{SS}[z^S][V][K][z^S]'}.\tag{A17}$$

The current in the driving coil is

$$I_o^D=[0\ 1]\{I_o\}.\tag{A18}$$

Substituting (A17) into (A10) and the result into (A18) gives

$$\begin{aligned}I_o^D=F_oL_2&\frac{\left(\frac{z_{oo}^{SS}}{z_{oo}^{SD}}[z^S][V][k][y-y^M]'-[z^D][V][k][y-y^M]'\right.}{1-L_1L_2z_{oo}^{SS}[z^S][V][K][z^S]'}\\&\frac{\left.+L_1L_2z_{oo}^{SS}[z^S][V][K][z^S]'[z^D][V][k][y-y^M]'-L_1L_2z_{oo}^{SS}[z^S][V][K][z^D]'[z^S][V][k][y-y^M]'\right)}{1-L_1L_2z_{oo}^{SS}[z^S][V][K][z^S]'}\\&\left(\frac{1}{z_{oo}^{DD}}-\frac{z_{oo}^{SS}}{(z_{oo}^{SD})^2}-L_1L_2\frac{z_{oo}^{SS}}{z_{oo}^{DD}}[z^S][V][K][z^S]'+2L_1L_2\frac{z_{oo}^{SS}}{z_{oo}^{SD}}[z^S][V][K][z^D]'-L_1L_2[z^D][V][K][z^D]'\right.\\&\left.+L_1^2L_2^2z_{oo}^{SS}[z^S][V][K]([z^S]'[z^D]-[z^D]'[z^S])[V][K][z^D]'\right)\\&+E_o^D\frac{}{1-L_1L_2z_{oo}^{SS}[z^S][V][K][z^S]'}.\end{aligned}\tag{A19}$$

Substituting (A17) into (A11) gives

$$\begin{aligned}v_o=F_o&\frac{\left(\frac{1}{Y_{oo}}-L_1L_2[y-y^M][k][Z][V][k][y-y^M]'-L_1L_2\frac{z_{oo}^{SS}}{Y_{oo}}[z^S][V][K][z^S]'\right.}{1-L_1L_2z_{oo}^{SS}[z^S][V][K][z^S]'}\\&\frac{\left.+L_1^2L_2^2z_{oo}^{SS}[z^S][V][K][z^S]'[y-y^M][k][Z][V][k][y-y^M]'\right.}{1-L_1L_2z_{oo}^{SS}[z^S][V][K][z^S]'}\\&\frac{\left.+L_1L_2z_{oo}^{SS}[z^S][V][k][y-y^M]'[z^S][V][k][y-y^M]'\right)}{1-L_1L_2z_{oo}^{SS}[z^S][V][K][z^S]'}\\&\left(\frac{z_{oo}^{SS}}{z_{oo}^{SD}}[z^S][V][k][y-y^M]'-[z^D][V][k][y-y^M]'\right.\\&-L_1E_o^D\frac{\left.+L_1L_2z_{oo}^{SS}[z^S][V][K][z^S]'[z^D][V][k][y-y^M]'-L_1L_2z_{oo}^{SS}[z^S][V][K][z^D]'[z^S][V][k][y-y^M]'\right)}{1-L_1L_2z_{oo}^{SS}[z^S][V][K][z^S]'}.\end{aligned}\tag{A20}$$

The coefficient of L_2F_o in equation (A19) equals the coefficient of $-L_1E_o^D$ in (A20). Equations (A19) and (A20) are subjected first to the condition $v_o=0$ and then to the condition $I_o^D=0$. Eliminating E_o^D in (A19), when $v_o=0$, and F_o in (A20), when $I_o^D=0$, we obtain

$$\left.\frac{F_o}{L_1I_o^D}\right|_{v_o=0}=-\left.\frac{E_o^D}{L_2v_o}\right|_{I_o^D=0}. \tag{A21}$$

This is the reciprocity relation that exists in the combined electromechanical system.

Equations (A20), (A19), and (A17) can be written for brevity as

$$v_o=CF_o+AL_1E_o^D \tag{A22}$$

$$I_o^D=-AL_2F_o+BL_1E_o^D \tag{A23}$$

$$E_o^S=HF_o+NL_1E_o^D, \tag{A24}$$

where the constants A, B, C, H, and N depend only on the calibrator construction.

In eq (1) a relationship is given for the calibration factor, defined as $F=E_o^S/v_o$, as a function of the mechanical impedance, Y_p, of the object on the mounting table. We will determine this equation in terms of the calibrator constants A, B, C, H, and N of eq (A22) to (A24). If the force, F_o, is only the reaction to driving a mechanical impedance Y at a velocity v_o,

$$v_o=-F_o/Y. \tag{A25}$$

Substituting (A25) in (A22) and solving for F_o,

$$F_o=-E_o^D\frac{AL_1}{C+1/Y}. \tag{A26}$$

Substituting (A26) into (A24) and (A25) and forming the ratio E_o^S/v_o,

$$F=\frac{E_o^S}{v_o}=\frac{N}{A}+\left(\frac{NC}{A}-H\right)Y. \tag{A27}$$

We see that N/A in eq (A27) is a in eq (1) and $(NC/A)-H$ in eq (A27) is b in eq (1) when Y is Y_p.

$$a=N/A, \qquad b=(NC/A)-H. \tag{A28}$$

In experiment 1, section 2, the transfer admittance $G=I_o^D/E_o^S$ is determined for a series of weights, W, attached to the mounting table. Substituting (A26) into (A23) and (A24) and forming the ratio G,

$$G=\frac{I_o^D}{E_o^S}=\frac{B+(BC+A^2L_2)Y}{N+(NC-AH)Y}. \tag{A29}$$

In experiment 1, Y is the mechanical impedance $j\omega W/g$, where W is the weight on the mounting table, ω the frequency in radians per second, and g the acceleration of gravity, 386 in./sec^2. Making this substitution in (A29) and forming $W/(G-G_o)$, where G_o is the value of G when $Y=0$, we find

$$\frac{W}{G-G_o}=\frac{386}{j\omega}\frac{N^2}{A^2NL_2+ABH}+\frac{N^2C-AHN}{A^2NL_2+ABH}W. \tag{A30}$$

We see that the intercept J and slope Q found in determining $W(G-G_o)$ experimentally are

$$J=\frac{386}{j\omega}\frac{N^2}{A^2NL_2+ABH} \tag{A31}$$

$$Q=\frac{N^2C-AHN}{A^2NL_2+ABH}. \tag{A32}$$

In experiment 2, section 2, the voltage ratio, $R=E_o^S/E_o^D$, is determined when I_o^D is zero. Eliminating F_o between (A23) and (A24) and setting $I_o^D=0$, we see that

$$R=E_o^S/E_o^D=\frac{HBL_1+ANL_1L_2}{AL_2} \tag{A33}$$

Equation (4) is obtained when eq (A31) through (A33) are substituted into (A28) and L_1 and L_2 have the values given previously.

From eq (A29), $G_o=B/N$, when Y is zero, that is, G_o is the value of G when nothing is attached to the mounting table of the calibrator. If G_p is the value of eq (A29) when $Y=Y_p$, where Y_p is the mechanical impedance of a pickup to be determined, we find that

$$Y_p=\frac{N^2(G_p-G_o)}{(A^2L_2N+AHB)-(N^2C-AHN)(G_p-G_o)}. \tag{A34}$$

The substitution of eq (A31) and (A32) into (A34) gives eq (5) for determining the mechanical impedance of a pickup attached to the mounting table of the calibrator.

We are indebted to L. R. Sweetman for guidance in setting up the laboratory equipment, and to Richard Harwell, Jr., for the careful machining of the masses and the various fixtures used. Ruth Woolley performed the least-squares calculations and Carol Waldron prepared the figures.

8. References

[1] Richard K. Cook, Absolute pressure calibrations of microphones, J. Research NBS **25**, 489–505 (1940) RP1341.

[2] Horace M. Trent, The absolute calibration of electromechanical pickups, J. Appl. Mechanics **15**, 49–52 (1948).

[3] Albert London, The absolute calibration of vibration pickups, NBS Tech. News Bul. **32**, 8–10 (1948).

[4] Sanford P. Thompson, Reciprocity calibration of primary vibration standards, Naval Research Laboratory Rept. F–3337, 8 p. (August 16, 1948).

[5] M. Harrison, A. O. Sykes, and P. G. Marcotte, The reciprocity calibration of piezoelectric accelerometers, David Taylor Model Basin Rept. 811, 14 p. (March 1952).

[6] Ernst A. Guillemin, Communication networks (John Wiley & Sons, Inc., New York, N. Y., 1931).

[7] Horace Lamb, On reciprocal theorems in dynamics, Proc. London Math. Soc. **19**, 144–151 (1889).

[8] R. A. Frazer, W. J. Duncan, and A. R. Collar, Elementary matrices (MacMillan Co., New York, N. Y. 1947).

Washington, March 12, 1956.

Journal of Research of the National Bureau of Standards Vol. 57, No. 4, October 1956 Research Paper 2715

Method for the Controlled Burning of Combustible Materials and Analyses of the Combustion Gases[1]

Alan Schriesheim[2]

A method is described to burn a given quantity of a combustible material in a fixed amount of air at a selected initial temperature. Analyses of most of the gaseous combustion products were made quickly and comprehensively by means of a mass spectrometer. Hydrogen chloride was not detected with the mass spectrometer because of its adsorption upon the walls of the glass combustion chamber. The concentration of this gas was determined by titrating a water wash of the combustion chamber with a standard silver nitrate solution. Carbon monoxide when present in concentrations below 1,000 parts per million was determined by an indicator method, and when present in concentrations above 1,000 parts per million was determined by the mass spectrometer. Several organic coatings of different chemical composition were burned in a combustion space initially maintained at three temperatures. The lowest temperature (250° C) produced the smallest variety of combustion gases, whereas the highest temperature (550° C) produced the largest variety.

1. Introduction

Organic materials are widely used for various building purposes. When these organic materials are exposed in air to elevated temperatures, gaseous combustion products are formed. The principal combustion products are carbon monoxide, carbon dioxide, and water. Other gases, such as phosgene, hydrogen chloride, ammonia, cyanogen, and sulfur compounds, have been found upon the combustion of chlorinated hydrocarbons, wool, silk, and rubber [1 to 4].[3]

In order to study the gaseous combustion products of these organic materials, several investigators [1, 2, 3] have burned large built-up specimens, including actual rooms and buildings. Obviously, this procedure is costly and time consuming. Several laboratory methods have been developed [1, 2, 5], which, however, lacked (a) a quick and comprehensive method for analyzing the gases, and (b) a method for controlling the amount of air per unit of weight of the specimen at any initial temperature.

A laboratory procedure designed to burn or decompose a given quantity of material in a fixed volume of air, at different temperatures, is described. A procedure is also described that utilizes a mass spectrometer to increase the speed and extend the scope of the gas analyses.

2. Apparatus

Figure 1 is a schematic diagram of the entire apparatus. Figure 2 is a diagram of the combustion chamber alone.

The combustion chamber, figure 2, was constructed of Pyrex glass, except for the combustion tube extending through its center. This tube was a 12-in. length of silica combustion tubing, 1 in. in diameter, that had been cut in half along its axis for approximately half of its length. This combustion tube was sealed to the walls of the combustion chamber through a graded silica-Pyrex seal.

A strip of mica, 3.5 in. by 1.2 in., was placed on top of the open part of the silica tube, and 20 ft of platinum wire, 0.019 in. in diameter and coiled in a ¼-in.-diameter spiral, was wound around the silica tube and over the mica strip (fig. 2).

A thermocouple was placed below the mica strip, and both thermocouple and platinum lead-in wires entered the combustion chamber through openings that were sealed gas-tight with Wood's metal.

The combustion chamber was attached to a vacuum manifold through the glass spiral and two ball joints (fig. 1). The spiral was constructed of 5 turns of 7-mm Pyrex tubing, each turn having a diameter of 6 in. The combination of spiral and ball joint provided enough movement so that the combustion chamber could be inclined.

3. Procedures

Under ordinary conditions, an accidental fire starts at atmospheric pressure. This condition was duplicated in the combustion chamber by allowing the drawoff tube to remain open until the initial temperature was reached, and then closing it.

Because the combustion chamber was allowed to remain open to the atmosphere, different amounts of air were left in the system at each initial temperature. In order to maintain a constant ratio of the weight of the specimen to the amount of air at each initial temperature, the weights of the specimens were adjusted to compensate for the decrease in the amount of air in the system at the higher temperatures.

The ratio of the weight of the specimen to the amount of air in the system at room temperature was chosen as a reference point. The weights of the specimens to be used at the higher temperatures were calculated by means of the relationship

$$\frac{X_1}{X_2}=\frac{n_1}{n_2}, \tag{1}$$

[1] The experimental work was supported by the U. S. Air Force.
[2] Present address: Esso Research & Engineering Co., Linden, N. J.
[3] Figures in brackets indicate the literature references at the end of this paper.

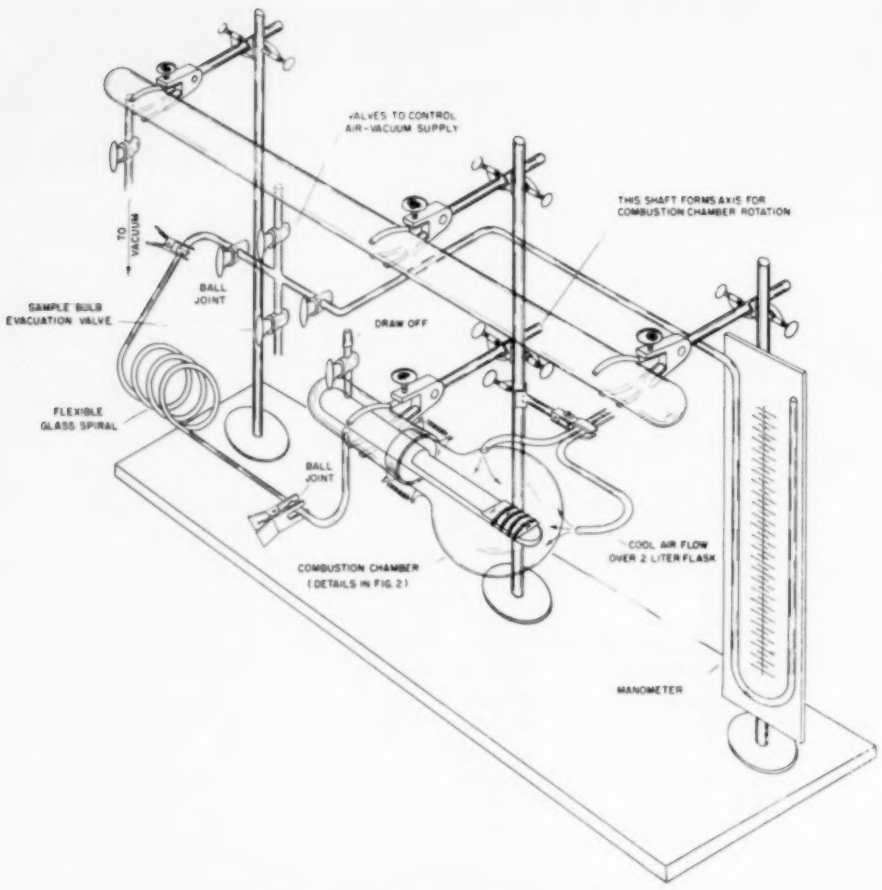

FIGURE 1. *Combustion apparatus.*

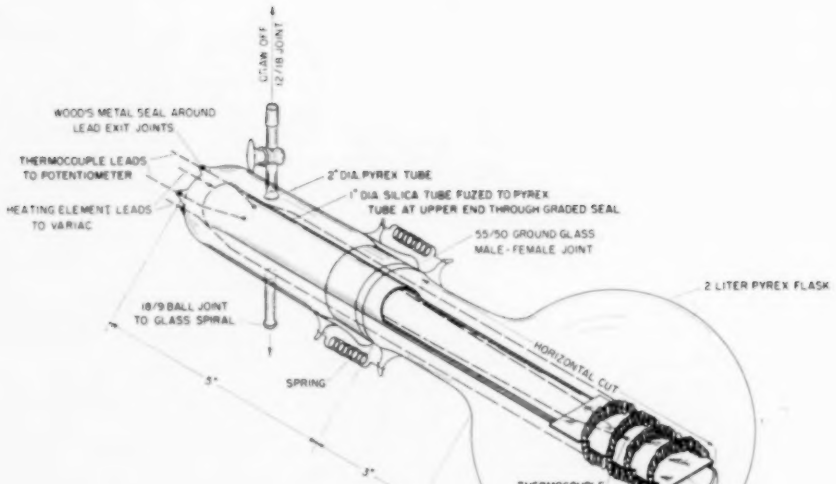

FIGURE 2. *Details of combustion chamber.*

where

X_1 = the weight of the sample at room temperature.
X_2 = the weight of the sample at the initial temperature.
n_1 = the number of moles of air in the system at room temperature.
n_2 = the number of moles of air in the system at the initial temperature.

The quantity n_1 can be derived from the perfect-gas equation,

$$P_1V_1 = n_1RT_1, \quad (2)$$

because the volume of the system, V_1, is known (2,230 ml), and P_1 and T_1 refer to the atmospheric pressure and room temperature, respectively.

The calculation of n_2, however, posed some difficulties. Although the initial temperature in the vicinity of the platinum coil was known, the temperature, T_2, of the entire system, encompassing the heated platinum coil, the air inside the system, and the cooled walls of the combustion chamber, was unknown. Hence, the following indirect method of calculating n_2 was employed.

Applying the perfect-gas equation to the open system raised to a higher temperature, T_2, the following relation is obtained:

$$P_1V_1 = n_2RT_2, \quad (3)$$

where

P_1 = the atmospheric pressure.
V_1 = the volume of the system.
n_2 = the number of moles of air left in the system at system temperature T_2.

If the system is closed at room temperature and pressure, and the platinum coil then heated sufficiently to raise the system temperature to T_2, the situation is described by

$$P_2V_1 = n_1RT_2, \quad (4)$$

where

P_2 = the pressure at system temperature T_2.
V_1 = the volume of the system.
n_1 = the original number of moles of air in the system (room temperature and atmospheric pressure).

Dividing eq (3) by eq (4),

$$\frac{P_1}{P_2} = \frac{n_2}{n_1}, \quad (5)$$

and n_2 may be calculated from an experimental measurement of the pressure developed when the closed system is heated to temperature T_2.

For the purposes of this investigation it was unnecessary to know the actual value of the system temperature at which the determinations were made. Hence, it was sufficient to measure the pressure developed in the closed system when a selected heating-coil temperature had been reached, and to calculate the value of n_2 produced by those conditions without further defining them. In turn, X_2 can be calculated from n_2 by means of eq (1). To avoid a separate measurement of this pressure at the beginning of each run, a calibration curve of pressure versus heating-coil temperature was made, and the closed-system pressure for the run temperature selected was read from the curve. In practice, therefore, to avoid pressure buildup before combustion, the drawoff tube could be left open during the initial period of heating the equipment.

This method of avoiding a preliminary pressure buildup was considered preferable to one that had been used by other workers, which utilized a balloon into which the gases expanded [1]. A balloon introduces errors arising from (a) the difficulty of washing adsorbed gases, as hydrogen chloride, from the fabric; (b) the possible introduction of organic vapors into the samples; and (c) the diffusion of gases through the fabric.

At the beginning of each run the specimen was placed in a porcelain combustion boat, which was placed in the silica tube as far from the platinum coil as possible. Then the 2-liter glass bulb was placed in position and the two springs attached. The combustion chamber was cooled by the air coming from the jets shown in figure 1.

The combustion chamber was evacuated by opening the stopcock to the vacuum manifold. This evacuation removed any organic vapors that might have been present from a preceding run. After evacuation, the vacuum stopcock was closed and the drawoff valve opened to the atmosphere. Current was then applied to the platinum coil.

When the initial combustion temperature, as indicated by the thermocouple, was attained, the drawoff tube was closed. Then the combustion chamber was inclined, causing the combustion boat containing the specimen to slide down the silica tube into the hot platinum coil, which ignited the specimen.

The input to the heating coil was maintained constant for 12 min, the current was turned off, and the apparatus was allowed to cool to room temperature. The gases were then collected as described below.

Several sample bulbs having volumes of 50 ml and 2,000 ml were constructed by sealing vacuum stopcocks and 19/38 ground-glass female joints to bulbs of appropriate size. The 50-ml bulbs were used for the mass-spectrometer analyses, and the 2,000-ml bulbs were used for the carbon monoxide determinations. Before a run, the sample bulb used was evacuated by attaching it to the vacuum manifold. The apparatus was cooled to room temperature, and then the evacuated sample bulb was placed on the drawoff arm and the drawoff stopcock opened. Approximately one-fourth of the air was immediately transferred out of the drawoff arm by expansion of the air from 1 atm to roughly ¼ atm. Assuming negligible subsequent mixing, the above procedure would lead to dilution of the combustion gases with

about 8 percent of air. In order to allow subsequent diffusive mixing, the sample stopcock was not opened until 10 min after the drawoff arm was opened. Thus, the actual contamination, although unknown, was probably somewhat less than 8 percent. For the colorimetric carbon monoxide determinations the error introduced by this method was negligible. Both stopcocks were then closed, and the sample bulb was attached either to the mass spectrometer or to the carbon monoxide apparatus.

After the combustion chamber cooled to room temperature, a partial vacuum was invariably present within the apparatus. In those cases where hydrogen chloride was expected, the drawoff arm was attached, by means of a piece of plastic tubing, to a beaker containing dilute (pH=10) sodium hydroxide. This solution was drawn into the combustion chamber and allowed to stand for 15 min. Due to the high affinity of hydrogen chloride gas for water, any of this gas not adsorbed upon the vessel walls was expected to dissolve in the base. After 15 min the springs were removed, and the solution was poured into a beaker. The combustion chamber was then washed several times with distilled water, and these water washings were combined and analyzed by the method described below.

4. Analyses

The 50-ml sample bulb containing combustion gases was placed on the inlet system of the mass spectrometer. An analysis was carried out for gases having a mass number of 1 to 100. The analytical results are recorded in table 1.

Carbon monoxide was determined by two methods. When it was present in concentrations above 1,000 ppm, the mass spectrometer was used. When present in concentrations below 1,000 ppm, the mass spectrometer was not sensitive enough to give an accurate analysis. It was, therefore, necessary to use the indicator technique [6]. The 2,000-ml sample bulb was filled with combustion gases, and the pressure reading on the manometer was recorded. The bulb was attached to a source of carbon monoxide-free air under pressure, and this air was allowed to enter the bulb until the pressure was slightly above 1 atm. Then the bulb was attached to an indicator tube [6], and the gases passed through the indicator at a constant rate, as determined by a flowmeter. At the end of a given time period, the color of the indicator was compared with a color chart, and the concentration of carbon monoxide in the sample bulb was determined.

TABLE 1. *Results obtained upon burning combustible materials in air*

Specimen	Material	Relative weights * per unit area	Temperature	Concentration of gases															
				Carbon dioxide	Carbon monoxide	Oxygen	Nitrogen	Methane	Methyl chloride	1,2-Dichloroethane	Ethane	Ethylene	Propylene	1,3-Butadiene	Benzene	Toluene	Hydrogen chloride	Hydrogen	Sulfur dioxide
ASSEMBLIES																			
			°C	%	%	%	%	%	%	%	%	%	%	%	%	%	%	%	%
1	Marine-grade plywood	1.0	250	0.9	0.1	17.9	73.8												
			400	19.4	1.4	2.7	74.2	1.4											
			550	17.1	3.6	2.8	71.9	1.0				2.4	Trace	Trace	Trace	Trace			
2	Marine-grade plywood, medium-density plastic overlay.	1.2	250	5.3	0.4	16.2	77.1												
			400	17.4	1.5	4.6	75.7												
			550	16.0	6.5	2.0	71.4	1.4			0.2	0.2	Trace		Trace	Trace			
3	Marine-grade plywood, Fire-retardent paint	1.1	250	1.2	0.6	19.6	78.1												
			400	11.0	.4	11.2	75.4	0.3											
			550	16.8	4.7	2.7	73.5	.9				.2			Trace	Trace		0.3	
4	Marine-grade plywood, Fire-retardent paint, Polyvinyl chloride plastic	1.7	250	1.9	0.3	18.7	78.2								do	do	1.6		
			400	16.3	4.4	2.9	74.0	1.6							0.1	do	2.8		
			550	17.1	5.1	2.1	72.2	1.4	0.2		.5	.1	0.1	0.1	Trace	do	3.0		
5	Asphalt aluminum paint, Marine-grade plywood, medium-density plastic overlay.	1.2	250	1.3	0.3	21.8	74.4												
			400	16.1	1.4	7.1	74.0												
			550	17.4	6.0	0.3	70.4	0.13			.1	Trace	.1					.3	
6	Marine-grade plywood, Fire-retardent paint, Polyester plastic	2.7	250	0.9	0.1	20.0	77.2								Trace	Trace	0.7		
			400	17.6	.1	2.7	77.3	.8	.4	0.2					do	do	1.7		
			550	14.7	13.2	2.6	64.1	1.9	.4	.7			Trace	Trace	do	do	3.8	.4	
COATINGS																			
7	Polyvinyl chloride plastic	0.8	250	0.7	0.1	17.7	74.0										2.4		
			400	11.1	.6	6.4	81.0										3.3		
			550	10.1	5.8	0.3	77.7	1.0	0.1	Trace		0.5	0.1	0.1	Trace	Trace	4.7	0.7	
8	Fire-retardent paint	.06	250	0.4	0.1	20.0	77.3												
			400	1.4		19.3	77.4												
			550	3.6		18.2	77.2								Trace				
9	Asphalt aluminum paint	.03	250	0.9		20.9	77.2												0.1
			400	1.4		19.8	77.8											Trace	.1
			550	2.7		19.8	76.7											do	Trace
10	Vinylidine chloride plastic	.05	250	0.2		18.7	78.2										0.6		
			400	.8		21.4	76.2										.8		
			500	.4		17.0	81.4									Trace	1.1		

* This column is the ratio of the weight of each material for a certain area to the weight of the exterior plywood for the same area.

Hydrogen chloride was adsorbed upon the walls of the combustion chamber, along with water produced during the course of combustion. Because of this adsorption, it was not possible to determine hydrogen chloride by means of the mass spectrometer. Instead, the water washings used in the procedure outlined previously were adjusted to a *p*H of 6.0 to 7.0 and titrated with standard 0.1 *N* silver nitrate, using fluorescein as an indicator [7].

5. Materials

To illustrate the utility of this method, several samples of organic wall and ceiling coatings were burned, and an analysis of their gaseous combustion products was carried out. These materials are listed in table 1.

In order to duplicate field conditions, the volume of a structure in field use was calculated, as was the area of the walls and ceiling of this structure. The area of each specimen was then adjusted so that the ratio of the specimen area to the volume of the combustion chamber was equal to the ratio of the ceiling and wall area to the volume of the structure.

6. Results and Discussion

The results of the analyses of the combustion gases are recorded in table 1.

Each material was organic, and gave rise to carbon monoxide and carbon dioxide upon combustion. The plywood apparently contained only carbon, hydrogen, and oxygen, and only gases composed of these elements were detected.

The plastic coatings contained chlorine as well as carbon, hydrogen, and oxygen, and gave rise to hydrogen chloride and chlorinated hydrocarbons, in addition to carbon monoxide and carbon dioxide. Hydrogen chloride has been found in the combustion gases of several types of chlorinated plastics, although there appears to be little information on the presence of chlorinated hydrocarbons [1].

The sulfur dioxide from the combustion of the asphalt aluminum paint probably came from the asphalt-resin base. It is known that the sulfur content of asphalt can be as high as 5 percent, depending upon its source [8]. No sulfur dioxide was found when the plywood material surfaced with the asphalt aluminum paint was burned (specimen 5). This was probably due to the adsorption of the sulfur dioxide, by the water formed upon combustion of the plywood, on the walls of the combustion chamber.

For every material the greatest variety of gases occurred at the highest initial temperature (550° C.). At this temperature, cracking and decomposition occurred, and small molecular fragments, such as methane and hydrogen, were formed from many of the specimens.

The chlorinated plastics liberated chlorinated hydrocarbons at the higher temperatures, whereas the only chlorinated material produced at the lowest temperature was hydrogen chloride. In each case the amount of hydrogen chloride increased as the temperature increased.

The assemblies and the polyvinyl chloride plastic coating are the heaviest materials listed in table 1. The quantities used were sufficient to consume all the oxygen if they were to burn entirely to carbon dioxide and water. As might be expected, these materials produced the largest concentrations of combustion gases, and caused the greatest decrease in the oxygen concentration.

For these materials, the combustion gases had oxygen concentrations of 0.3 to 3 percent at the highest initial temperature. This low oxygen concentration is typical not only of the closed system used here, but also of large, open, ventilated systems. For example, Kingman [5] and Olsen [2] report very low oxygen concentrations as the result of analyses of the combustion gases of ventilated and unventilated burning rooms. In general, the gases produced in most fires are the products of combustion and destructive distillation on decomposition [2]. In the method described in this paper, the above condition was approximated by forced heating of the specimen, after the oxygen concentration had dropped to a level below which flames could be sustained.

The foregoing procedure, while not capable of extreme accuracy, will give a quantitative estimate of the concentrations of combustion gases produced from commercially available organic coatings. Such information is of importance when designing a dwelling for use under certain conditions, and in producing organic coatings with special thermal-breakdown properties.

The author thanks the following Bureau staff members: S. Gunther, F. Elder, and S. Schuhmann for the mass-spectrometer analyses and the carbon monoxide determinations, and J. Loftus for the hydrogen chloride determinations.

7. References

[1] E. H. Coleman and C. H. Thomas, J. Appl. Chem. **4,** 379 (1954).
[2] J. C. Olsen, G. E. Ferguson, and L. Scheflan, Ind. Eng. Chem. **25,** 599 (1933).
[3] L. B. Berger, H. A. Schrenk, I. A. Gale, R. W. Stewart, and L. E. Sieffert, U. S. Bureau of Mines Rept. R. I. 4134 (Oct. 1947).
[4] Fire Eng. **99,** 148 (1946).
[5] F. E. T. Kingman, E. H. Coleman, and D. S. Rasbash, J. Appl. Chem. **3,** 463 (1953).
[6] M. Shepherd, Anal. Chem. **19,** 77 (1947).
[7] I. M. Kolthoff and E. B. Sandell, Textbook of quantitative analyses, p. 475, 572 (The Macmillan Co., New York, N. Y., 1949).
[8] H. Abraham, Asphalts and allied substances, p. 73 (D. Van Nostrand Co., New York, N. Y., 1945).

WASHINGTON, May 17, 1956.

U. S. GOVERNMENT PRINTING OFFICE: 1956

Recent Publications of the National Bureau of Standards

Journal of Research of the National Bureau of Standards, volume **57**, No. 2, August 1956 (RP2694 to RP2700, incl.). 60 cents. Annual subscription $4.00.

Technical News Bulletin, volume **40**, No. 8, August 1956. 10 cents. Annual subscription $1.00.

Basic Radio Propagation Predictions for December 1956. Three months in advance. CRPL 144. Issued August 1956. 10 cents. Annual subscription $1.00.

Journal of Research, volume 57, No. 2, August 1956. 60 cents. Single copies of Research Papers appearing in the Journal are not available for sale. The Superintendent of Documents, U. S. Government Printing Office, Washington 25, D. C., will reprint 100 or more copies of a Research Paper. Request for the purchase price should be mailed promptly to that office.

Research Papers

RP2694. Thermal properties of aluminum oxide from 0° to 1,200° K. George T. Furukawa, Thomas B. Douglas, Robert E. McCoskey, and Defoe C. Ginnings.

RP2695. Stress-strain relationships in yarns subjected to rapid impact loading: 4. Transverse impact tests. Jack C. Smith, Frank L. McCrackin, Herbert F. Schiefer, Walter K. Stone, and Kathryn M. Towne.

RP2696. Thermal expansion of polytetrafluoroethylene (Teflon) from −190° to −300° C. Richard K. Kirby.

RP2697. Preparation of D-arabinose-5-C^{14} from D-glucose-6-C^{14}. Horace S. Isbell, Nancy B. Holt, and Harriet L. Frush.

RP2698. Thermal expansion of binary alkali silicate glasses. Herman F. Shermer.

RP2699. Investigation of an alternating-current bridge for the measurement of core losses in ferromagnetic materials at high flux densities. Irvin L. Cooter and William P. Harris.

RP2700. Ionization and dissociation of the trifluoromethyl halides by electron impact. Vernon H. Dibeler, Robert M. Reese, and Fred L. Mohler.

Circulars

C573. Phase of the low radiofrequency ground wave. J. R. Johler, W. J. Kellar, and L. C. Walters.

Publications in Other Journals

Standard test for photoflash cells. H. J. DeWane. Mag. of Standards (70 E. 45th St., New York 17, N. Y.) **26**, No. 5, 135 (May 1955).

How strong must a building be? George N. Thompson. Mag. of Standards (70 E. 45th St., New York 17, N. Y.) **27**, No. 3, 68 (Mar. 1956).

How the National Bureau of Standards contributes to building codes. James P. Thompson. BOCA News (Building Officials Conference of America, Inc., 110 E. 42d St., New York 17, N. Y.) **4**, No. 12, 1 (May 1956).

Corrosion technology, the third year anniversary. J. G. Thompson. Corrosion Technology (Stratford House, Eden St., London, N. W. 1, England) **3**, No. 4, 105 (Apr. 1956).

Publications for which a price is indicated are available only from the Superintendent of Documents, U. S. Government Printing Office, Washington 25, D. C. (foreign postage, one-third additional). Reprints from outside journals are not available from the National Bureau of Standards but can often be obtained from the publishers.

UNIVERSITY OF MICHIGAN
GENERAL LIBRARY
DOCUMENTS DIVISION
1276 ANN ARBOR MICH

UNITED STATES
GOVERNMENT PRINTING OFFICE
DIVISION OF PUBLIC DOCUMENTS
WASHINGTON 25, D. C.

OFFICIAL BUSINESS

PENALTY FOR PRIVATE USE TO AVOID PAYMENT OF POSTAGE, $300 (GPO)

Journal of Research of the National Bureau of Standards Vol. 57, No. 4 October 1956

Contents

		Page
Infrared spectra of D-talose monobenzoate and related substances. H. S. Isbell, J. E. Stewart, H. L. Frush, J. D. Moyer, and F. A. Smith.	RP2708	179
Small oil-free bearings. Hobart S. White.	RP2709	185
Preliminary spectroradiometric measurements of the solar constant. Ralph Stair and Russell G. Johnston.	RP2710	205
Infrared spectrum of acetylene. Harry C. Allen, Jr., Eugene D. Tidwell, and Earle K. Plyler.	RP2711	213
Variation of peak temperature with heating rate in differential thermal analysis. Homer E. Kissinger.	RP2712	217
Mass spectrum of sulfur vapor. Paul Bradt, Fred L. Mohler, and Vernon H. Dibeler.	RP2713	223
Calibration of vibration pickups by the reciprocity method. Samuel Levy and Raymond R. Bouche.	RP2714	227
Method for the controlled burning of combustible materials and analyses of the combustion gases. Alan Schriesheim.	RP2715	245

Single copies of the above Research Papers are not available for sale, but the Superintendent of Documents, U. S. Government Printing Office, Washington 25, D. C., will reprint 100 or more copies, and request for the purchase price should be mailed promptly to that Office.

[A list of recent NBS publications is given on page 3 of the cover.]

For sale by the Superintendent of Documents, U. S. Government Printing Office, Washington 25, D. C. Price 60 cents (single copy). Subscription price: $4.00 a year; $1.25 additional for foreign mailing.

UNITED STATES GOVERNMENT PRINTING OFFICE, WASHINGTON : 1956